Ministry of Higher Education and Scientific Research
University of Baghdad
Institute of Laser for Postgraduate Studies

Optical No Core Fiber Sensor for Temperature and Strain Measurement

A Thesis Submitted to the Institute of Laser for Postgraduate Studies, University of Baghdad in Partial Fulfillment of the Requirements for the Degree of Master of Science in Laser / Mechanical Engineering

By

Mohammad Muzahim Hasan

B.Sc. Mechanical Engineering – 2007

Supervisor

Assist. Prof. Dr. Hanan J. Taher

2021AD **1443 AH**

بِسْمِ اللَّهِ الرَّحْمَنِ الرَّحِيمِ

"نَرْفَعُ دَرَجَاتٍ مَنْ نَشَاءُ وَفَوْقَ كُلِّ

ذِي عِلْمٍ عَلِيمٌ" ﴿٧٦﴾

صدق الله العظيم

سورة يوسف الاية (76)

Certification

I certify that this thesis was prepared under my supervision at the Institute of Laser for Postgraduate Studies, University of Baghdad, as a partial fulfillment of requirements for the degree of "Master of Science in Laser/ Mechanical Engineering".

Signature:

Name: **Dr. Hanan Jaafar Taher**

Title: **Assistant Professor**

Address: Institute of Laser for Postgraduate studies,University of Baghdad.

Date: / / 2021

(Supervisor)

In view of the available recommendation, I forward this thesis for debateby Examining Committee.

Signature:

Name: **Dr. Hanan Jaafar Taher**

Title: **Assistant Professor**

Address: Institute of Laser for Postgraduate studies,University of Baghdad.

Date: / / 2021

Examination Committee Certification

We certify that we have read this thesis “Optical No Core Fiber for Temperature and Strain Measurement" and as Examination Committee, we examined the student in its content and in our opinion, it is adequate with standards as a thesis for a degree of Master in science in Laser /Mechanical Engineering.

Signature:
Name: **Dr. Abdulhadi Mutashar Abd**
Title: Professor.
Address: Institute of Laser for Postgraduate Studies/ University of Baghdad
Date: / / 2021
(Chairman)

Signature:
Name: **Dr. Ziyad Ayad Taha**
Title: Assistant Professor.
Address: Institute of Laser for Postgraduate Studies/ University of Baghdad
Date: / / 2021
(Member)

Signature:
Name: **Dr. Ahmed Riyadh Abbas**
Title: Assistant Professor.
Address: Collage of laser and optoelectronic engineering/Al Nahrain University
Date: / / 2021
(Member)

Signature:
Name: **Dr. Hanan Jaafar Taher**
Title: Professor.
Address: Institute of Laser for Postgraduate Studies, University of Baghdad.
Date: / / 2021
(Supervisor)

Approval by the Deanship of Institute of Laser for Postgraduate Studies, University of Baghdad.

Signature:
Name: **Prof.Dr. Hussein A.Jawad**
Title: Dean.
Address: Institute of Laser for Postgraduate Studies, University of Baghdad.
Date: / / 2021

الإهداء

إلى من كرست حياتها في سبيل راحتنا.. أمي الحبيبة.

إلى من سعى دائما لننعم بحياة كريمة ..أبي الحبيب.

إلى سندي في كل لحظة .. زوجتي الغالية .

إلى مشرفتي العزيزة التي كانت دائما مصدر تشجيع و دعم .

إلى جميع أساتذتي الكرام.

إلى جميع أصدقائي و زملائي و زميلاتي.

و قبلهم جميعا إلى وطني الذي جمعهم كلهم العراق.

ACKNOWLEDGEMENTS

'**ALLAH**' my merciful God is the first who I would like to thank, the sustainer who has been always with me along my life until this moment. I would like to express my endless love and appreciation to my mother, her prayers enlightened my way through this scientific journey.

My highest words of thank to my supervisor, **Dr. Hanan Jaafar Taher**, her keen support, encouragement and motivation were a great inspiration to me. Her guidance and scientific background made my steps easier to the bottom line.

She was supportive, kind and positive since the startup and until the end .

I would also like to thank **Dr. Hussein A. Jawad**, the dean of Institute of Laser for Postgraduate Studies, and **Dr. Jawad A. Hasan**, the deputy of dean of the institute of laser for postgraduate studies.

Thanks to **Dr. Tahrir S. Mansour,** head of the engineering and industrial application department for her kind support.

I would like to express my sincere appreciation to every single staff and colleague in the Institute of laser for postgraduate studies for their efforts and cooperation.

I would like to express a special word of thank to **Mr. Saif Akeel Mohammed**, for his continuous encouragement and his kind support since the beginning of my project.

A great Thank to **Dr. Abdulhadi Al Janabi,** for facilitating my work is his laboratory.

My greatest words of thank to all my family members, and my colleagues for being so positive and encouraging along my masters journey. Eventually I would like to express my truthful love to my wife and my three kids. Thanks for being in my life and thanks for your continuous support.

ABSTRACT

Optical fiber sensors have been showing proven outcomes in temperature and strain sensation applications, their sophisticated properties and precise results such as, the invulnerability to electromagnetic interference, compactness, corrosion resistance, high temperature resistance have made them superior to electronic sensors. In this thesis, a state of art yet, simple to fabricate temperature sensor built on the basis of Mach-Zehnder interferometer is experimentally demonstrated. Structuring the sensor was straightforward by fusing a segment of no-core fiber between two single-mode fiber and inducing tapers. Two various structures tapered and untapered sensors retaining the factory-made acrylate polymer coating are examined, the tapered structure showed the highest sensitivity for temperature measurement of around -1.9438 nm/^{0}C and a resolution of 1x10^{-2} ^{0}C in the range of 30-45 ^{0}Cand 3.5 seconds response time. The high temperature sensitivity of the temperature sensor might be due to the high negative thermo-optic coefficient, higher thermal expansion coefficient of the acrylate coating along with the tapering effect. Then, a uniaxial bi-directional strain sensor structured based on the same principles by utilizing apiece of no-core fiber between two single mode fibers, the strain sensor exhibited an excellent sensitivity as compared to previously published works, the strain sensor showed a sensitivity of -16.37 pm/με in the range of 0-1000 με and a resolution of 0.8185 pm and a perfect repeatability .Both strain and temperature sensors are cost effective, easy to fabricate and simple in structure. To the best of our knowledge this is the first time of using polymer coated tapered no-core fiber as a temperature sensor and highest strain sensitivity reported in no-core fiber so far. The sensors can be deployed in many temperature and strain sensation applications especially in the fields of biomedicine and biomechanics.

LIST OF CONTENTS

LIST OF TABLES

LIST OF FIGURES

LIST OF SYMBOLS AND ABBREVIATONS

BBS	Broadband source
CTE	Coefficient of thermal expansion
EMZI	Extrinsic Mach-Zehnder interferometer
FBG	Fiber Bragg grating
FPI	Fabry-Perot interferometer
GI	Graded index
IMZI	Intrinsic Mach-Zehnder interferometer
MI	Michelson interferometer
MMF	Multi-mode fiber
MMI	Multimodal interference
MZI	Mach-Zehnder interferometer
NCF	No core fiber
OFS	Optical fiber sensors
OPD	Optical path difference
OSA	Optical spectrum analyzer
PCF	Photonic crystal fiber
PMMA	Poly methyl methacrylate
R^2	Linear regression coefficient
RI	Refractive index
SI	Step index
SMF	Single mode fiber
SMS	Single mode- multimode- single mode
SNS	Single mode- no core fiber- single mode
TCF	Twin core fiber
TOC	Thermo-optic coefficient
UV	Ultraviolet

LPG	Long period grating
SNS-PC	Single mode-no core fiber-single mode polymer coated
TSNS-PC	Tapered single mode-no core fiber-single mode polymer coated
με	Microstrain

Chapter one

Introduction and Basic Concepts

1.1 Introduction and Motivation

Temperature and strain are crucial parameters and essential to be monitored in a variety of industrial and medical applications[1,2].These two parameters are key parameters in structural health monitoring[3],biomechanical application[4], biomedical application[5], automotive[6],space crafts[7],military applications[8], and so on. A robust, yet a precise sensing system for monitoring these influential parameters gave rise to optical fiber sensing systems. Optical fiber sensors have unique advantages such as, the invulnerability to electromagnetic interference (EMI), compactness, anti-corrosive properties and being inert to the vast majority of chemicals [9].

In the past three decades a large number of researches have been conducted in a competition to develop the best optical fiber temperature and strain sensors. The competition was in terms of the best sensitivity, resolution, and repeatability. Many fiber temperature sensor structures been developed based on single mode fibers (SMFs)[10], single-mode-multimode-single-mode fibers (SMSs)[11],photonic crystal fibers (PCFs)[12] ,and single-mode-no-core-fiber-single-mode fiber SNS[13].

In the advancement of fiber temperature sensors, some research groups employed fiber Bragg grating as thermometric fiber sensors[14].Although very interesting results might be obtained in some special fiber optic strain and temperature sensors, yet mechanical toughness, repeatability, simplicity, and cost effectiveness have limited these valuable outcomes to be utilized in real sensation applications.

Tapering effect have proven results in temperature sensation applications whereas an increased sensitivity attained [15,16,17,18].The enhanced sensitivity are mostly due to mode filtering and evanescent wave penetration to the outer medium, however a good understanding to tapering influence and tapering parameters are significant in designing tapered fiber temperature sensors. Unlike opto-mechanical sensors, in which the optical fiber sensor would be subjected to direct or indirect mechanical forces, fiber biosensor[19] , fiber chemical sensors[20], and fiber temperature sensors

are not imposed to any mechanical forces , thus tapering which is considered an extra weaker point in opto-mechanical sensors, can significantly enhance the sensitivity in fiber temperature sensors. Optical fiber sensors in mechanical sensing applications have replaced traditional sensors in many industrial and engineering applications; they have drawn a great attention due to their necessity and performance. Many opto-mechanical sensors have been present as hot research topics such as, fiber torque sensor[21], fiber deflection sensor[22], fiber stress sensor[23],fiber-optic vibration sensor[24] fiber load sensor [25], and fiber strain sensor[26].These fiber sensors are used in structural status monitoring, bridges, railways and aircrafts[27,28,29].

Optical fiber strain sensor need a relatively tougher structure to withstand cycles of repetitions especially the deployed in real sensing application. Operation principles of these sensors are concluded from the photoelastic phenomenon which refers to the variation of the refractive indices of the optical fiber due to the effect of an acting force. If strain applied parallel to the direction of the light wave inside the fiber, it can be considered axial strain.

Various fiber strain sensor structures are reported in the past decade such as , SMS structure[30], tapered structure single-mode-twin core fiber -single mode SM-TC-SM structure[31], cascaded single-mode-photonic crystal-multimode-single-mode fibers sensors SM-MM-PCF-SM[32].A governing equation to outweigh the reliability, cost effectiveness, compactness, ease of fabrication, simplicity, repeatability, linearity ,sensitivity and resolution can break the barrier and enable many researches to leave the laboratory boundary to observe a real deployment in actual measurement systems.

In the first part of this work, an optical NCF temperature sensor with excellent sensitivity is planned to be achieved by designing a tapered SMF-NCF-SMF retaining the factory-made UV-curable acrylate coating. The structure is simple yet repeatable and can be utilized in biomechanical and biomedical applications. The well applicable selected temperature range covers human body and the majority of mammals. The sensor is enhanced by inducing tapers according to empirical predefined tapering dataset .In the second part ,a bi-directional axial strain sensor

based on NCF is developed and demonstrated , then benefitting from the temperature sensor parameters the cross sensitivity to temperature is analyzed in the strain sensor. Both temperature and strain sensors are functioning according to wavelength modulation mechanism through multimodal interference theory MMI .In the temperature sensor, the utilization of the polymer protective coating saves both time and coating cost along with improving the thermal sensitivity .The removal of the coating was significant in reducing the temperature crosstalk in the strain sensor.

1.2 Characterization of optical fibers

Fiber-optic is information transmitting medium basically made of silica and other materials can be doped in the matrix, Germanium as an example. Optical fiber can also be made of plastic as polymer optical fibers. Light-wave propagates through the center of the fiber which is the core, whereas core is surrounded by an optical material called the cladding that traps light in the core forming an optical phenomenon known as the total internal reflection[33]. The fiber-optic is coated by a buffer which protects the fiber from damage. In the vast majority of fiber-optics the core and the cladding are made of pure silica, the core is made to have a higher refractive index than the cladding for enabling the total internal reflection to take place. In addition to the primary buffer, another layer of protection is provided in the manufacturing process which is the jacket coating[34].An illustrative image of typical optical fiber is shown in Fig.(1.1).The dimensions of the two concentric cylinders the core and the cladding depend on the type of the optical fiber. In SMFs the core diameter can range from (5-9) μm while the cladding diameter is usually 125 μm, whereas in MMF, the core can range from (50-100) μm and the cladding from (125-200) μm .

The physical structure of optical fiber might slightly differ from a manufacturer to another , however the basic operation concepts remains the same regardless of enforcement techniques and custom designs such as those of specific applications uses.

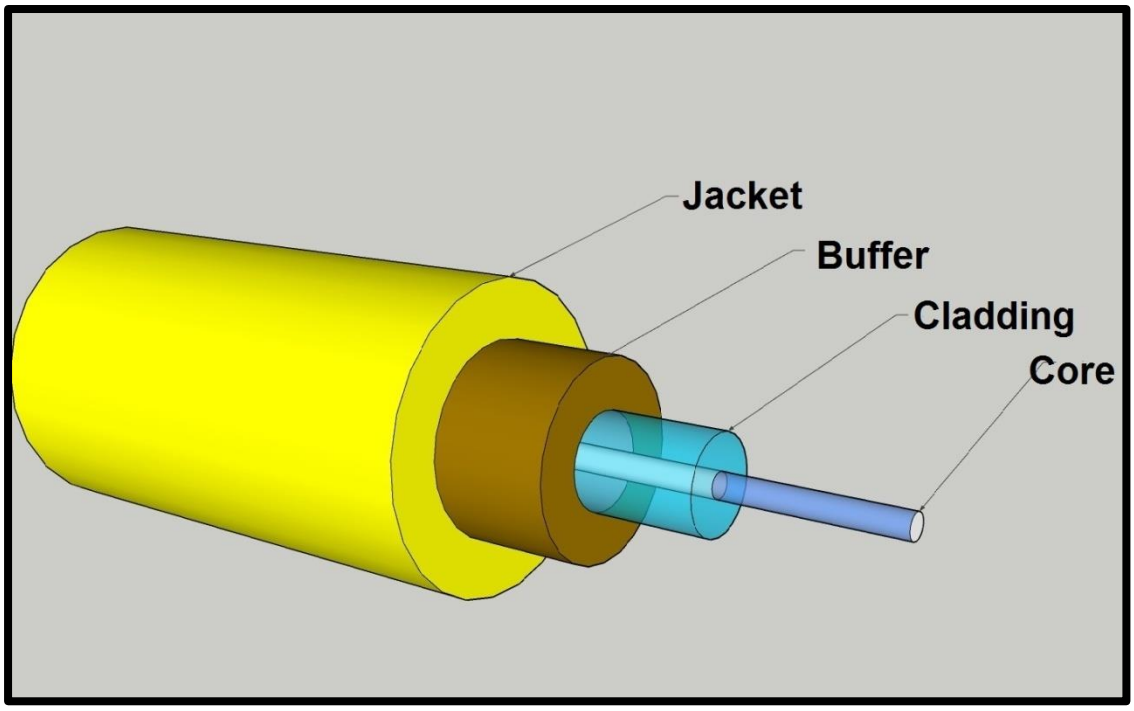

Figure(1.1):Typical optical fiber structure

Utilizing Snell's law when the angle of incident light is greater than the critical angle, light is reflected while the value of the incident angle is less than the critical angle light will escape through the cladding and the total internal reflection will fail.

A schematic graph of the total internal reflection phenomenon is depicted in Fig.(1.2)

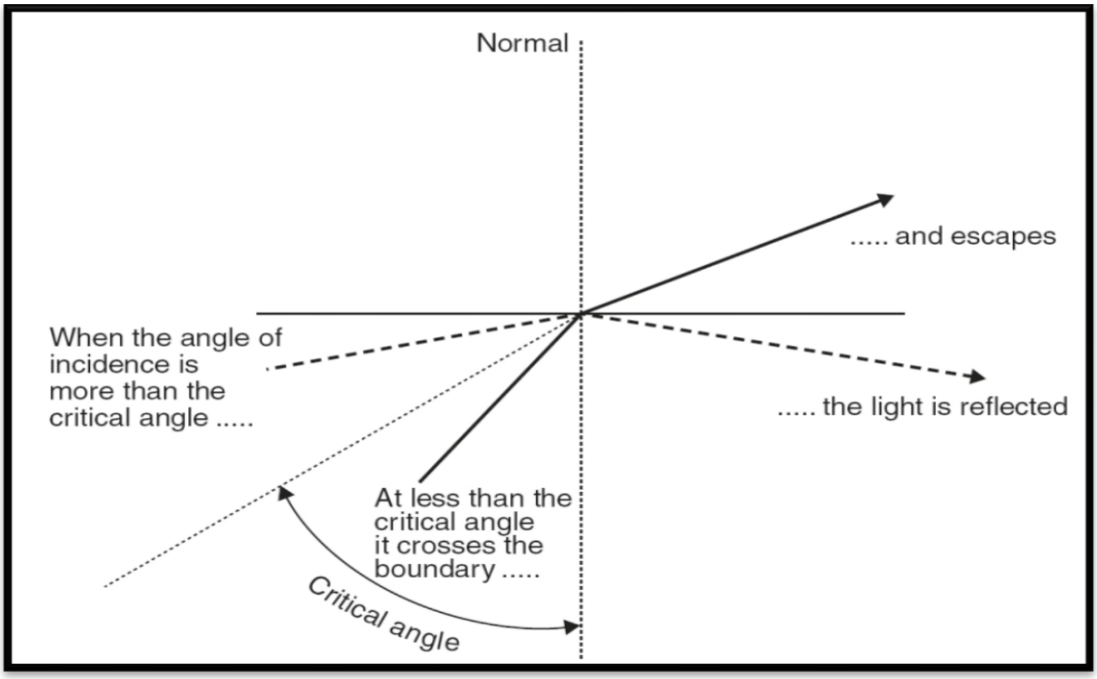

Figure(1.2):Total internal reflection in optical fibers[35]

1.3 Classifications of optical fibers

Optical fibers are classified according to the allowed numbers of modes that propagate through the fiber to: SMF which technically one mode will advance in the fiber, and MMF which many modes will make their way through the fiber core. These types are different in specifications, dimensions and transmission distance. Optical fibers have some special types as well such as, photonic crystal fibers (PCF) and, thin core fiber and NCFs.

1.3.1 Single mode fibers (SMFs)

This type of optical fibers has a smaller core dimensions. It is able to transmit a large amount of data for longer distance in long-haul telecom backbones. Lower attenuation as function of wavelength, less than 0.5dB/km for 1200nm-1600nm window and 0.19 dB/km for 1550 nm window.It exhibits lower vulnerability to dispersion and pulse widening in longer transmission spans. The most common operated wavelength are 1310,1550 nm windows [36].

1.3.2 Multi-mode fibers (MMFs)

Multi-mode fibers have larger core dimensions; it can transmit data in short distances usually within buildings, campuses and schools. MMF suffers higher attenuation than SMFs, around 3 dB/km in the 850 nm window, which is high. Higher dispersion occur in MMFs because of the fact of the intermodal dispersion as multiple mode travel through the same core of fiber. The most common operating window is 850 nm. MMFs can be classified to step index fiber (SIF) and graded index fiber (GIF) [37].

1.3.2.1 Multi-mode step-indexed fibers (MM-SIFs)

The term step-index refers to the abrupt change between the index of refraction of the core and the cladding in this type of MMFs, the change that follows a step function.[38] .

1.3.2.2 Multi-mode graded-index fibers (MM-GIFs)

In this type of MMFs the index of refraction of the core is not constant along the radial distance to the center of the fiber; it decreases as the radial distance increases toward the core-cladding interface that concluded the term "Graded" [38]. An illustrative graph of SMF, MM-SIFs and MM-GIF are shown in Fig. (1.3), where n_1,n_2 are the core and cladding refractive indices , respectively.

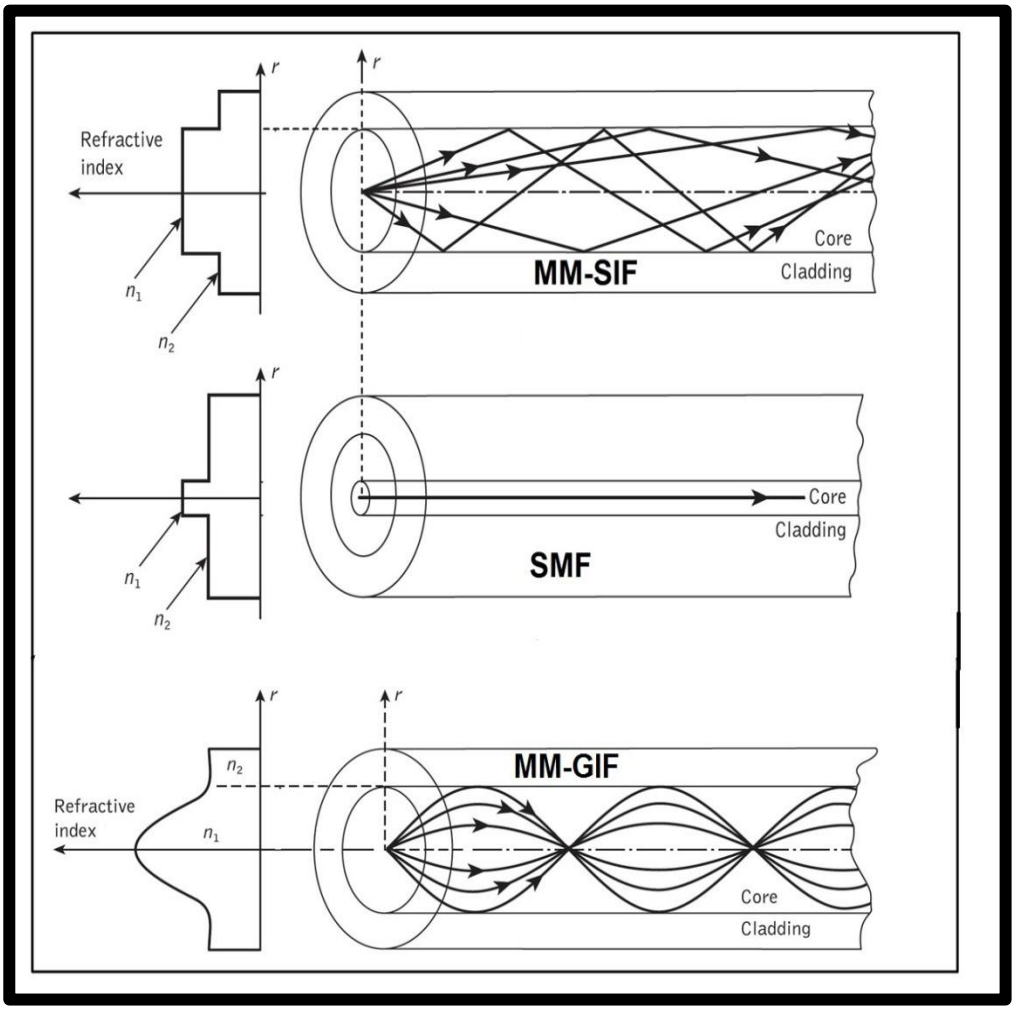

Figure(1.3):Different kinds of fiber-optics[38]

1.4 No-core fibers (NCF)

No-core fibers NCFs are special variants of MMFs where no cladding present, sometimes called coreless fiber. This type of optical fibers has shown interesting results in fiber sensing applications, especially in refractive index (RI) sensing of various liquids [39]. In NCF no clad etching is required to promote the evanescent light penetration to the surrounding .The simple structure of NCF enables the ease of fabrication procedure as its geometry made of one cylinder of glass coated with the primary buffer and that makes it both time and cost saving in sensing applications.

1.5 Optical fiber sensors (OFS)

The sophisticated advantages of OFSs cannot be limited to the points which mentioned in the introductions of this chapter, for instance, electronic sensors have limited capability in distribution sensing , therefore a large numbers of these sensors needs to be deployed which is both expensive and hard to maintenance.

A better understanding of optical sensors working mechanism is important. OFSs utilize light to convey the data, the sensor is designed to respond only to the intended measurands, generally there are two sensing mechanisms employed in OFSs; intrinsic and extrinsic. The main difference between these two techniques is the location in which the modulation occurs. In intrinsic sensors the light-wave remains inside the fiber where the modulation actually take place, whereas in extrinsic OPFs, the sensor is a bulky optical instrument such as; electro-optic crystals, or strain birefringence. These extra components sometimes situated amongst cross polarizers, hence the modulation is undergoing outside the optical fiber with another assisting component [40].An illustrative chart in Fig.(1.4) refers to the main differences between the two techniques, to clarify the operation concepts few examples are given within the same figure .

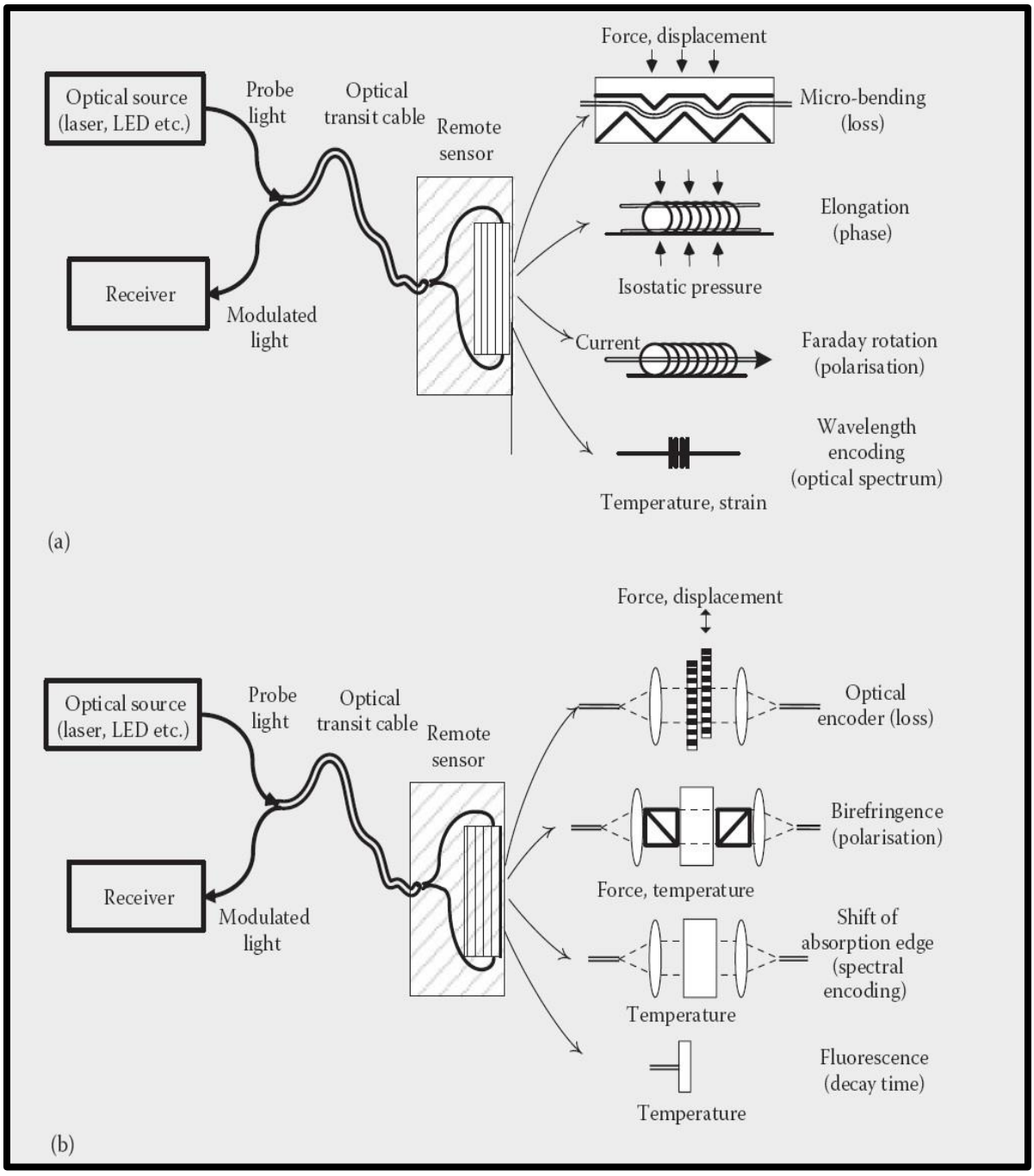

Figure(1.4):Operation mechanism of fiber-optic sensors (a) intrinsic and (b) extrinsic[41]

1.6 Interferometric optical fiber sensors

An optical fiber interferometer utilizes the phenomenon of interference between two traveling light beams which have advanced across various optical paths

within the same fiber or within two different fibers. As a result, they need beam splitting and beam recombining devices regardless of being intrinsic or extrinsic.

As a matter of fact, one of the optical paths must be prepared to get easily affected by external disturbances usually named the sensing beam, and the other beam will continue the propagation through the sensing fiber without being affected by the perturbations which is named reference bema. Accordingly, measurands might be quantitatively calculated using different techniques of detection. These techniques can rely on; studying the variance in the intensity, wavelength, polarization, or the phase of the emerging signals. As a result OFS is able to give a magnificent performance in a wide dynamic range. The recent trends of fiber-optic interferometric sensor are to minimize the sensing system size for micro-system applications. Thus, conventional bulky optical parts such as, beam combiners, beam splitters and lenses have been promptly substituted with mini-scaled fibers. That makes the sensor to function on fiber size scales. The best example of implementing minimized fiber-optic interferometers is in-line structures, an optical fiber itself as a sensor. Inside the optical fiber, light has two different optical paths in a single physical line .The intrinsic setup offers many advantages such as, higher coupling efficiency , ease of alignment and better stability[42-44] .

1.6.1 Mach-Zehnder interferometer (MZI) based sensors

Mach-Zehnder interferometers (MZIs) have been extensively used in a large variety of fiber sensation devices owing the simple in configuration. An incident ray of light is divided into two arms via a fiber coupler then, re-coupled by another coupler. The recombined ray has the component of interference according to the optical path difference (OPD) between the two arms. For sensing purposes, the reference arm is isolated from external perturbations whereas the sensing arm is imposed to the measurand. Then, the variance in the sensing arm determined such as, RI change, strain, and temperature .The optical path difference (OPD) of the Mach-Zehnder can be detected by analyzing the variation in the signal of the interference [44-46].

1.6.1.1 Extrinsic Mach-Zehnder interferometer (EMZI) based sensors

Former MZI which is the extrinsic type had a couple of separated arms which are, the reference arm and the sensing arm.In this type, there are two different physical paths for each light beam to pass through. The original light source is divided via beam splitter into two beams the reference and the sensing arm. Usually 3dB couplers are utilized for the splitting at the first point and for the combining at the second point [45-47].

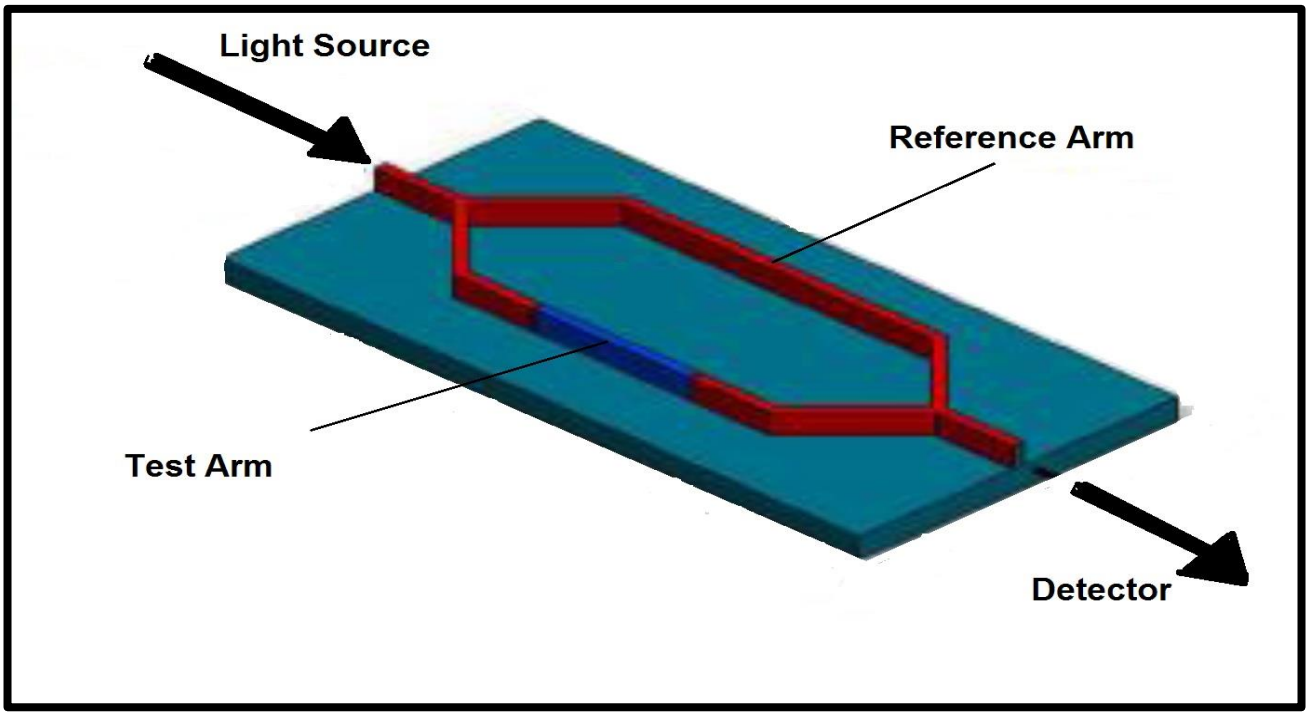

Figure(1. 5):Traditional extrinsic Mach-Zehnder interferometer [45]

1.6.1.2 Intrinsic Mach-Zehnder interferometer (IMZI) based sensors

The IMZI is an ideal replacement to the EMZI for many advantages such as, compact size, better coupling efficiency and ease of coupling. In the recent era of OFS researches, the vast majority of the sensing structure that employs Mach-Zehnder interferometers are IMZIs .They are easy to fabricate and less materials involved in the interferometer structure. The splitting and the coupling occur within the splicing joints of the sensing segment inside the same fiber. Because of these

advantages, intrinsic sensors can simply embed in many measurement systems. The intrinsic structure contains less optical components, hence less errors percentage and more cost effectiveness. The same medium contains both of sensing arm and reference arm [46, 47].A schematic figure of IMZI is illustrated in Fig.(1.6)

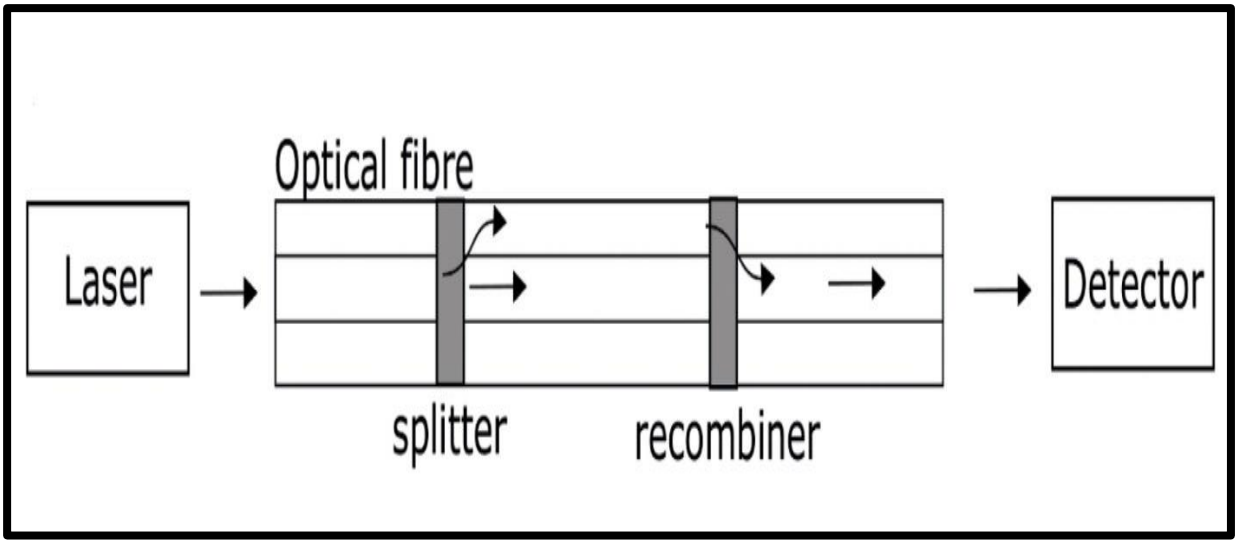

Figure(1.6):Intrinsic Mach-Zehnder interferometer [47]

1.6.2 Fabry-Perot interferometer (FPI) based sensors

Fabry-Perot interferometer is another interferometric system which employs the reflection phenomenon between two reflecting surfaces as operation principle. It can be structured by end-coating fibers to form the interferometer to enable the best reflectivity by multi-layer coating. There are two types of Fabry-Perot interferometers; the intrinsic (IFPI) and the extrinsic (EFPI). In the IFPI the ends of the fiber is coated by a highly reflective coating then, those ends are fused to an intermediate segment to form the cavity. The EFPI is formed by an air-gap between two reflecting uncoated fibers, the cavity is fixed via an alignment tube, and the fibers are held by glue or epoxy to prevent the cavity form movement. The use of EFPI, is identified by analyzing the fully reflected spectrum of the sensor to find out the optical path difference, accordingly, the measurand encoded information [48-50]. An illustrative sketch of both IFPI and EFPI is shown in Fig.(1.7),both IFPI and EFPI interferometers are extensively used in strain sensing applications.

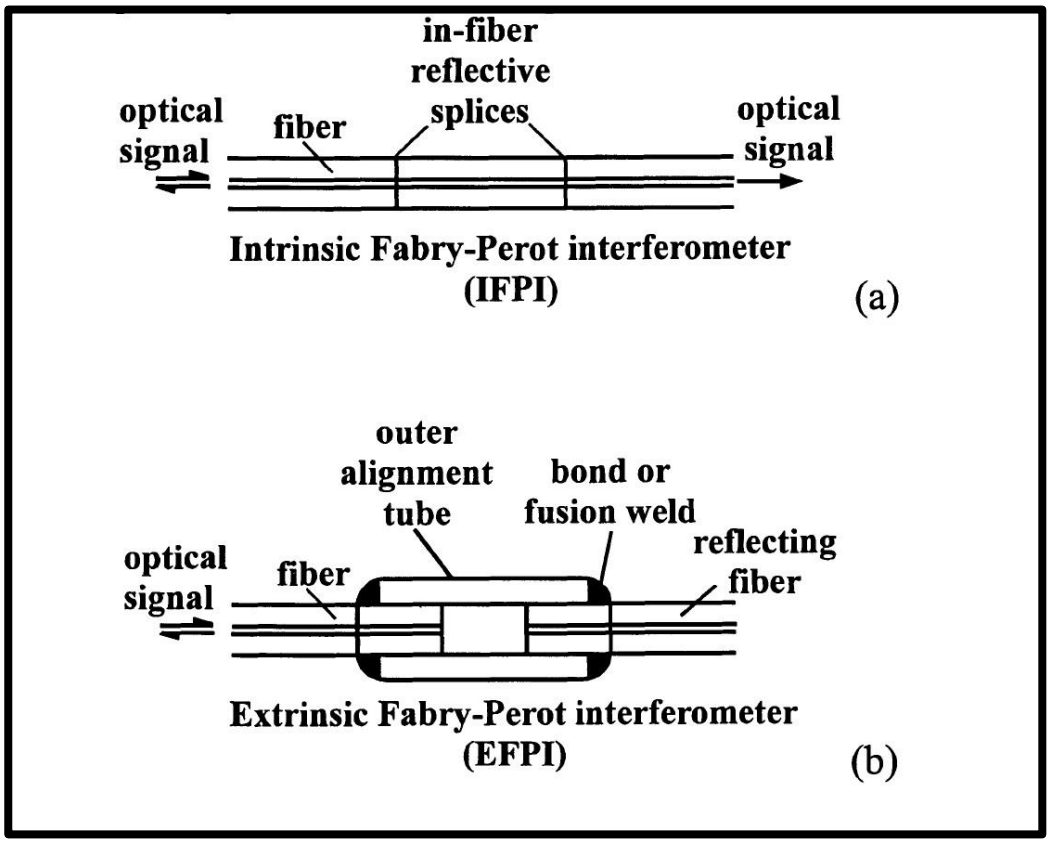

Figure(1.7): (a) Intrinsic Fabry-Perot cavity (b) Extrinsic Fabry-Perot cavity [49]

1.6.3 Michelson interferometer (MI) based sensors

A Michelson interferometer is constituted utilizing two separate pieces of fibers to the output ports of a fiber-coupler and putting a fully reflecting mirrors or fiber Bragg gratings at the other end of the fibers [50]. Bragg gratings (BG) completely reflect the light which its wavelength falls within the no-pass band of the grating. A Michelson interferometer operates same as MZI with a major difference the light-wave advancing in its two split beams is forced to undergo interference at the same coupler where they firstly suffered the split. Due to this property, Michelson interferometer performs like a nonlinear mirror the same as Sagnac interferometer (SI).The difference between MI and SI is that the interfering optical fields do not share the same physical path in MI. Nonlinear Michelson interferometers might also be made via bulky optics (mirrors and beam splitters) [50,51].A sketch of Michelson interferometer is illustrated in Fig.(1.8).Where Lx and Ly are the distances between the mirrors and the beam splitter.

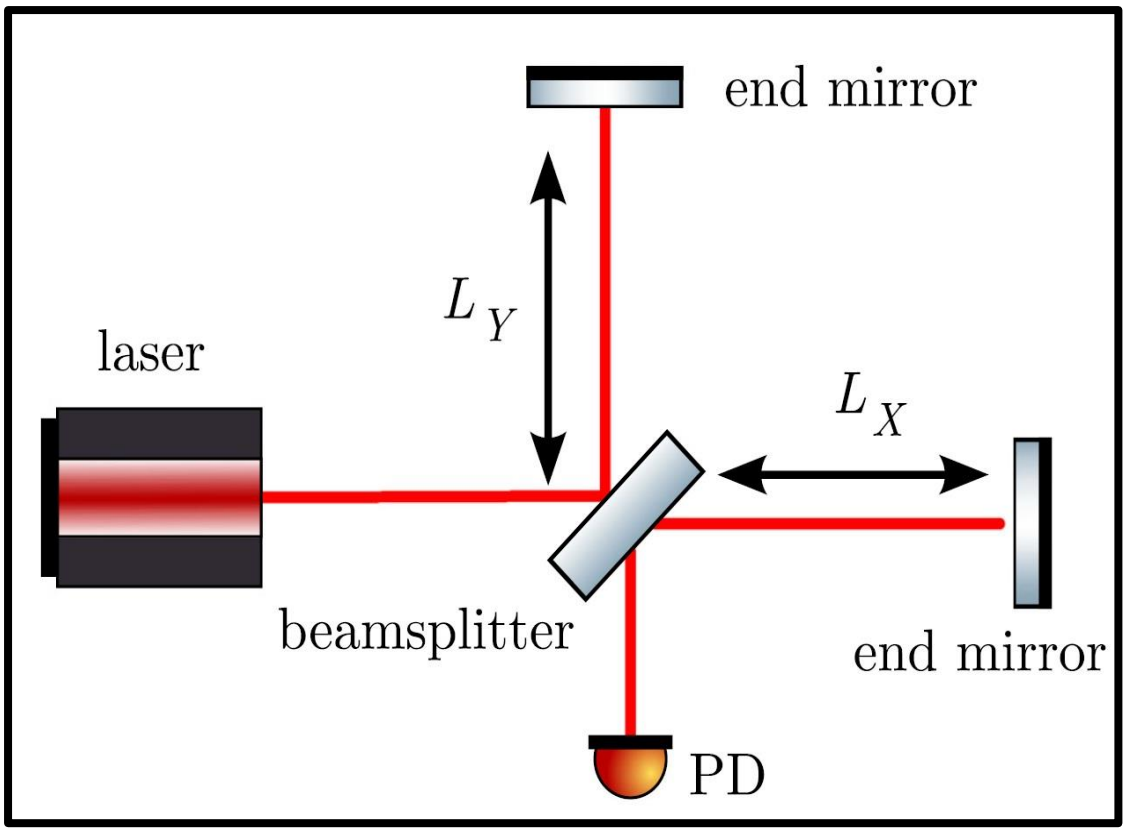

Figure(1.8): A schematic graph of typical Michelson interferometer [51]

1.6.4 Sagnac interferometer (SI) based sensors

The Sagnac effect manifests the proportional phase-shift of two light beams that propagate on an identical path in opposite directions within a rotating frame. Recent navigation systems and optical fiber gyroscope employ Sagnac interferometer working principle. Extremely precise measurements of spinning and rotation of around $10^{-4} – 10^{-5}$ click/hour is obtained in SI [52].

A typical configuration of Sagnac interferometer is shown in Fig.(1.9).The SI is in triangular form containing a source of light, mirrors M_1, M_2, a beam-splitter S, and a sighting surface. All these components are situated on a rotating base at a fixed angular speed X around a rigged axis. The axis of rotation not necessarily normal to the plane of the interferometer. The light source and the sighting plane are situated on the same rotating base of M_1, M_2, and S. [52-55]. In one round-trip between the source and the sighting surface, the clockwise-emerging beam suffers four reflections, whereas the counterclockwise beam undergoes two reflections (M_1, M_2)

and two transmissions (both at S). Given the 90 degree difference of phases between the transmission and reflection of the counter-advancing beams reach the sighting plane with a relative-phase of 180 degree. Accordingly, one beam will cancel the other resulting in a dark or no fringes. Even a slight phase difference between both beams will affect the signal strength at the sighting plane as the system rotates. Usually interference fringe shifts are seen only when a slight misalignment of the system take place which leads to separation of the counter-advancing beams as it hits the beam-splitter S [54].

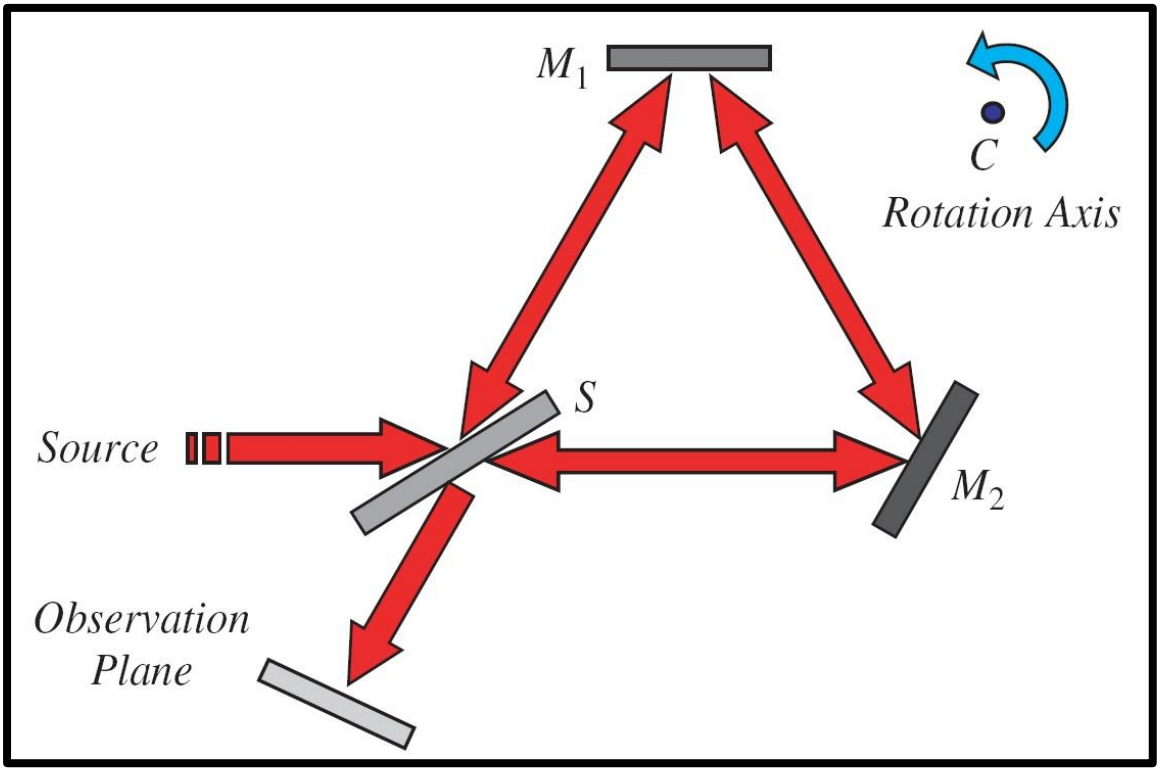

Figure(1.9): A schematic diagram of triangular Sagnac interferometer [54]

The main characteristics of a Sagnac interferometer can explain as:

1. The obtained relative phase between counter-advancing beams within the Sagnac loop is proportional to (a.v), where a is the loop area and v is the loop angular velocity, regardless of the loop shape, or the location and rotation axis orientation.
2. Doppler-shifts induced as a result of reflections from the rotating mirrors and the beam splitter will not cause a variation in the counter-advancing beams frequency.
3. The index of refraction of the media that the counter-advancing beams has no

effect on the relative phase of these beams, knowing that the media itself is rotating with the rest of the system [55].

1.7 Acrylate polymers

UV-curable Acrylate polymers have substantial properties that promote the use of these materials as coating for optical fibers. These materials are deposited on the glass fiber in a liquid form then, cross linking of the polymer hardening process on the silica fiber is performed using ultraviolet ray (UV).They are basically transparent, easy to remove, provide protection against moisture, improve the mechanical strength ,non-toxic and cost effective. These polymers can be applied as a single layer of coating or multi-layer of coating Acrylate[56].Optical and thermal properties of some common UV-curable polymers are listed in the Table.(1.1).From the table below, most of these polymers have a high negative thermo-optic coefficient TOC and high coefficient of thermal expansion as compared to silica fiber.

Table.(1.1) optical and thermal properties of polymers used in fiber coating[57]

Polymer type	Material state	TOC $x10^4$ $°C^{-1}$	CTE $x10^4$ $°C^{-1}$
Epoxy	Glassy	-1.0	1.7
PMMA	Glassy	-1.3	2.2
Sol-gel/diphenysilane	Glassy	-2.3	3.9
Silicone	Rubbery	-3.1	5.9
PEMA	Glassy	-1.1	1.9
tB-PEEK	Glassy	-1.0	1.7
Polycarbonate	Glassy	-0.9	1.7
Polystyrene	Glassy	-1.2	2.2
Sol-gel	Glassy	-2.1	3.5
Urethane acrylate elastomer	Rubbery	-4.2	7.2

Polymer coatings have been showing excellent results in improving temperature sensitivity in optical fiber sensors. Hats mostly due to their higher CTE and high negative TOC which induces a high thermal response in OFSs [58-61].

1.8 Wavelength modulated fiber temperature sensors

Understanding the operation principles and enhancement techniques are the key success in designing all-fiber temperature sensors. The racing to focus on the best sensitivity only and forgetting the mass production criterion might not be a good idea. Trials to achieve the highest sensitivity at any cost is encouraging; however a great numbers of these sensors might remain in the boarder of the laboratories and remain as a research material only. Fiber-optic temperature sensors are designed depending on different modulation techniques of the propagating light[62].The modulation techniques can change one or more characteristics of the light-wave. In wavelength modulated interferometric temperature sensors, an interference pattern will be intentionally created utilizing one of the previously mentioned interferometers. The interference pattern can be constructive or destructive depending on the phase variation of the interfering waves and the path difference amongst traveling modes [63].When fiber sensors subjected to temperature variation, a shift in the interference peak or dip occur. This shift can be toward either longer wavelength (red-shift), or shorter wavelength (blue-shift. To improve the sensitivity, a broad-range of modifications can be adapted. These modifications can be either by modifying the structure itself such as; inducing tapers, offsets, core mismatch, cascading different types of optical fibers and macro bending [64-66].Or by the addition of thermo-sensitive coatings that have higher response to temperature variation such as; polymers, heat sensitive nano-coatings, metal coatings and heat sensitive liquid coatings sealed in a capillary tubes[67-69].Further enhancements can be obtained by a combination of two or more from above. These enhancements will affect the difference in the effective index of refraction between core mode and cladding modes of the propagation light, leading to various coupling constants along the sensing segment.

The NCF used in structuring a multimode based temperature sensor can be more enhanced by utilizing a combination of temperature sensitivity enhancements. For instance, keeping the acrylate coating which has a high CTE, a high negative TOC and adding tapers. This combination can promote mode filtering and evanescent wave penetration to the outer medium at the same time.

1.9 Intensity modulated fiber temperature and strain sensors

Light intensity modulation is another approach which is widely adapted in designing fiber temperature sensors [70].In intensity modulated sensors, the perturbation will modify the intensity of the light falling on the detection system. For instance, When light propagate through a segment of NCF that is sandwiched between two SMFs and sealed with alcohol inside a capillary tube, if the sensing segment is exposed to increase in temperature, the emerging light towards the detector might suffer from either an increase or a decrease in the intensity. These variations can be due to the change in the absorbance of evanescent light in the sensing part of the NCF under thermal effects thus, sensitivity is a function of intensity [71].Another concept is applying sensitive coatings (e.g.) nano-particles. Adding heat-sensitive nanostructured materials to the sensing part might manipulate the amount of light that can be absorbed as it passes the sensor in response to heat variations. Nanostructured materials have super interaction properties due to the unique surface area to volume ratio value. An example of these sensors is a nano-coated cladding removed SMF intensity modulated temperature sensor [72].In large strain or displacement applications, a common technique which widely adapted in some fiber sensors is the utilization of two separated fibers. These fibers are optically aligned but not fused to each other, light propagates from one fiber, passing the air gap and emerging the second fiber. When strain is applied, the distance between two optical fibers will increase leading to degradation in the intensity that leaves the second fiber and hits the detector. In such structure, the strain or displacement if applied in the opposite direction, both fiber ends will converge, thus the amount of light intensity hitting the detector will

increase. Intensity variation on the detector is the indicator of the system for strain or displacement in either direction [73]. This method can be used in structural health monitoring, bridges, railways and to identify cracks in buildings. A schematic diagram of some intensity modulated temperature and displacement sensors shown in Fig.(1.10)(a-b).

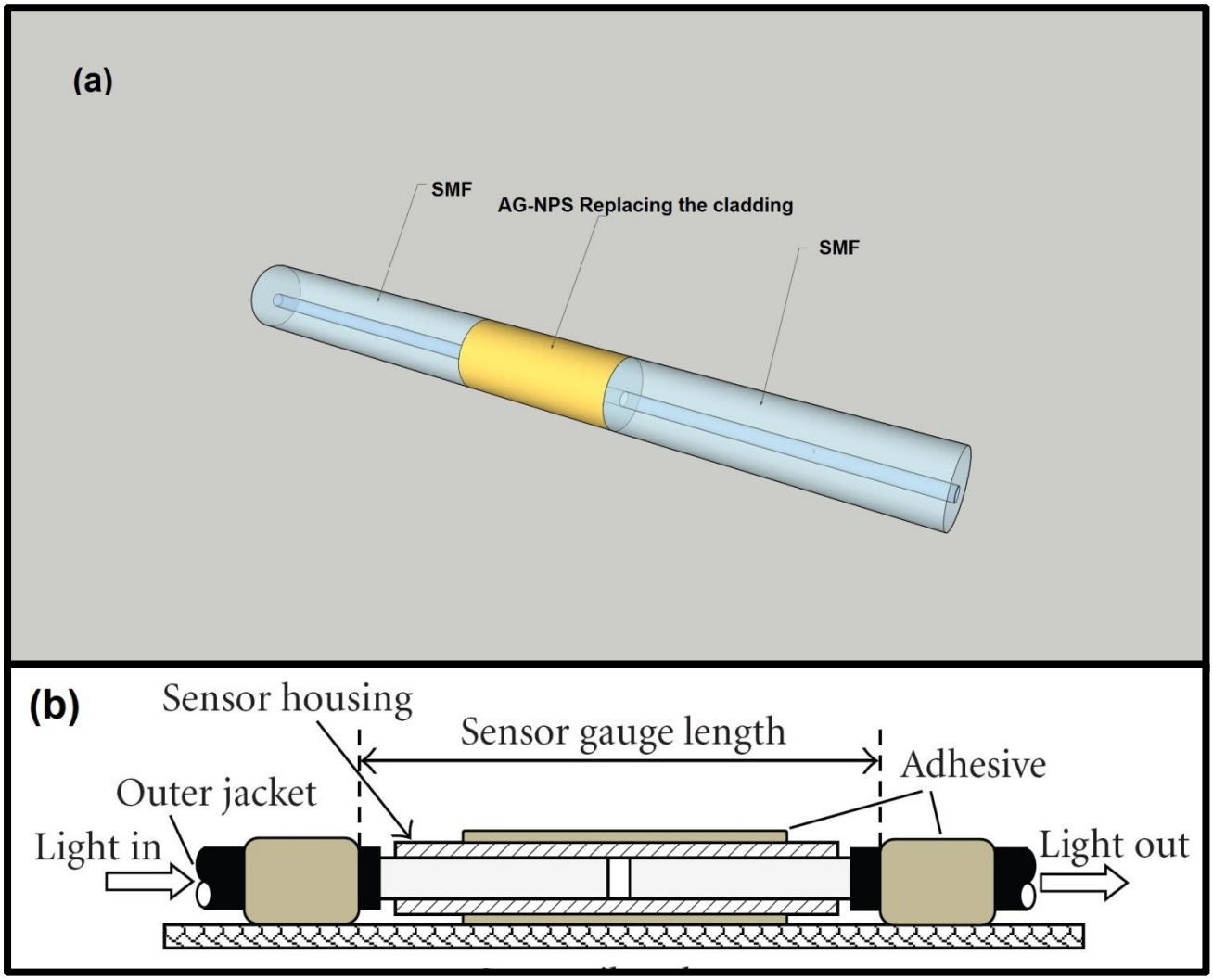

Figure(1.10): A schematic diagram of intensity modulated sensor for (a) temperature sensor and (b) displacement sensor [72,73]

1.10 Polarization modulated fiber sensors

The polarization direction of the electric field of an electromagnetic ray is known as the state of polarization. The classification of polarization types are linear, circular, and elliptical polarization states. In a linearly polarized light, the direction of the electric field follows a constant behavior on the same propagation line as light is

advancing from a point to another. While in elliptically polarized light, the direction of the electric field changes during the light propagation, plotting all the points in this state will constitute an elliptical shape. Exposing the fiber sensor to any kind of perturbations will induce a change in refractive indices. Accordingly, there is an induced variation in phase between various polarization directions. Fig.(1.11) shows a typical configuration for a polarization based fiber-optic sensor. Light can be polarized by a polarizer, a polarization maintaining fiber or a birefringence [74].

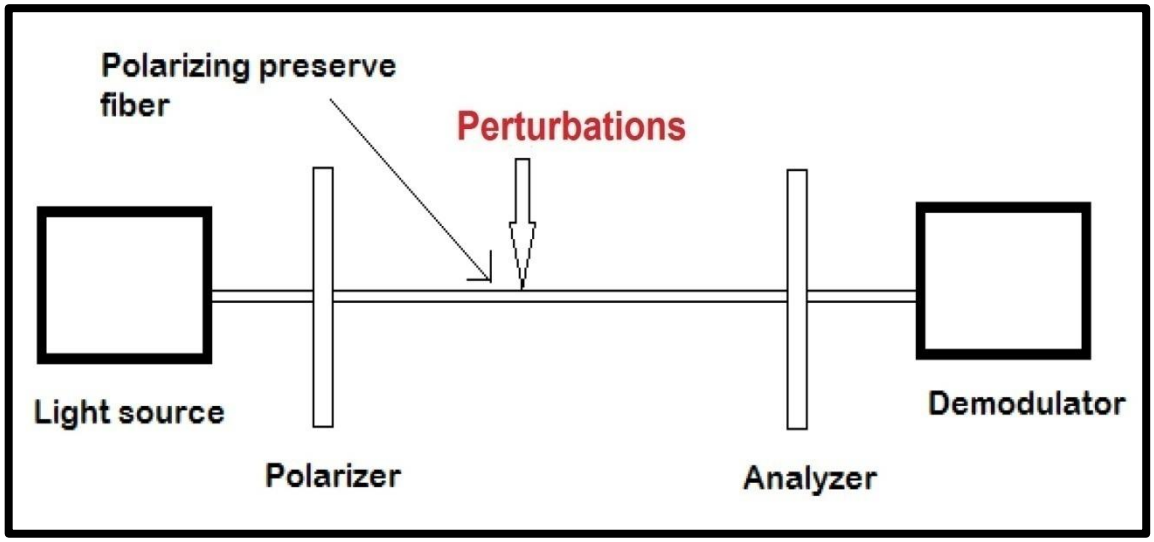

Figure(1.11): A schematic diagram of a typical polarization modulated fiber sensor [74]

1.11 Multimodal interference (MMI)

A multimode sensor needs a waveguide that allows multimodal propagation to observe multimodal interference phenomenon. This can be simply obtained in multimode fiber-optics. The MMI phenomenon has been greatly demonstrated in developing diverse OFSs. The mostly used sensing structure to obtain an MMI sensor is shown in Fig.(1.12).

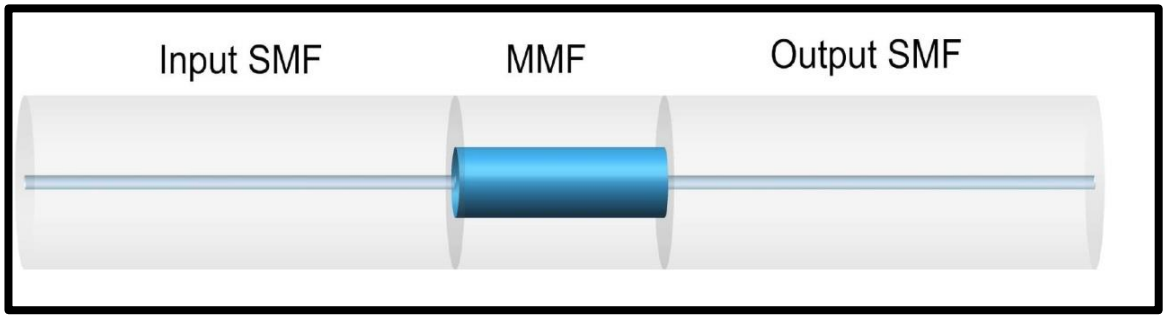

Figure(1.12): A schematic diagram of a convnentional MMI based sensor[75]

A traditional SMS fiber is made of a short segment MMF fused between a lead-in and a lead-out SMFs. The injected light-wave is guided via the lead-in SMF into the MMF section and propagates through the MMF core. Some modes emerge out as evanescent wave to interact with the external media. As a result, a sensitive structure to the ambient state variations [76].An important statement to mention is that, the complete dependence is on the structure. Accordingly, if no evanescent wave leakage of the SMS structure occurs to the surrounding medium, no sensitivity to any measurand will be obtained. OFSs relying on MMI phenomenon been studied for decades now, the concepts, basics, and operation principles to govern the mathematical equations is expressed in [77, 78].

1.12 Temperature sensor for biomechanical and biomedical applications

Biomechanics is the science that studies the mechanics that is utilized by living creatures with exceptional emphasis on human body. It is a quantitative subspecialty referring to the devices that are required to assess a broad-variety of physical parameters [79].Optical sensors can be encapsulated or enclosed in surgical operations, metallic tubes, catheters, or even needles. OFSs been increasingly utilized during invasive procedures [80-82].These sensors are preferred as no risks of electrical shock because they purely operate by light-wave [83-84]. Thus, they are safer to be used intrinsically in mammals or humans. The remote sensing capabilities enable researchers in biomechanics to study deep sea creatures as well. An OFS is able to operate as a transceiver by pushing a larger amount of data to a long distance [85,86]. In dental medicine OFSs are successfully presented to evaluate temperature and strain in dental splints before and post to disposition within oral cavity [87-88]. Bone-cements are very important in implant fixations and prostheses. Their stability in a long term manner is critical in joint-biomechanics. Temperature and strain characterization employing PMMA-manufactured bone-cements for femoral prostheses is successfully achieved at various loads and temperatures using OFSs [89].

1.13 Operation principle of the tapered polymer-coated temperature sensor TSNS-PC

The TSNS-PC fiber structure is created by fusing a part of NCF amongst dual fibers of standard single mode. As the fundamental core mode advances from lead-in single mode fiber (SMF) and reaches the first tapered region, higher order modes are excited. These modes will advance in the NCF suffering many reflections then re-couple in the second taper, they continue the propagation to the lead-out SMF constituting an interferometric pattern based on MZI. Since the taper can be attained via a fusion splicer, the formed taper shape can flexibly be designed by adjusting arc-current, arc- time, and arc-power. This fact facilitates obtaining different coupling constants from the lead-in SMF to the NCF section, consequently, an adjustable design of the sensor structure [90]. The TSNS-PC fiber sensor is a typical SMS design where the no-core fiber (NCF) lays amongst two optically aligned single-mode fibers (SMFs). The NCF segment and its protective polymer coating signify the multimodal waveguide core and the correlated cladding, respectively. The easiest way to examine the principles of MMI impacts in fiber-optics can be maintained by fusion splicing an SMF straightly with a step-indexed type MMF. As light-wave is conjoined into the MMF, the input domain could be disintegrated into guided modes. The proportionate spectral shift induced by temperature variance can be given as [91]

$$\frac{\Delta\lambda a}{\lambda} = (\alpha a+\xi a)\,\Delta T\,, \qquad (1.1)$$

Where αa and ξa are, respectively, coefficient of thermal expansion (CTE) and thermo-optic coefficient (TOC) of the NCF material. If the polymer coating was stripped-off, according to equation (1.1), temperature rise would allow the interference dip location to move linearly to longer wavelengths (red-shift), and the thermal sensitivity would purely be dependent on the specification of the NCF glass

material. The TSNS-PC fiber configuration; however, is also sensitive to the index of refraction variation of the protective acrylate coating which acts as a cladding in this case. Assuming the TOC of the acrylate polymer coating is ξb, the spectral shift introduced by the acrylate polymer coating index variations due to temperature rise can be addressed as [92].

$$\frac{\Delta\lambda b}{\lambda} = \rho\xi b\Delta T , \qquad (1.2)$$

Where ρ is a constant. When ξb is large negative, the impact of thermo-optic response of the protective polymer coating presents a negative sensation rate of temperature to the sensor. As the sensor is not strained the proportionate total wavelength shifting induced by the variation of temperature would be as in [92,93]

$$\Delta\lambda = \Delta\lambda a + \Delta\lambda b$$

$$= [(\alpha a+\xi a) + (\rho\xi b)]\Delta T \qquad (1.3)$$

The theoretical calculation of Eq. (1.3) can predict that the wavelength shift is dependent on both NCF glass and the polymer coating. Accordingly, the thermal sensitivity of the sensor is affected by the thermal properties of the NCF material and the polymer coating. For silica fibers, $\alpha a \approx 2.6 \times 10^{-6}$ /°C and $\xi a \approx 6.9 \times 10^{-6}$/°C. The factory made protective polymer coating (UV-curable acrylate) with a large negative TOC ≈ -4×10^{-4} retained in the fabrication of the temperature sensor, as (ρξb) term is a large negative value, (blue-shift) is expected [94,95].

1.14 Strain in a general definition

Geometric measure of material deformation in response to the relative dislocation among atoms or terms of recovery to the original shape is called strain. It can be classified into two types: elastic and plastic. An external load or constrains usually is the cause. Elastic strain is usually refers to the state where the material will recover

its original shape after the cancelation of the external effecting load. Whereas in plastic-strain the material suffers a permanent deformation even if the external constrain is no more [96].Stress-strain diagram of a polymer optical fiber is given in Fig.(1.13).

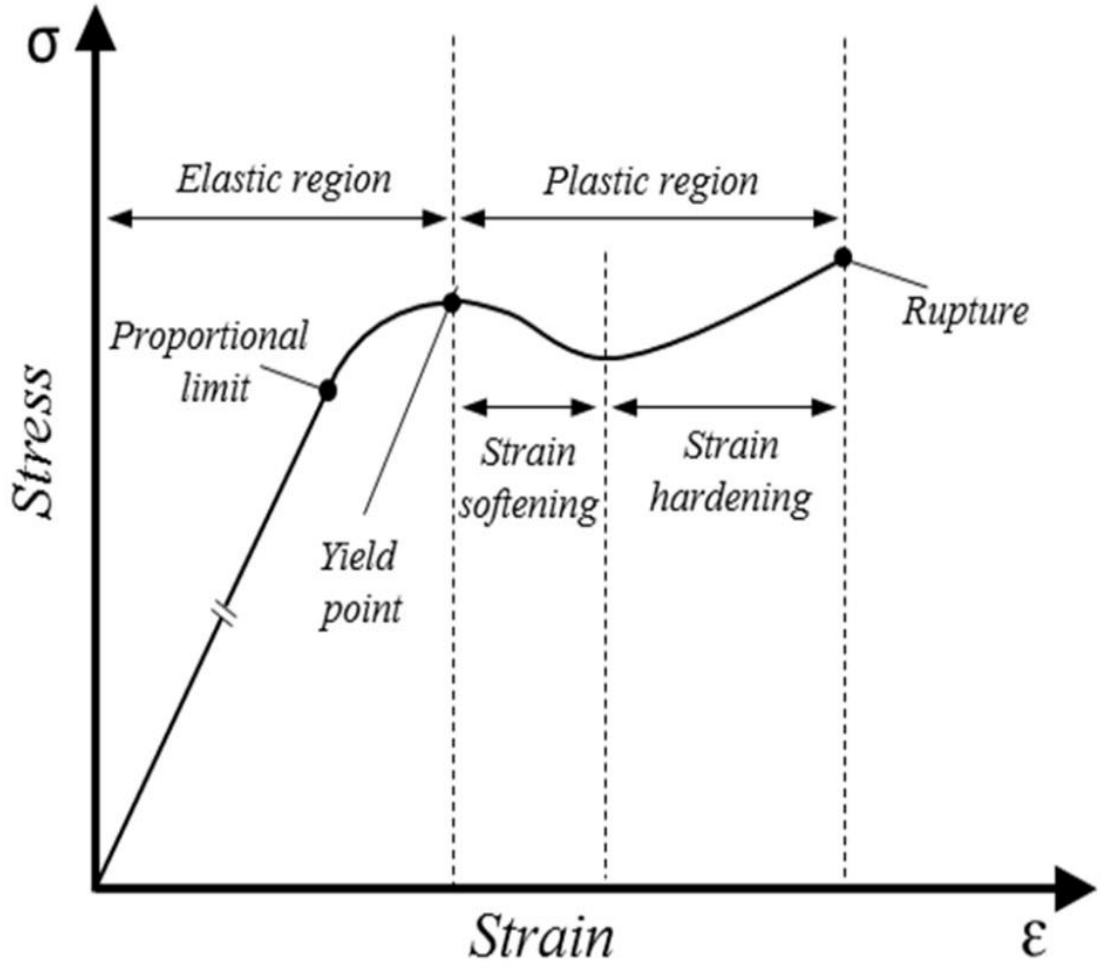

Figure(1.13):Stress-strain diagram of polymer optical fiber [97]

1.15 The effect of strain on optical fibers

Optical fibers are sensitive to changes in length and in the RI, they reveal sensitivity to small changes in length as little as few picometers (pm).The fact behind this sensitivity is derived from the variation of the optical path variance of different traveling modes along the fiber in response to tensile force. When Axial force applied to the fiber photoelastic effect leads to RI variation, by understanding this phenomenon fiber strain sensors can be developed .In an SMS structure, optimal

length selection is influential to the pattern of the MMI dip and the sensitivity. Most optical fibers are made of silica which exhibits negligible elasticity owing glass is a brittle material by nature. Accordingly, optical fiber strain sensors must be designed to withstand the applied extension to prevent failure .The majority of fiber strain sensors operate in the range of 0-1000 μm and minority strain sensors operate in the ranges beyond 1200 μm [98].

Micro strain can be calculated as [99]

$$\Delta\mu\varepsilon = \frac{\Delta L}{L} \times 10^6 \qquad (1.4)$$

Where $\Delta\mu\varepsilon$ is the value of strain in μm, ΔL is the variation of length of the sensor, and L is the initial length.

1.16 Micromechanical sensors

Mechanical sensors represent a type of sensors that exhibit sensitivity to variations in mechanical characteristics. Along with the micromachining technology, micromechanical sensors such as microcantilevers [100], thermistors [101], and acoustic sensors [102] have been playing an important role in micro-size detection and micro-sensing applications. In the majority of micromechanical sensors, there are two general strategies: by detecting stresses (or strains) induced on the cantilever (or membrane) surface, or by detecting the change in resonant frequency of a mass-spring system. There is a long history of piezoelectric and piezoresistive phenomenon being used in transduction schemes allowing for extremely sensitive response to deflection or mass change.

Micromechanical sensors can cover a broad range of sensors to cover a wide variety of application which might be beyond the concentration scope of this thesis however, micromechanical sensors have been used to replace the bulky mechanical sensors such as those of micro electromechanical systems MEMS and in robotics [103,104].

In the field of micromechanical sensors, the microcantilevers, the acoustic wave and the, micro thermistors have been dominating the field of research. There still are large

numbers of these sensors utilized in various applications and cannot be replaced by optical fiber sensors.

1.16.1 Temperature micromechanical sensors and their applications

Many types of thermal sensors transduce a thermal signal directly into electrical signals. Such types of sensors include thermocouples, thermistors, and transistors. Other types of thermal sensors convert a temperature change into mechanical deflection that can be transduced into an electrical signal such as microcantilevers [105].

A bilayer cantilever is one of the best well-known micromechanical sensors, it consists of two layers of different materials. The temperature is found by measuring the deflection of the cantilever, the micro deflection is induced from the different thermal expansion coefficients of the top film and the probe body. If a piezoelectric material is a part of the bi-material cantilever, the deflection will result in a measurable voltage produced. These cantilevers are also useful in the application of actuators. Let us consider a bilayer cantilever where a thin film is deposited on a relatively thick cantilever body to form bilayers. If the temperature and the thermal expansion coefficients of the two materials are known, the thermal deflection can be found .microcantilevers are used in actuators, climate control circuits and electronic circuits [106-108].

CMOS (complementary metal-oxide-semiconductor) sensors are devices fabricated by the standard silicon microfabrication process. CMOS is a standard of circuit design that is integrated into circuit chips,CMOS temperature sensors can be categorized as a special type of thermistor that uses silicon as the sensing material. Since the carrier concentration of silicon is dependent on the temperature, any type of electrical element integrated onto silicon including a resistor, a diode, and a transistor can be potentially utilized as a temperature sensor. The temperature can be found by measuring the temperature-dependent voltage-current (V-I) characteristics. Most CMOS temperature sensors are bipolar transistors. The base-emitter voltage and saturation current have good temperature characteristics. Temperature is determined

by the signals generated from the base-emitter voltage and the saturation current all the integration is done on the surface of a microchip, making it not only extremely portable but also mass producible. CMOS is used in cellphones, laptop computers and electronic devices [109,110].

1.16. Strain micromechanical sensors and their applications

A piezoresistive material is a type of material that changes its electrical resistivity as a result of mechanical stress. Semiconductors usually show piezoresistivity that can be used for strain gauges. Doped silicon exhibits a strong piezoresistive effect in which the resistance of the doped region changes reliably when it experiences a stress due to deflection. Therefore, piezoresistive cantilever sensors are usually constructed of doped silicon. Piezoresistive elements are embedded at the top surface where the largest strain is induced. The method of sensing the cantilever deflection in AFM imaging by integrating piezoresistors on the cantilever was initially developed by two groups: Tortonese et al. at Stanford University in 1993 and Rangelow et al. at Kassel University in 1995 [111,112].

In addition to strain gauges, various applications use piezoresistive microcantilevers such as; commercial accelerometers, force sensors, pressure sensors, and torque sensors. [113-115].

1.17 Literature survey

In the past few years, numerous researches have been conducted to developed temperature and strain sensors based on NCF and MMI phenomenon. Each research represents a unique structure and a different experimental setup. The trials to achieve the best sensitivity were either by modifying existed structures or designing novel ones. To compare the obtained sensitivities in both sensors, the present work is listed in contrast to a short survey which contains some recently reported achievements in both temperature and strain fiber sensing systems. Table (1.2), and Table (1.3) respectively.

Table.(1.2) A summary of recently reported temperature sensors

C. Author	Year	Sensor structure	Range°C	Sensitivity pmC^{-1}	Ref.
Lin MA et al.	2015	SMF-NCF-SMF	30-100	38.7	[116]
Vanita Bhardwaj et al.	2016	SMF-Silicone rubber-coated NCF-SMF-tapered SMF	30-75	253.75	[117]
Jui-Ming Hsu et al.	2016	SMF- NCF-taper-SMF	20-60	1560	[118]
Jia Zhenan et. al	2017	SMF-tapered MMF-SMF	30-80	41	[119]
Tianmin Zhou et al.	2018	double tapered SMF ethanol coated	24-38	-900	[120]
Yun-Cheng Liao et al.	2019	double macro-tapered SMFs	89-950	113	[121]
D. A. May-Arrioja et al.	2020	SMF-NCF-SMF Eythanol-glycole	20-80	444	[122]
Jie Dong et al.	2020	Symmetrical double groove SMFs	20-90	230	[123]
Qingzhuo Wang et al.	2020	SMF-tapered TCF-SMF	25-80	65	[124]
Fang W. et al.	2020	SMF- tapered folded NCF-SMF	20-90	59.8	[125]
S. K. Al-Hayali et al.	2020	SMF-NCF-SMF nano coated CuO-PVA	25-235	101	[126]
Mohammad M. et al.	**Present work**	**Tapered SMF-NCF-SMF**	**30-45**	**-1943**	

Table.(1.3) A summary of recently reported strain sensors

C. Author	Year	Sensor structure	Range με	Sensitivity pm $με^{-1}$	Ref.
Zhi-bo Liu et al.	2014	SMF-NCF-SMF	0-730	-2	[127]
Lin Ma et al.	2014	SMF-NCF-SMF	0-2600	-2.06	[128]
Ke Tian et al.	2017	SMF-MMF-FPI-MMF-SMF	0-1000	-2.6	[30]
Yuan Sun et al.	2017	SMF-twisted MMF-SMF	100-1000	-7	[129]
Chuanbiao Zhang et al.	2019	SMF-taperTCF-TCFtaper-SMF	0-841.5	6.11	[31]
Fan Yang et al.	2018	SMF-MMF-PCF-SMF	0-1724	-14.89	[32]
S.-C. Yan et al.	2020	Double S taper -offset SMF	0-800	-6.63	[130]
Leigang Dong et al.	2020	SMF-THCF-SMF	0-2100	2.7	[131]
Shuo Zhang et al.	2020	SMF-LCMMF-SMF	0-1200	-10.10	[132]
Yu Wang	2020	SMF-HCBG-FPI-SMF	0-1389	2.02	[133]
Mohammad M. et al.	**Present work**	**SMF-NCF-SMF**	**0-1000**	**-16.37**	

1.18 Aim of work

In the present work, the intention is to achieve the following goals:-

1- Designing and fabricating an SNS-PC temperature sensor.

2- Improving the sensitivity via tapering effect.

3- Studying the intensity behavior with temperature variation in the SNS-PC and TSNS-PC temperature sensors.

4- Designing and fabricating an SNS strain sensor.

5-Investigating the temperature crosstalk in the SNS strain sensor.

6-Examining the influence of NCF length on strain sensitivity in the SNS strain sensor.

Chapter Two

Experimental Tools & Setup

2.1 Introduction

In this chapter, the double tapered single-mode -no-core-fiber-single-mode polymer coated temperature sensor TSNS-PC, and single-mode-no-core fiber-single mode strain sensor design and fabrication is explained in details. The working mechanism, simplicity of design and the key points of improving the sensitivity are listed. The optimal length selection for both temperature sensor and strain sensor are explained in details as well .As both sensors rely on multimodal interference phenomenon, the operation principles of both sensors are similar except of the testing parameters are different. The temperature sensor is fabricated by fusion splicing a part of NCF between a couple SMFs, and then tapers are induced in the splicing joints. The UV-curable acrylate coating is not removed on the NCF sensing segment to improve temperature response .In the strain sensor a segment of NCF is fused between two SMFs. The polymer coating is removed to reduce temperature influence on the strain sensor, this will minimize temperature cross sensitivity. A walkthrough to select the optimum length by studying the transmission spectra characteristics for both sensors is explained as well. All necessary tools and devices that used in the experiments are listed and explained in details. The experiments conducted in the photonics lab of institute of laser for postgraduate studies. A simple chart of chapter two is illustrated in Fig.(2.1)

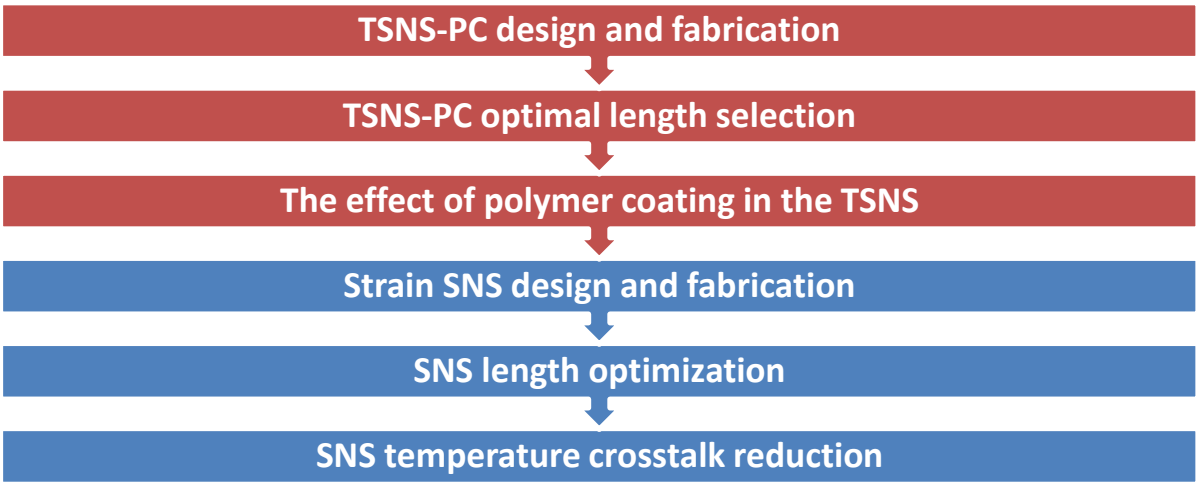

Figure(2.1): Chapter two summerization chart

2.2 Temperature sensor experimental setup

The experimental setup of the tapered interferometric sensor based on NCF is illustrated in Fig.(2.2). The information of every single part utilized in the setup is explained in details in the coming subsections.

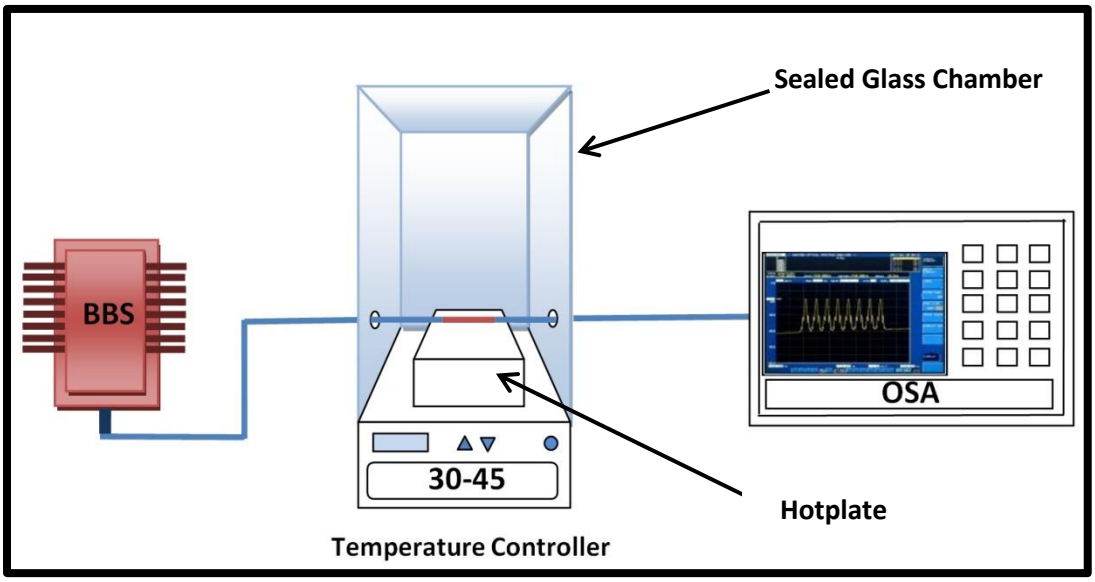

Figure(2.2): Experimental setup of TSNS-PC sensor

2.2.1 Optical spectrum analyzer (OSA)

Optical spectrum analyzers (OSA) are instruments that measure the optical power as a function of wavelength or frequency. These devices can operate over a specific range of wavelengths or frequencies, usually the x-axis represents the wavelength and the y-axis refers to the optical power. In this experiment, the utilized OSA is (Yokogawa,AQ6370) , the specifications of the device can be summarized as follow :

- The range of wavelength is 600-1700 nm.
- The accuracy of the wavelength is ±0.01 nm.
- The wavelength resolution is 0.02 nm.
- Dynamic range 78 dB.
- Power level range - 90 to +20 dBm.
- Measurement time 0.2 sec at 100 nm span.
- Operates on both SMF and MMF.

2.2.2 Super luminescent diode broadband source (BBS)

A butterfly-packaged super-luminescent diodes (Thorlabs SLD1550S-A1) operating in the range of 1450-1650 nm spectra is used as a broadband infrared source (BBS). The output spectrum of the BBS has a near Gaussian profile with a slight ripple. It consists of a current controller, an integrated circuit chip with a 14-pin butterfly package along with a thermoelectric cooler and a thermostat to dissipate heat for a stable output light. The integrated circuit is situated on the thermoelectric cooler via a sub-mount (heat sink) that has a high thermal conduction capability to push heat away from this chip as much as possible. The device has an optical coupling setup to couple the infrared beam to the optical fiber; the output connector is a SMF pigtail of 1m length terminated with an FC/APC connector. [Appendices A, B, and C].

2.2.3 No-core fiber (NCF)

The special structural property of no-core fiber (NCF) has broadened the sensing applications based on multimodal interference self-imaging, evanescent wave absorption and materials coating. NCFs extensively used in measuring various physical, chemical and biological parameters, presented to confirm the potential value of NCF-based sensors in bio-sensing.

In this experiment (Thorlabs FG120LA) NCF with Ø125 µm is utilized, this variant of MMF has an outer diameter that is equal to the cladding diameter of standard SMF-28 fiber, all specifications of this optical fiber is specified in[Appendix D]

2.2.4 Sealed glass chamber and hotplate

A sealed cube-like glass chamber is used as a thermal isolator in the experiment. The usage of this chamber is to provide a stable thermal environment to the sensor. This prevents any possible result alteration due to outside temperature. The heat source in the experiment was a digital hotplate temperature (SH-4C digital magnetic

stirrer hot plate) controller with maximum heating power of 600 watt. The upper temperature limit of the hotplate is 350 Cº

2.2.5 Single-mode fiber specifications (SMF)

Standard SMF which is the key component in optical fiber communication is used to couple both ends of the NCF to the OSA and the BBS in the present experiment. Corning SMF-28 most common operation windows are 1310 nm and 1550 nm which used in telecom synchronous digital hierarchy SDH and dense wavelength division multiplexing DWDM systems, respectively. It can push a large amount of data for long distances with a lower vulnerability to attenuation and dispersion, Table (2.1) highlights the most important specifications of a standard Corning SMF-28.

Table (2.1): Optical Specs of Corning (SMF-28) [Appendix E].

Maximum attenuation	
Wavelength (nm)	Value dB/km
1310	≤0.32
1550	≤0.18
Dispersion	
Wavelength (nm)	Value ps/(nm.km)
1550	≤0.18
1625	≤0.22
Attenuation vs. wavelength	
Wavelength (nm)	Value dB/km
1285-1330	0.03
1525-1575	0.02

2.3 Tapered single-mode-no-core fiber-single-mode polymer-coated temperature sensor TSNS-PC

An illustrative graph of the temperature sensor is depicted in Fig.(2.3).In the fabrication process of the temperature sensor a segment of NCF (FG125LA by Thorlabs) with 125 μm glass diameter retaining its acrylate polymer coating of 62.5

μm thickness cleaved and spliced between two (Corning SMF-28) pigtails . A set of parameters were configured using a fusion splicer (SWIFT KF4, America Ilsintech). The fusion splicing parameters are listed in Table (2.2). The taper lengths and waist diameters are L_1, L_2, $d_1$and d_2 and their dimensions are 462.592 μm, 464.884 μm, 90.782 μm, 86.269 μm, respectively. The retained polymer protective coating length is labeled *l*, and is ≈ 2.96 cm where Z_1=Z_2 ≈ 2 mm stripped of polymer from both ends of the NCF to enable fusion splicing with the single mode fibers.

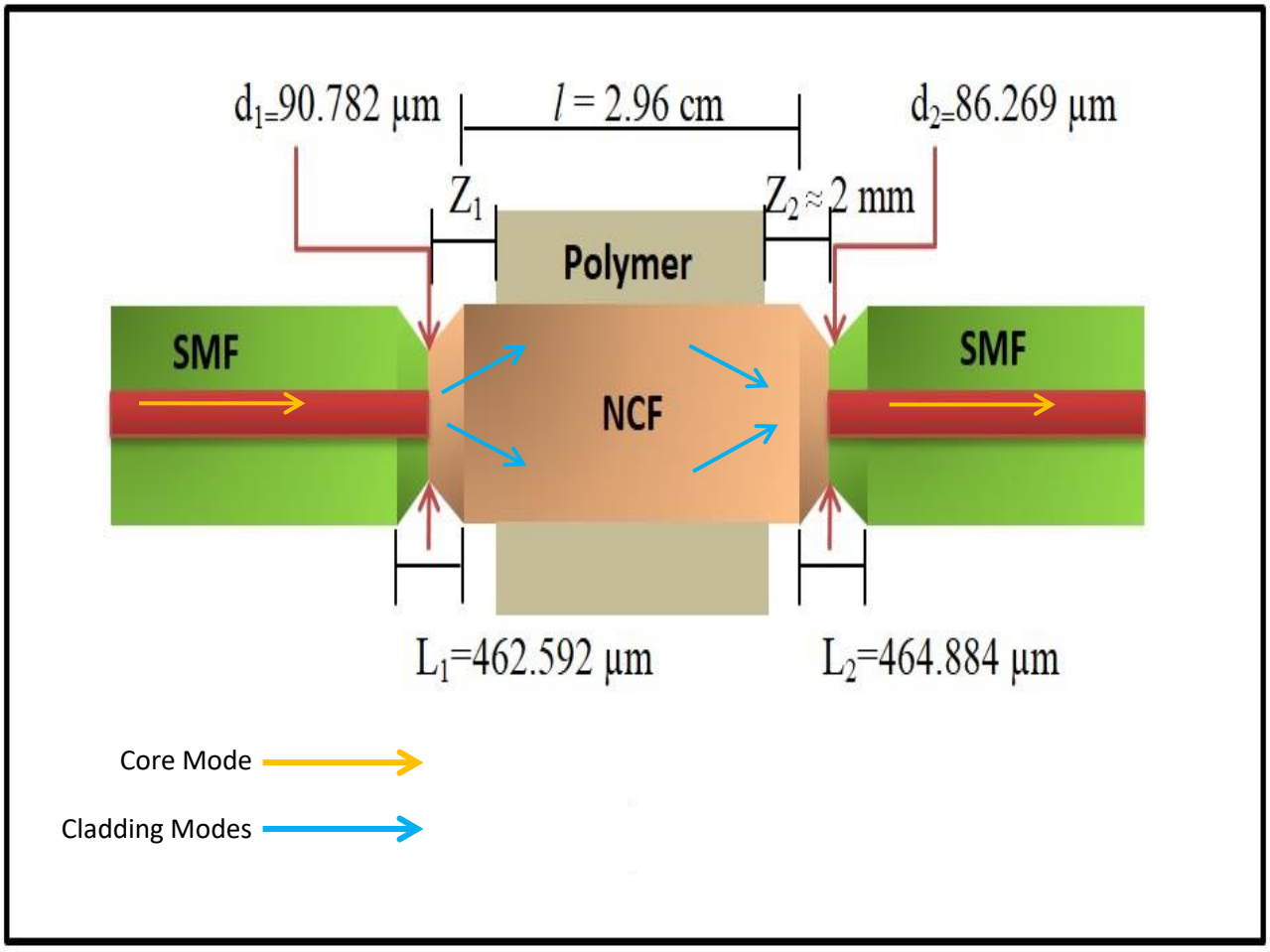

Figure (2.3): A schematic graph of the TSNS-PC temperature sensor

The tapering length and waist diameter were decided after a trial-and-error procedure. Reduced taper waist below 80 μm denoted to more optical intensity degradation in the transmission spectrum and a higher power loss. Accordingly, the tapering parameters were fixed for the best tapering waist and length as listed in Table (2.2).

Table.(2.2) Fusion splicing parameters for the tapered regions

Fiber Type	Proof test	Fiber angle limit	Gap(μm)	Arc current (bit)	Rearc time(ms)	Offset(dB)
MM-SM	on	1.0◦	18	125 ≈ 15.6 mA	1000	0.00

The tapers in the fabricated SNS-PC sensor were also examined via an optical microscope. The microscopic images were for confirming the homogeneity and non-existence of any distortion on the splicing joints.Non-smooth tapers if exist can greatly affect the coupling efficiency and alter the results. Fig.(2.4) shows the microscopic images for both tapers , the magnification power used to take the images is 40 X.

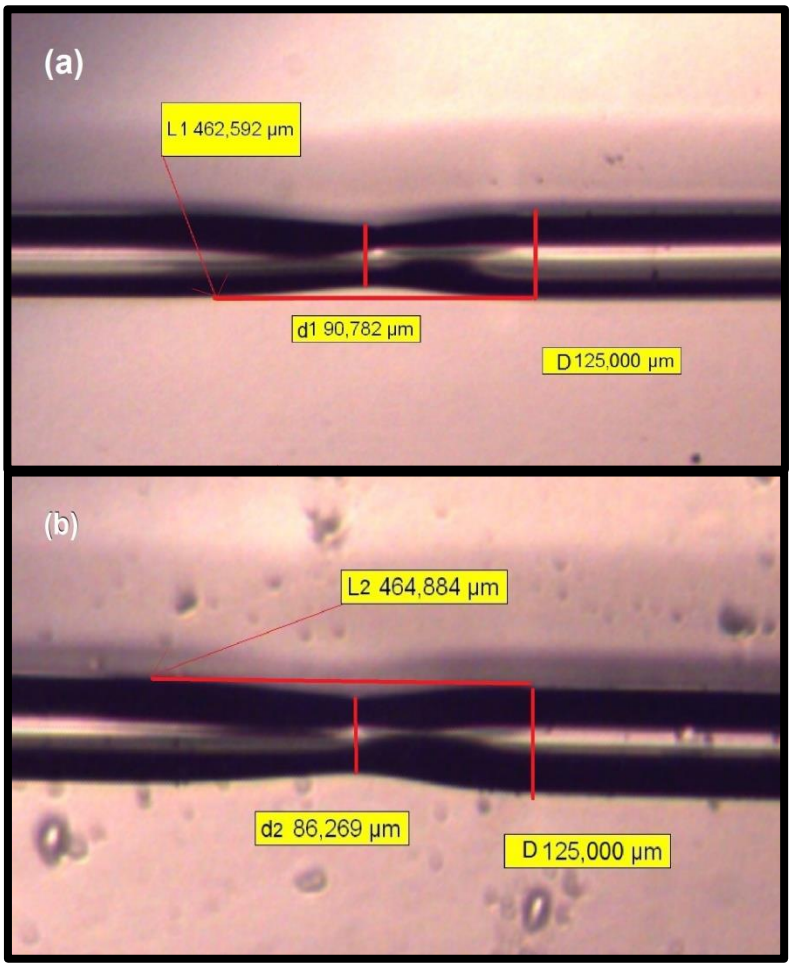

Figure (2.4): Microscopic images of the tapered joints 40 X (a) first taper (b) second taper

2.4 Length optimization and transmission spectra study of the temperature sensor

In pursuance of the optimal length selection for the temperature sensor, the spectra of transmission for the three varying NCF lengths investigated 2 cm, 3 cm and 4 cm for both tapered and untapered splicing joints. From Fig.(2.5)(a-b) it can be seen that for 2 cm length, resonance dips are virtually imperceptible with relatively small extinction ratio. This can be due to less signal coupling into higher order modes and more optical power in the fundamental mode. As the length is increased to 4 cm, more than two interference dips were observed with good extinction ratios, however the dips were either overlapping or adjacent, forming interference patterns which are obvious but undistinguishable. This might be due to the significant optical power loss because of the variance in optical path lengths of different propagating modes along the NCF length. Furthermore, at 3 cm length, one interference dip was observed in the untapered SNS-PC with a reasonable extinction ratio 16.3 dB, while two dips were observed in the TSNS-PC at extinction ratio of 23.8 dB for the first dip.

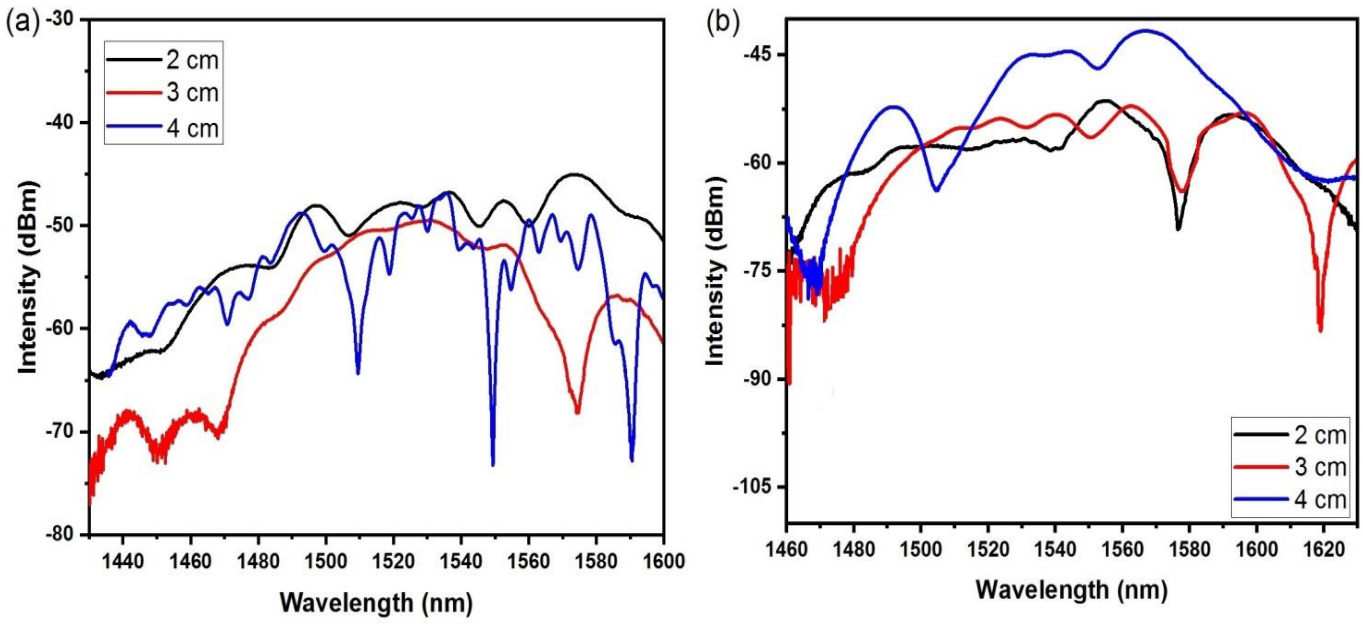

Figure (2.5): Spectra of transmission of the SNS-PC sensor at varying lengths: (a) without tapering, (b) with tapering

For the second dip the extinction ratio was around 12.5 db. Both dips were followed up in the investigation process for sensitivity comparison. Thus, with 3 cm length tapered sensor, most advantageous interference minima were obtained as well as good extinction ratios. The spectral span between the dips for the untapered sensor was good as well as those of the tapered sensor. The selected length is also advantageous as it is easily fabricated and can be repeated in few minutes in case of fracture. Unlike complicated structures which are both cost and time consuming, the proposed structure is easy to fabricate.

2.5 Strain sensor experimental setup

The experimental setup of the SNS strain sensor is depicted in the Fig.(2.6). A more detailed explanation about the fabrication method, utilized tools and the experimental setup is in the next sub-sections.

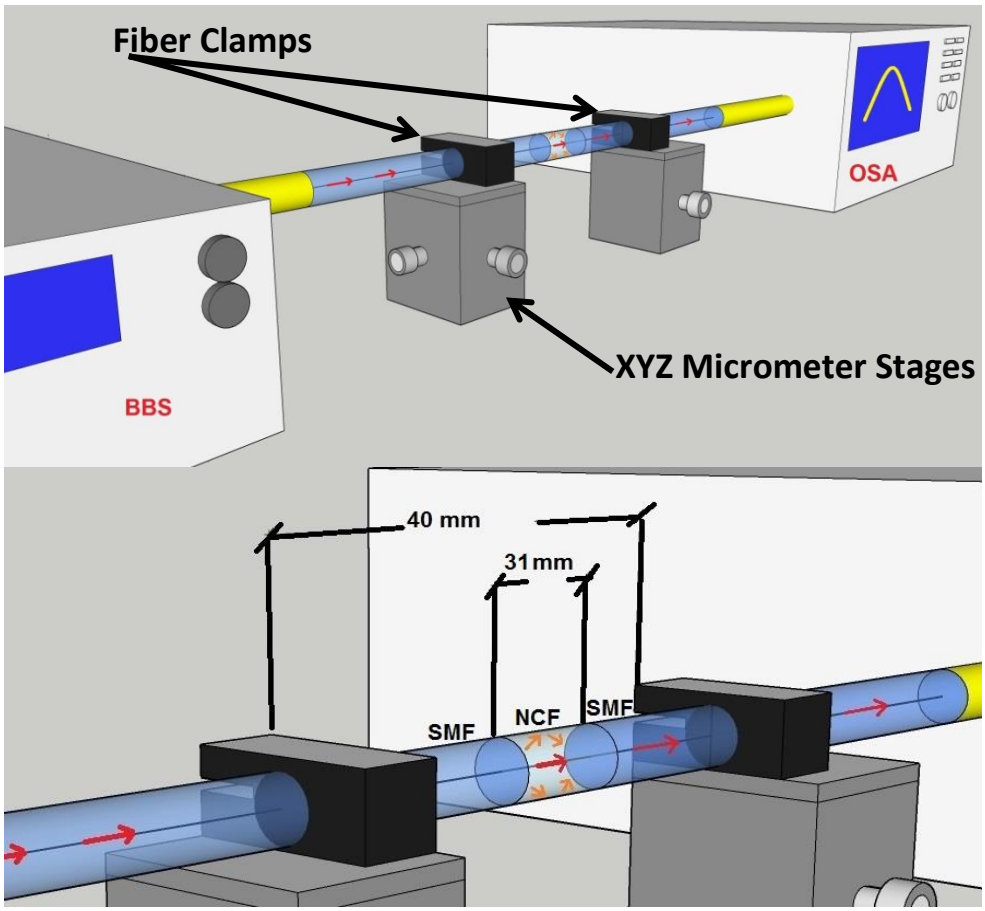

Figure (2.6): Experimental setup of SNS strain sensor

2.5.1 Optical fiber holders

In the strain sensing experiment, a pair of optical fiber grippers is used to hold tight the optical fiber sensor during applying axial tension. Thorlabs HFF003 Quick-Release Ø150 µm to Ø341 µm Fiber V-Groove for multi-axes stages can tightly grip optical fibers in the mentioned range. These special fiber holders do not exert fracture force to the fiber as the upper hold is made of polymeric rubber. The polymeric rubbers have a high friction coefficient to prevent slip. The HFF003 is a passive component and can be mounted to the X-Y-Z micrometer stage via various methods. The V-groove fiber holders are typically used to clamp fibers with the coating intact. The coating serves to protect the cladding of glass fibers from particulates that may land on the surface of the fiber, causing it to become brittle. Although this layer may also have optical properties that allow it to double as a second cladding, it is still referred to as the coating layer due to the protective properties. The term “buffer” is often used instead of “coating” when the layer surrounding the cladding is composed of (ethylene-tetrafluoroethylene) which commercially known as Tefzel.

These materials bonds differently to the glass cladding than other common coating materials, such as acrylate or TECS. Some fibers might also have an additional jacket, or buffer applied on top of the coating layer. [Appendix E].

2.5.2 Micrometer stages and optical alignment

Results alteration is common when bending occur in optical fiber sensors. Optical fibers are extremely sensitive to bend, this concludes why bend base interferometric sensor are developed. Bending in optical fiber as a general term is something undesirable, especially in communications. In this experiment, a pair of Newport; XYZ micrometer stages utilized to generate the driving tensile force. The advantages of using three-dimensional stages are to maintain alignment on all axes. In this experiment, a realistic strain inducing model is used. This is what makes this setup superior to recently fiber strain sensing setups. Many reported setups use one

micrometer stage and fix the other end of the fiber, which is considered one directional strain. In the present work, perfect alignment is maintained on all axes. Axial tension applied in x-direction inward and outward. No bending induced to the fiber during the experimental procedure, the tensile force is applied in steps.

2.6 SNS strain sensor fabrication

Prior to the fabrication process of the proposed SNS strain sensor, the length of the NCF segment is optimized according to the transmission spectrum study of the output signal. A detailed explanation about the length optimization is presented in the section 2.7. The schematic graph of the proposed SNS strain sensor is illustrated in Fig.(2.7)

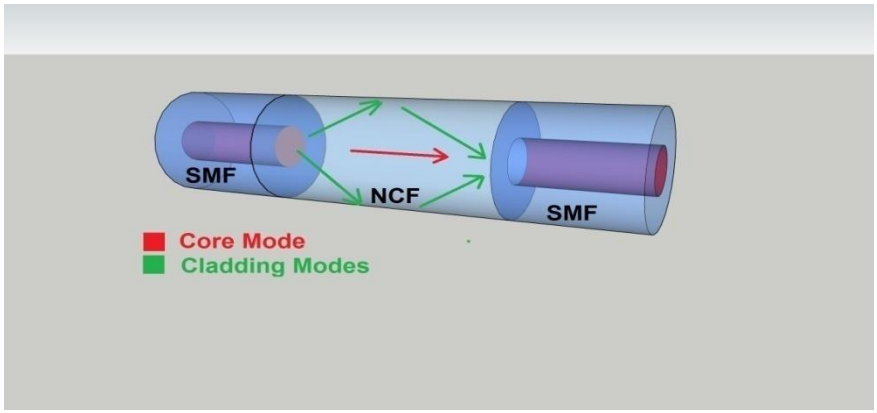

Figure (2.7): A schematic graph of SNS strain sensor

In the fabrication process of the SNS sensor, a piece of (Thorlabs, FG125LA) no-core fiber is fused between a couple of SMFs, the cladding diameter of the used NCF is 125 μm diameter. The outer diameter is equal to the outer diameter of standard SMF. The sensing fiber cleaved and spliced using (Fujikura, 60S) fusion splicer. The structure then mounted on a couple of (Thorlabs, HFF003) fiber holders, these holders are glued to a wood foundation which is fixed on two (Newport, XYZ micrometer stages) via screws, to maintain perfect structural rigidity.

Three dimensional alignment is crucial to avoid any possible bending that can alter the calculations. Accordingly, both Y and Z axes optically aligned to enable X-axis movements only .The front end of the SMF is coupled to an infrared broad-band source (Thorlabs SLD1550S-A1) and the other end is connected to an optical

spectrum analyzer (Yokogawa, AQ6370).The experimental procedure commenced by applying axial tension in steps of 100 μm per each side of the SNS sensor. The driving force is generated in both directions by rotating the X-axis lever on each micrometer stage by 100 μm in opposite direction. That makes the total count of one step equal to 200 μm. The zero strain length was equal to 40000 μm which is the initial distance between two fiber gripper's edges.

The resolution of the OSA is 20 pm and the wavelength range of the BBS is 1400-1600 nanometer .Laboratory images of the setup are illustrated in chapter three Fig.(3.8). In the fabrication of the strain sensor, the polymer coating removed to reduce temperature cross sensitivity. Polymers are known to have high negative thermo optic coefficient and a higher coefficient of thermal expansion coefficient than silica [134].

2.7 Length optimization and transmission spectra study of the strain sensor

The optimization of the strain sensor length is decided based on changing the sensing element's length and examining the corresponding transmission spectrum at zero strain. Length optimization is decided depending on two important interference spectrum criteria; the first in obtaining a single dip non saw shaped and has a good extinction ratio, or two non-adjacent dips with acceptable extinction ratios. Good spectral separation between multiple-dip sensors is crucial. The sensing lengths are selected from 20 mm to 40 mm with steps of 5 mm and ± 2mm as maximum error tolerance. Dips with small extinction ratios are non-favorable to be relied on in interferometric sensors, these dips can vanish or disappear promptly due to less interference energy. The transmission spectrum of various sensor lengths are illustrated in Fig.(2.8)(a-b). For the 21 mm sensor length the transmission spectrum revealed small dips that are ineligible to follow up. The 25 mm sensing head transmission spectrum revealed two adjacent dips with different extinction ratios which might overlap if shifting occur. Accordingly, both these sensing segments are excluded. At 31 mm length an interference dip is revealed at 1455.9 nm with 13.3 dB extinction ratio, this dip had good characteristics and been followed up. Accordingly,

this sensing length is kept in the follow up list. When the length is 35 mm two interference dips obtained at 1465.2 and 1533 nm with 19.23 dB and 14.1dB, respectively. This segment is also added to the follow up list for comparison purposes. Increasing the sensing segment to 40mm and above, denoted to the appearance of irregular saw shaped interference patterns in the transmission spectrum. Accordingly, the 40 mm and above NCF segments are excluded as well. The explanation of obtaining distorted dips beyond 40 mm is because of large optical signal degradation in the NCF sensing head due to increased length. From Eq.(2.3) theoretical calculations, the interference wavelength found to be 1455 nm at 31 mm sensor length which is close to the experimental results for the selected self-image number, R=3.As a result, the 31 mm length is confirmed theoretically and from transmission spectrum study to be the proposed sensing length .The proposed strain sensor is manifesting a simple Mach-Zehnder interferometer form. When light is injected from the first single-mode fiber and reach the first coupling interface, the single-mode-no-core fiber splicing point (SMFNCF) excitation of higher order modes is induced. The phase difference between different advancing modes in the (NCF) will give rise to interference phenomenon among various traveling modes at different phases and speeds known as multimodal interference (MMI).

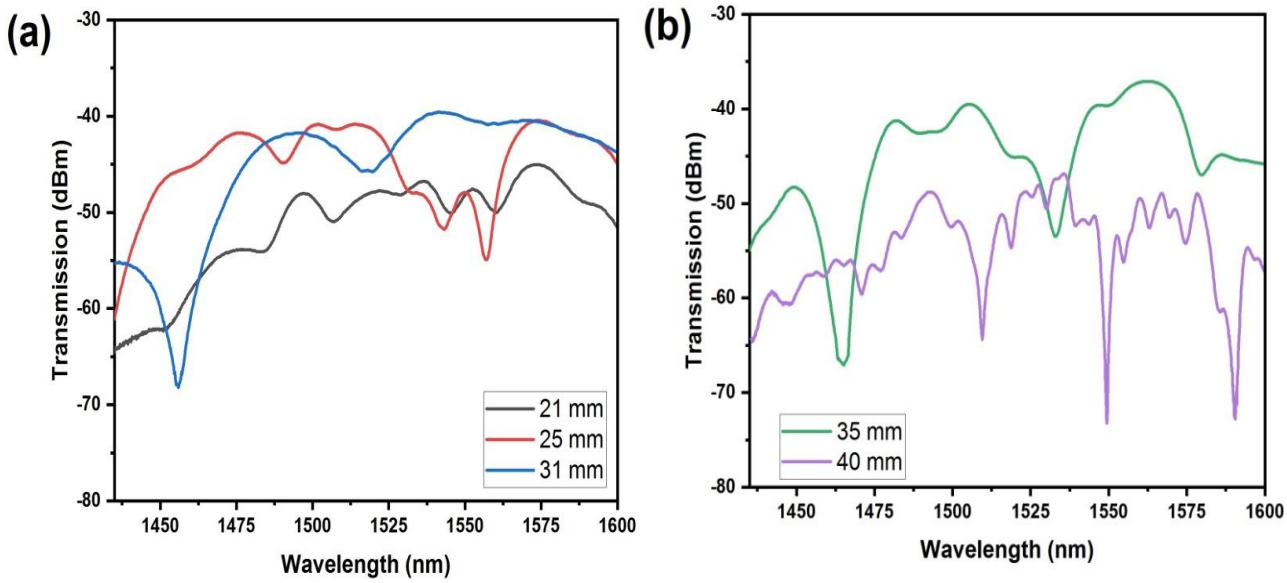

Figure(2.8):Transmission specrta of various strain sensor lengths

These propagating modes will eventually reach the second coupling interface which is the no-core fiber-single-mode fiber splicing point (NCFSMF).These modes undergo another re-couple and light will be ejected through the second (SMF)[135].

The interference between these different modes can be constructive which will constitute peaks in the output spectrum or destructive which will form dips in the output spectrum. According to the theory of multimodal interference the length of the sensing head NCF can be determined as in [136].

$$L = R\left(\frac{3L_b}{4}\right) \text{ with } R = 0,1,2,\ldots \qquad (2.1)$$

Where R is the self-image number and $L_{b\ is}$ equivalent to the length of the corresponding beat

$$L_b \cong \frac{4n_{NCF}D_{NCF}^2}{3\lambda_0} \qquad (2.2)$$

Where ^{n}NCF is equivalent to the index of refraction of the no-core fiber while ^{D}NCF is the diameter of the no-core fiber, and λ_0 is the free space wavelength. Merging the above equations , the free space wavelength can be determined via below equation.

$$\lambda_0 = R\left(\frac{n_{NCF}D_{NCF}^2}{L}\right), \text{ with } R = 0,1,2,\ldots \qquad (2.3)$$

Comparing the theoretical results with the experimental results, when $R=3$ agrees with the selected NCF length which is 31mm.

2.8 Temperature crosstalk analysis of SNS strain sensor

Temperature crosstalk is important to analyze in strain sensors, temperature cross-sensitivity examination setup is illustrated in Fig.(2.9). To investigate the influence of thermal effect on the strain sensor, the second SNS sensor was situated on the face of a hot-plate temperature controller. The structure is covered by a glass chamber, and then temperature rose from 20 °C to 70 °C in 10 °C steps, the temperature recordings taken each 10 minutes. The SMF ends connected again to the BB source and the OSA.

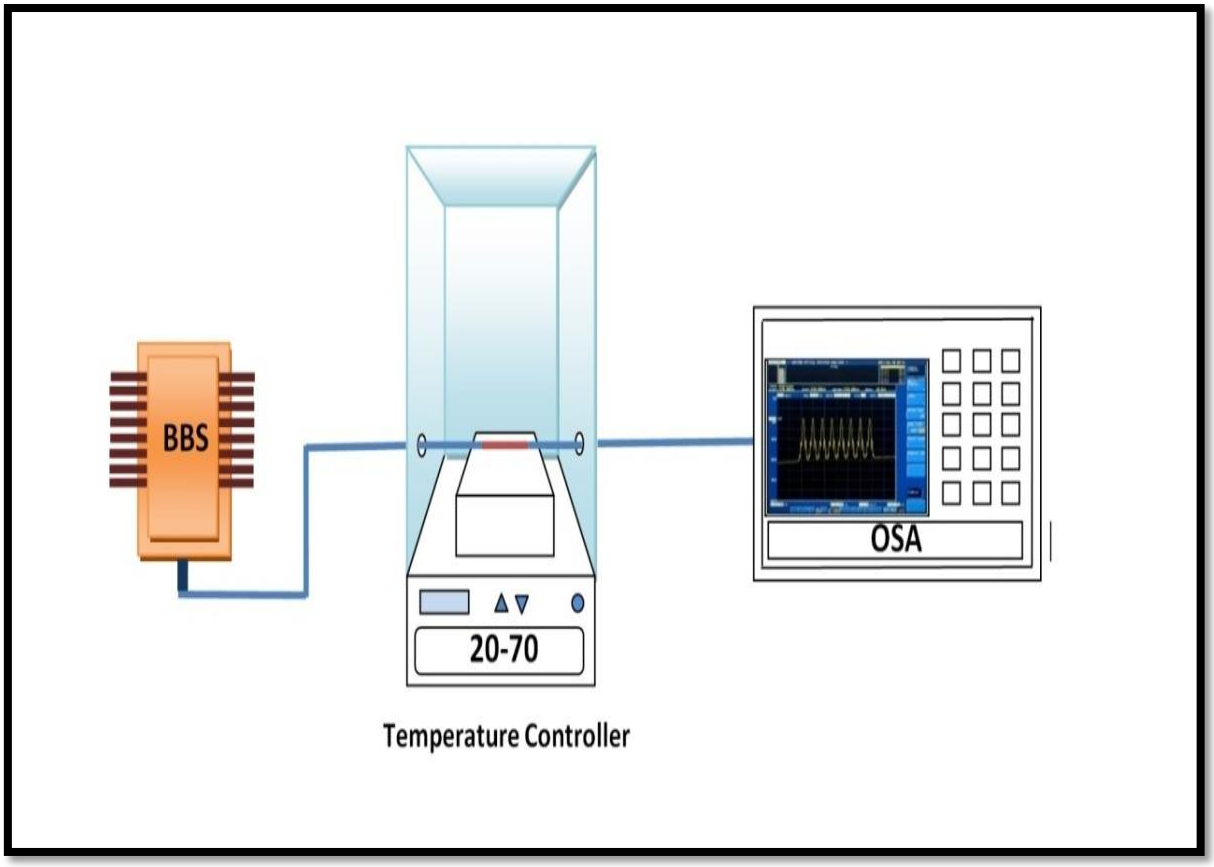

Figure(2.9):Temperature crosstalk investigation experimental setup

Chapter Three

Results & Discussion

3.1 Introduction

In this chapter, the investigations and the experimental results for both TSNS-PC temperature sensor and the SNS strain sensor are discussed. In the fabrication process of the temperature sensor, the transmission spectra for different sensing lengths of the SNS-PC and the TSNS-PC are examined. The optimal length was decided based on the specifications of the transmission spectrum. The experimental procedure carried out utilizing the OSA (Yokogawa AQ6360) and the BB source (Thorlabs SLD1550S-1).The factory made polymer coating is retained in the fabrication process for enhancing the temperature sensitivity. Acrylate polymer has a high CTE and higher negative TOC of which is approximately higher by two orders in magnitude as compared to that of bare silica. Post to selecting the optimum length and examining the temperature sensitivity of the SNS-PC. The TSNS-PC sensor with similar length of that of the untapered one is fabricated. The Induced tapers in the fusion splicing joints greatly improved the temperature sensitivity of about 53% as compared to the untapered temperature sensor. In the strain SNS sensor, the first consideration in the fabrication process was removing the polymer coating to reduce temperature sensitivity. Then the sensor length which is a crucial parameter is optimized based on theoretical calculation of self-imaging and practical experiments. The diameter of the NCF used in the strain SNS sensor structure kept constant; hence the varying parameter was the NCF length only. It’s a matter of fact that MMF based strain sensor’s sensitivity greatly depend on sensing segment length. All experiments conducted in the laboratory under standard conditions and performing safety precautions. Repeatability and reproducibility are also examined for both temperature and strain sensors. The temperature crosstalk is analyzed in the strain sensor. A schematic chart of chapter three summarization is depicted in Fig.(3.1)

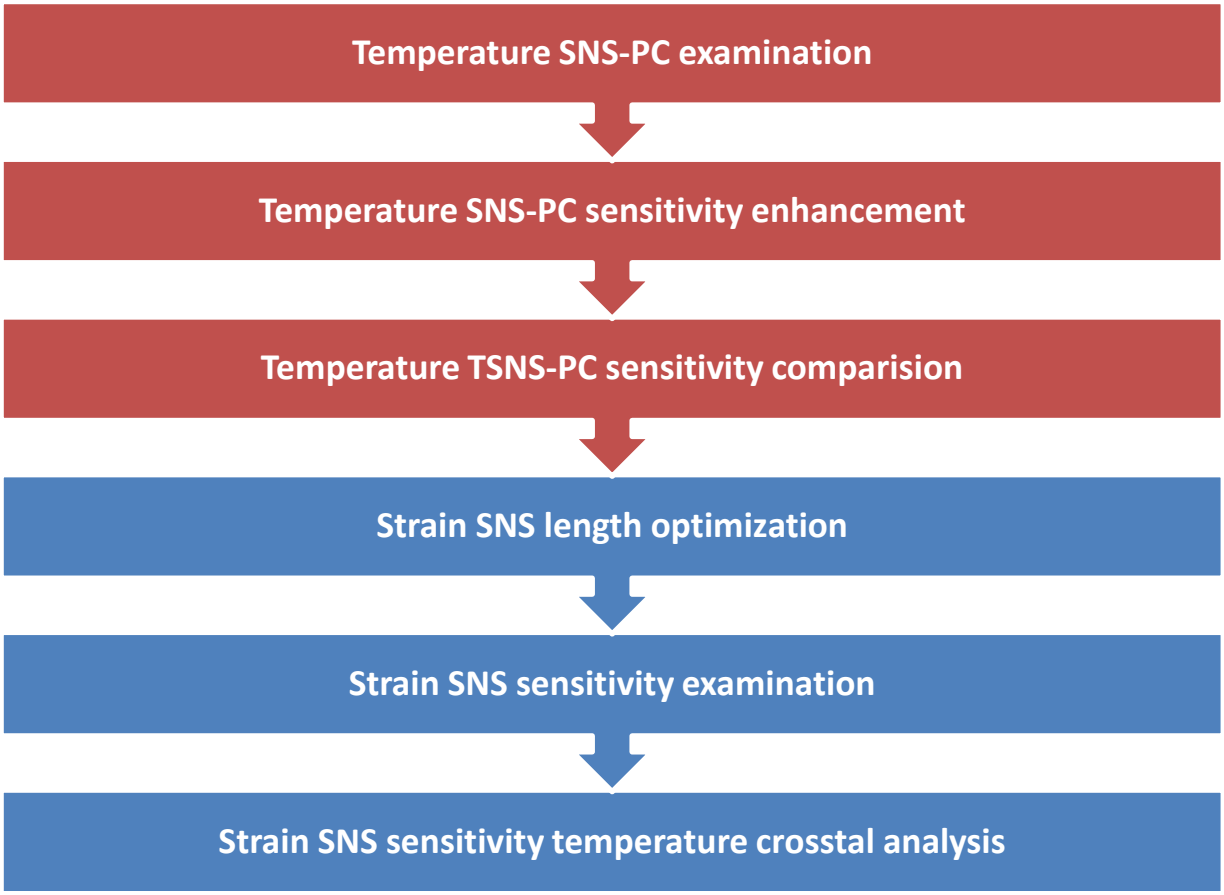

Figure(3.1):Chapter thee summerization

3.2 Results of SNS-PC and TSNS-PC temperature sensors

The fabrication of the temperature sensor is maintained via fusion splicing a segment of optimized length NCF between two SMFs, prior to this, the OSA was calibrated and maintained in a stable operational condition by one hour warm-up. The BB source was also tested on a standard SMF to inspect the operation status. The first structured temperature sensor was untapered, various transmission spectra of different lengths were examined. The exclusion of adjacent dips, saw shaped spectrum and small extinction ratio dips was carried out in some lengths. Small dips are unlikely to give precise readings as they can vanish promptly under different measuring conditions. Adjacent dips can overlap due to spectral shift which will prevent precise reading. Three dimensional schematic graph of the TSNS-PC sensor given in Fig.(3.2).

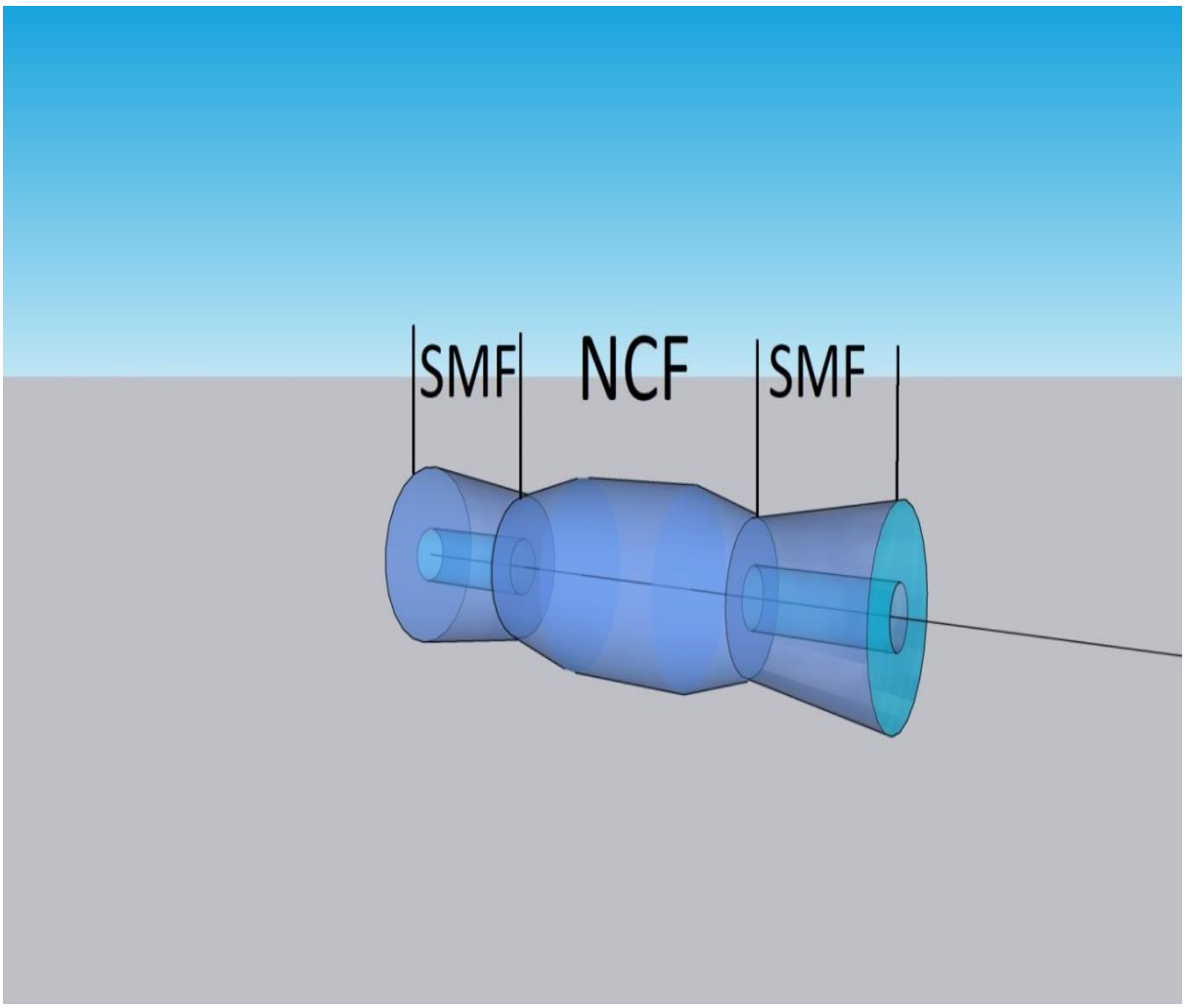

Figure(3.2):Three dimensional schematic graph of the TSNS-PC sensor

The first tested temperature sensor was the 3 cm length SNS-PC.The sensor is situated in direct touch to the outward area of a hot-plate without applying any tension to avoid strain. . Then the temperature is gradually increased from 30 ◦C to 45 ◦C step of 3 ◦C by an adjustable heat controller. The structure is covered by a sealed glass chamber. The selected temperature range covers several biomechanical and biomedical applications. The transmission spectrum of the un-tapered 3 cm NCF sensing head revealed interference minima at 1574.5 nm with around 16.3 dB extinction ratio. The spectral response of the un-tapered SNS-PC sensor is illustrated in Fig.(3.3)(a-b).The dip exhibits a shift toward shorter wavelengths with increasing temperature and exhibits a shift towards longer wavelengths with decreasing

temperature. Simultaneously, the optical intensity values decreased then increased with heating and cooling, sequentially. The wavelength response and the intensity response of untapered SNS-PC with increasing and decreasing temperature are given in Fig.(3.4)(a.b). Out of the obtained outcomes, the linear fitting graph of the spectral blue-shift and the intensity profile came out with a very good coefficient of linear regression. The values of R^2 for the spectral blue-shift and the corresponding intensity feedback were around 0.9985 and 0.9277, sequentially. The calculated spectral sensitivity and intensity slope were −1.2628 nm/ ◦C and 0.3178 dB/ ◦C, sequentially. The total wavelength shift induced by heating was around 19.2 nm. As indicated in the below graph, the wavelength shift induced by heating is heading towards shorter wavelength and the intensity linearly decreased in the untapered SNS-PC.The cooling cycle nearly exhibited an opposite behavior to the heating cycle which confirmed the steady behavior of the proposed temperature sensor in response to thermal effect.

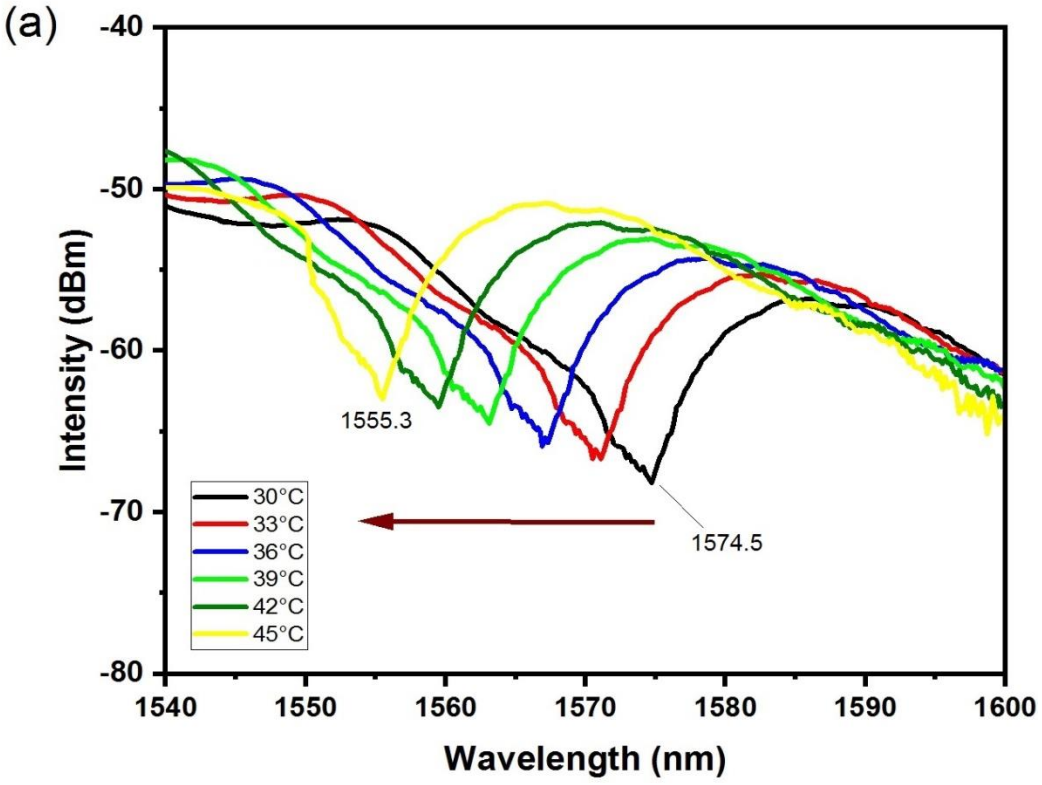

Figure(3.3)(a):Transmission spectrum of untapered SNS-PC sensor heating from 30-45◦C

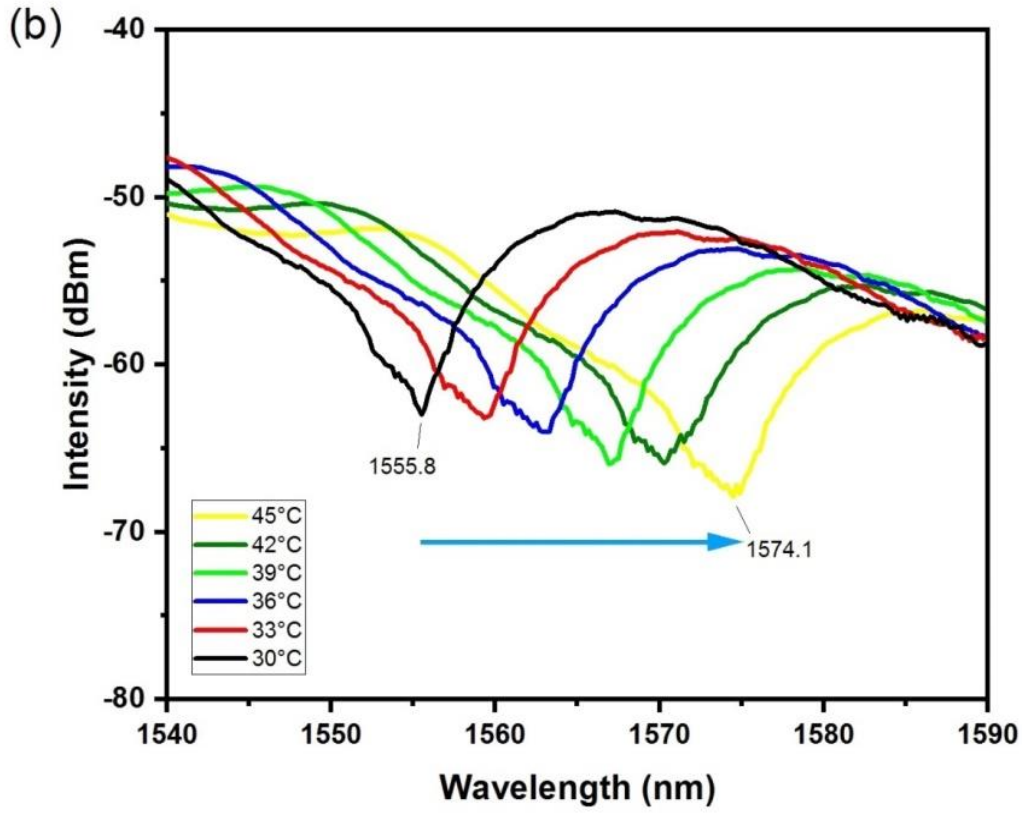

Figure(3.3)(b):Transmission spectrum of untapered SNS-PC sensor cooling from 45-30◦C

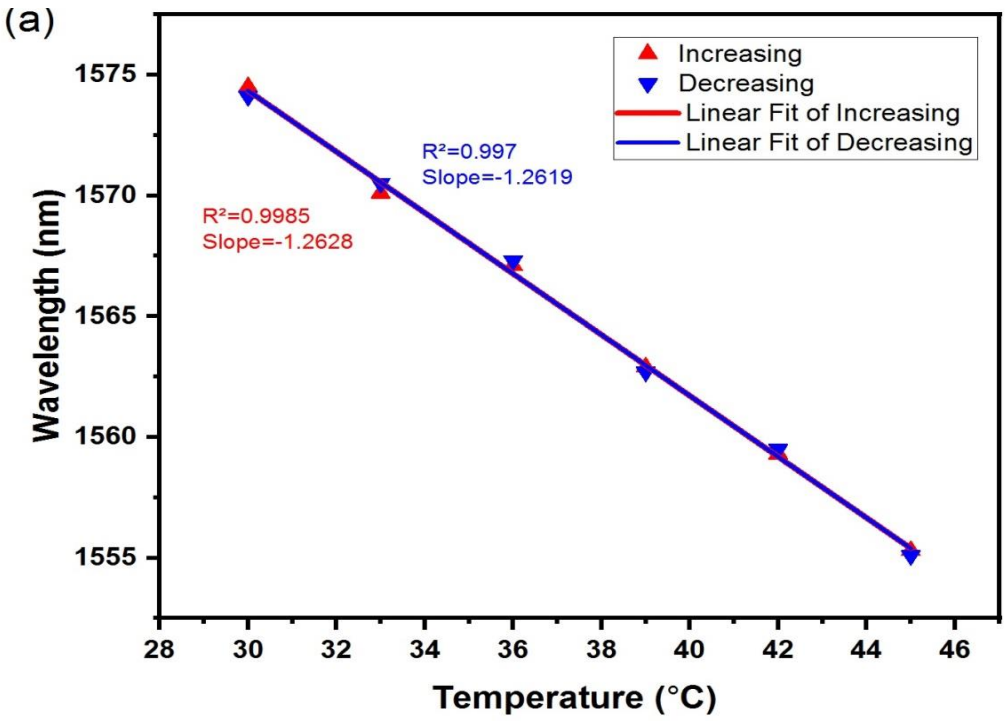

Figure(3.4)(a):Interference dip behavior with temperature variation against wavelength of the untapered SNS-PC

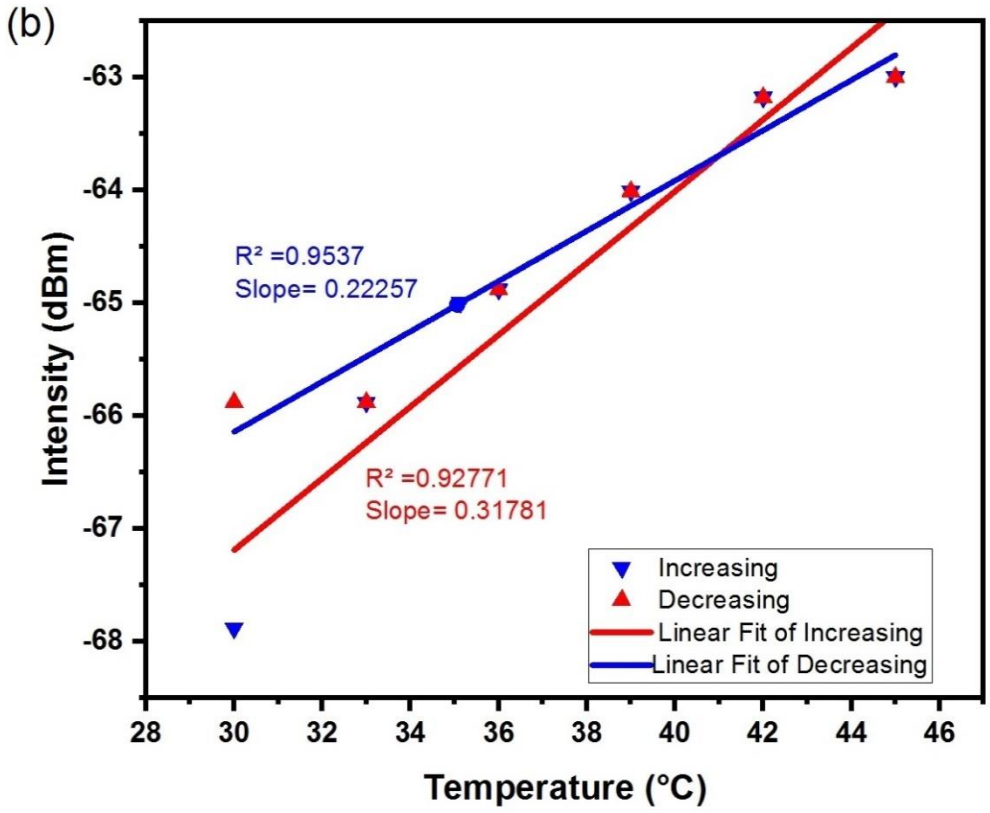

Figure (3.4)(b):Interference dip behavior with temperature variation against optical intensity of the untapered SNS-PC

Then, second active sensing head TSNS-PC of 3 cm length NCF with both splicing joints tapered is examined. From the spectral response which is depicted in Fig.(3.5)(a-b),the sensor showed two interference dips at 1618.9 nm and 1577.7, respectively. First dip revealed a very good extinction ratio of around 23.8 dB this dip wavelength exhibited an excellent blue-shift nearly 29.2 nm. However, the optical intensities of the output wavelengths experienced an increase then a consistent decrease along with temperature rising from 30 ◦C to 45 ◦C steps of 3 ◦C. Comparing the total wavelength shift between the untapered SNS-PC and the TSNS-PC, in the tapered sensor the shift is approximately 10 nm higher. This concludes the higher sensitivity which obtained by the tapering effect.

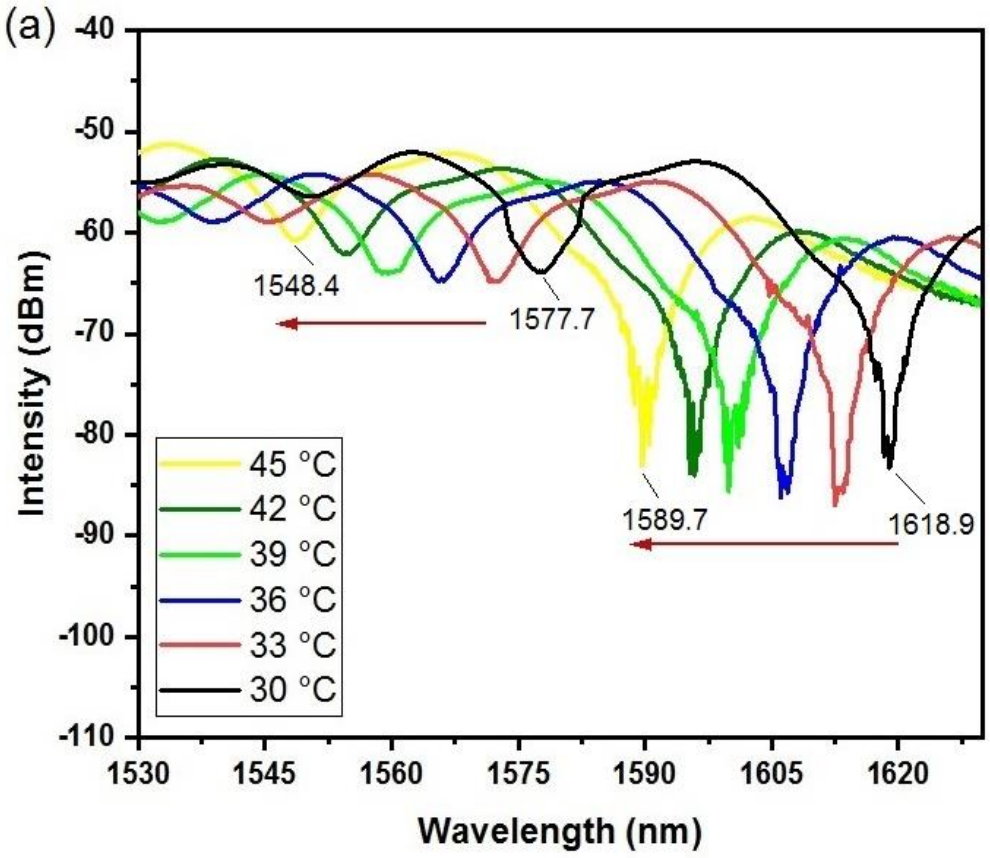

Figure(3.5)(a):Transmission spectrum of TSNS-PC sensor heating from 30-45◦C

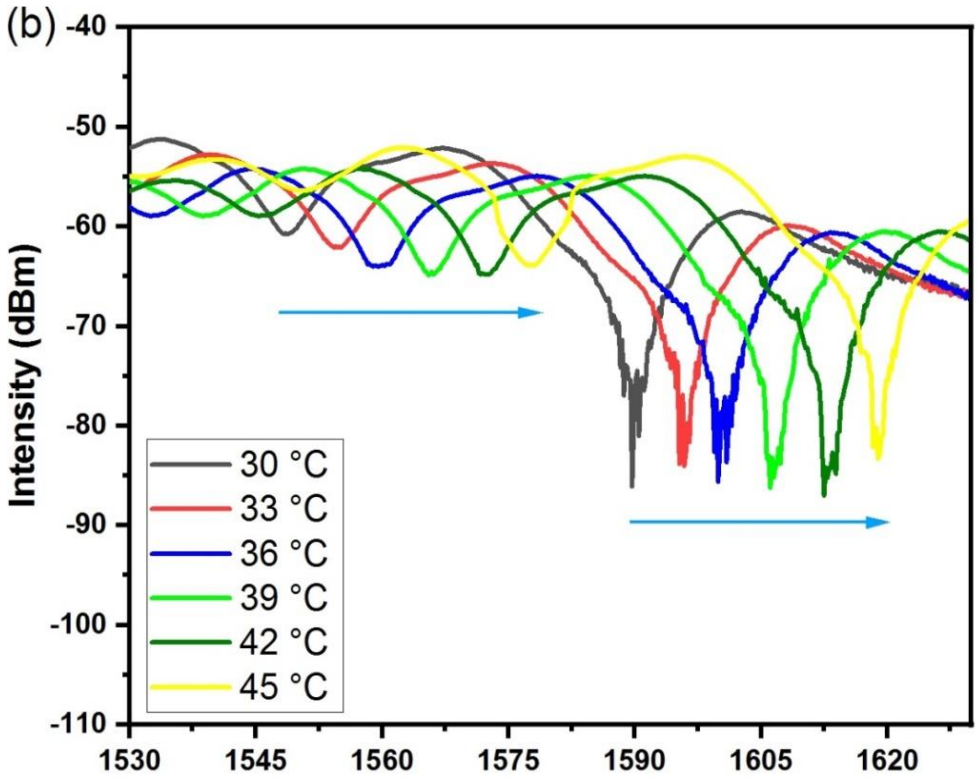

Figure (3.5)(b):Transmission spectrum of TSNS-PC sensor cooling from 45-30◦C

The determined sensitivity of the TSNS-PC is illustrated in Fig.(3.6)(a-b). For dip 1 it revealed a spectral sensitivity of around −1.9438 nm/◦C however, the optical intensity revealed a polynomial behavior. The linear fitting coefficient was 0.9969 for the wavelength feedback while the polynomial regression coefficient was 0.9164 for the optical intensity feedback. Herein, it's necessary to mention that the intensity response is studied for both temperature sensors for comparison purposes. The intensity response in the untapered SNS-PC followed a linear behavior with temperature variation; however, in the TSNS-PC the intensity profile exhibited a polynomial behavior with temperature variation in the first dip.

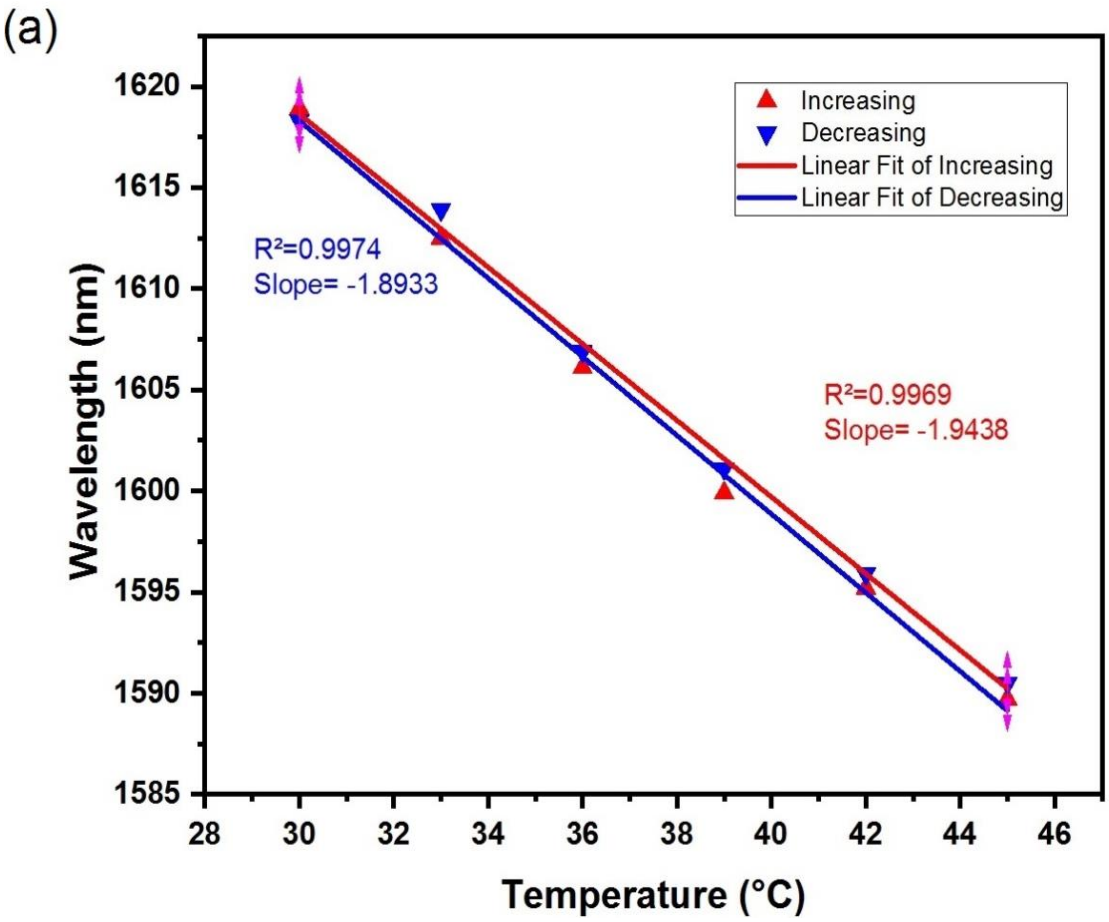

Figure(3.6)(a):Interference dip behavior with temperature variation against wavelength of the tapered TSNS-PC dip 1

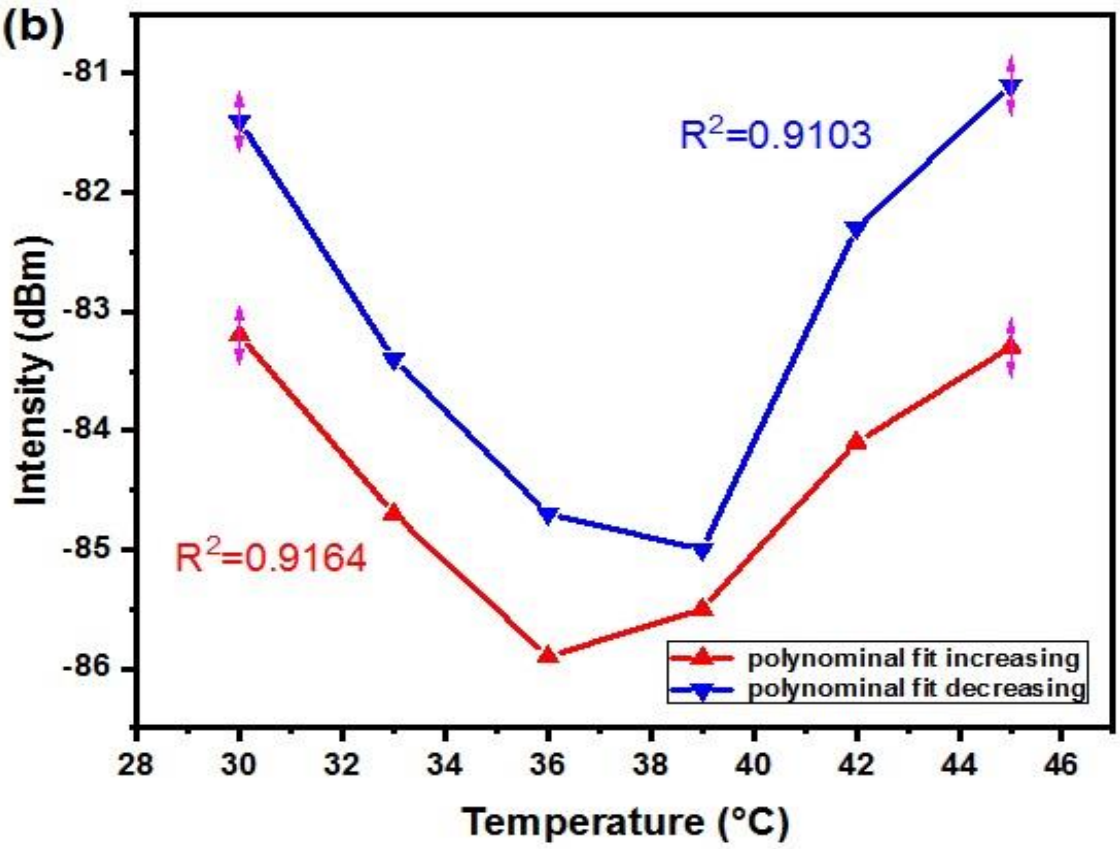

Figure(3.6)(b):Interference dip behavior with temperature variation against optical intensity of the tapered TSNS-PC dip 1

The second dip of the TSNS-PC examined as well, it revealed 12.5 dB extinction ratio at 1577.7 nm. The spectral shift of the second dip is illustrated in Fig.(3.5)(a-b).The second dip exhibited 29.3 nm shift toward shorter wavelengths as well. The calculated sensitivity of the second dip for both spectral responses and intensity profile with temperature variance is given in Fig.(3.7)(a-b).

From the obtained results of dip2, the behavior of both wavelength response and intensity feedback remained consistent as those of dip1, they revealed a linear response to the spectral shift and a nonlinear feedback for the optical intensity response due to thermal variance. The tapered sensor exhibited a similar

behavior with a previously published work, improved tapered temperature sensor with an approximately similar TOC coating [137].The shift towards shorter wavelengths of the fabricated sensor could probably associated with the bigger index of refraction of the polymer coating material, in addition to the refractive index of NCF being reduced because of the large negative TOC of the protective coating. The TOC value of the Acrylate coating is around – 4 x 10^{-4} ◦C^{-1} [138,139].The resolution calculation was estimated by dividing the spectrum analyzer resolution by the obtained sensitivity of the tapered sensor which its value was around 0.0102 ◦C.

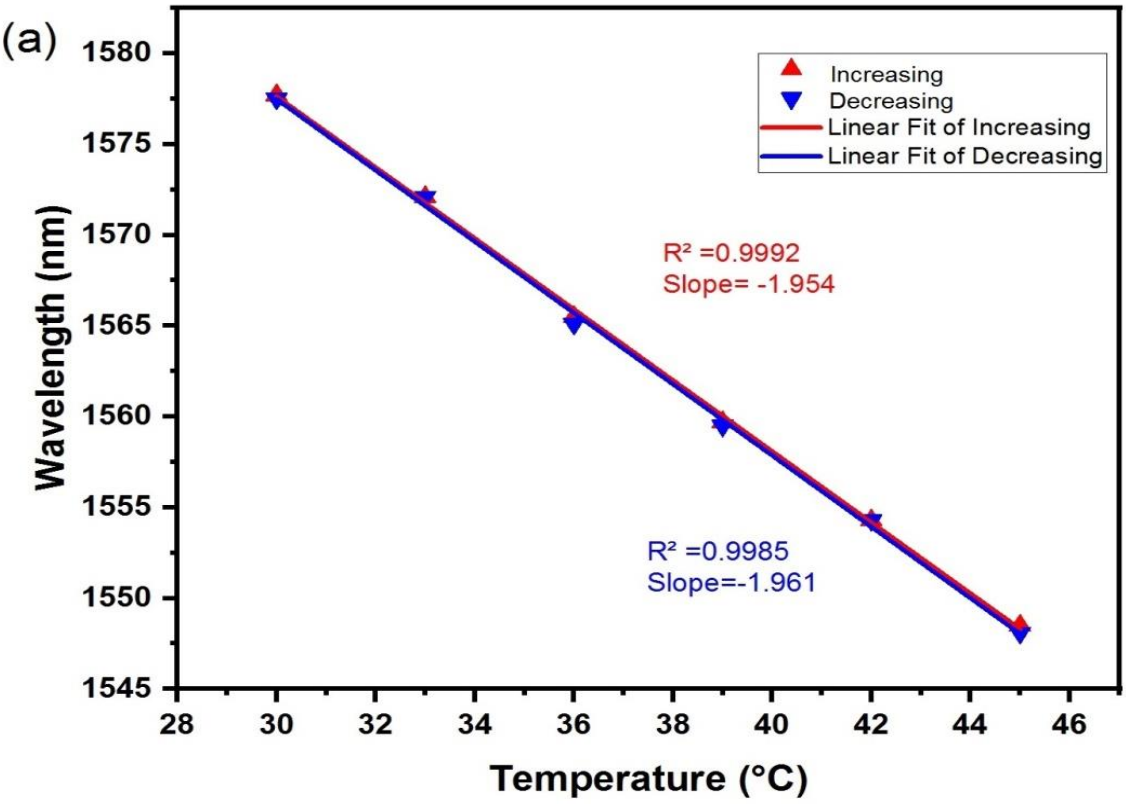

Figure(3.7)(a):Interference dip behavior with temperature variation against wavelength of the tapered TSNS-PC dip 2

It can be seen from the experimental results the tapering effect significantly improved the sensitivity about 53% in the TSNS-PC temperature sensor by allowing more evanescent waves coupling into the surrounding medium. For the TSNS-PC setup there is a powerful modal interferences at the tapered no-core fiber-optic segment. That is due to strong concentration of infrared light at the Lead-in taper transient part

and mode filtering effect. The filtering effect reduced the number of higher order modes propagation through the active sensing head. It been previously investigated that in the tapered sensors, higher order mode counts that are along the Lead-out taper transient section are fewer than those of the untapered multimode sensing fiber structure. Consequently, a significantly enhanced sensitivity [140].

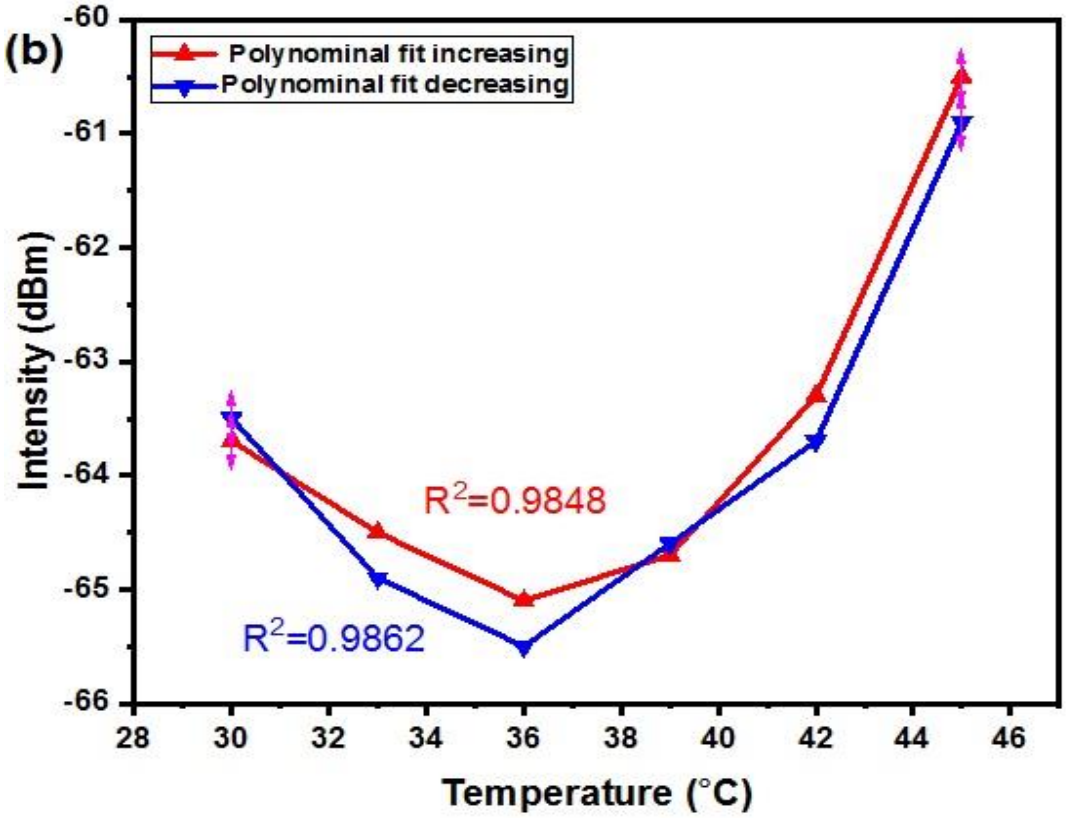

Figure(3.7)(b):Interference dip behavior with temperature variation against optical intensity of the tapered TSNS-PC dip2

3.3 Tapering effect Mode filtering and evanescent wave effect

The tapering effect can enhance the sensitivity by permitting more evanescent wave to couple with the surrounding medium and reducing the number of higher order modes contribution in the coupling. Consequently, more optical power in the LP_{01} and LP_{11}.This increases the chance of more interference energy to take place between the fundamental mode and the first higher order mode, which will give rise for an obvious interference pattern than can be easily observed and followed in the transmission spectrum. Thus, better sensing performance.

A conventional SMS fiber setup with typical MMF between two SMFs is not considered a perfect option in various parameter sensing such as; humidity, RI, sucrose concentration and temperature. Since the thick cladding of the MMF part reduces the interaction between the propagating light otter environment. Accordingly, in order to allow typical SMS sensing structure to work better in fiber sensing systems, various techniques are utilized such as; hydrofluoric acid etching, side polishing, core mismatch, bend based structures, and grating writing [141-143]

3.4 Results of the strain sensor

A photo-image graph for the experimental configuration of the strain sensor is illustrated in Fig.(3.8) .

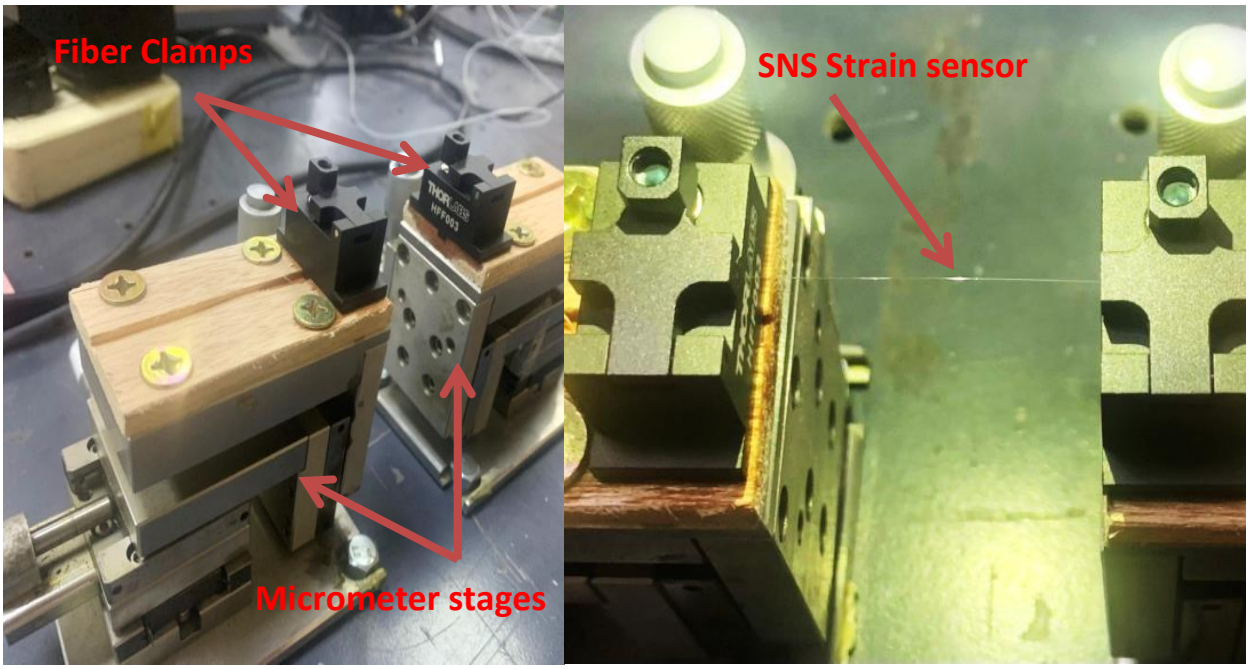

Figure(3.8):laboratory photo image of NCF strain sensor

Axial bi-directional strain is maintained by applying longitudinal steps of 100μm per each stage, the wavelength shift of the first strain sensor is illustrated in Fig.(3.9) . The interference dip experienced a linear blue-shift as strain is increased from 0-1000 με in steps of 200 με. For the reverse strain cycle, the first sensor exhibited a red-shift as the strain is oppositely decreased until reaching the zero strain point. The first strain sensor followed a stable behavior in the selected strain range. The experiment

is conducted at ambient temperature. To examine the mass production capability of the proposed SNS strain sensor, reproducibility and repeatability is taken in consideration.

It's important to design a robust repeatable strain sensor that can withstand many repetition cycles for real world measurement systems.

The concentration to rebuild the strain sensor based on the best length selection which previously mentioned in chapter2.

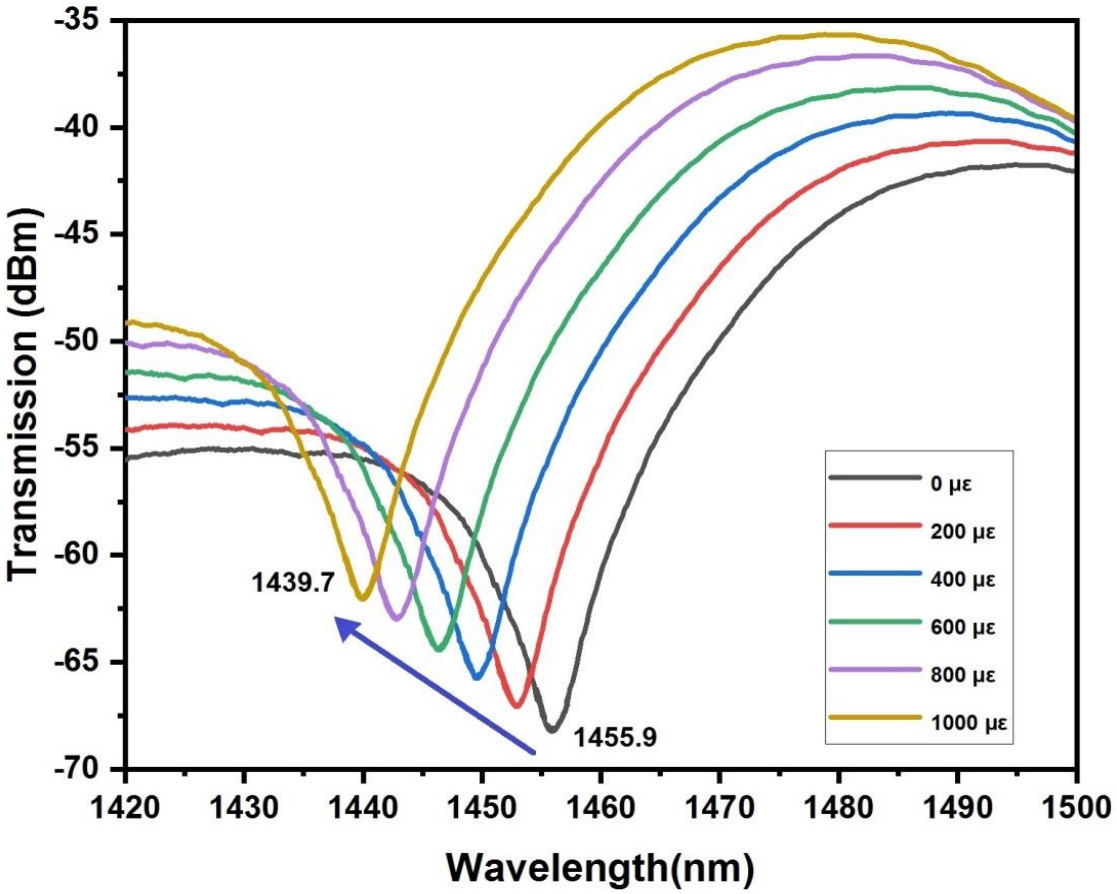

Figure(3.9):Transmission spectrum of strain sensor #1

Utilizing the given results of strain sensor #1 the linear fitting curve is drawn, the first sensor exhibited an excellent linear behavior, the coefficient of linear regression R^2 is 0.9961 for straining and 0.9968 for reducing strain.

The obtained sensitivity of straining and reducing strain are recorded as -16.27 pm/με and 15.73 pm/με، respectively .The linear fitting curve of sensor# 1 is illustrated in Fig.(3.10).

The interference dip of the first sensor experienced spectral shift as a result of the variation of refractive indices of multiple traveling modes along the sensor, this variation is primarily caused by the photo-elastic effect of the sensing NCF.

When tensile is applied, the length of the fiber sensor will vary slightly .As a result, the effective refractive indices between the fundamental propagating mode and the higher order modes will suffer a proportional change.

This change will affect the output transmission spectrum by moving the location of the interference dip to a specific direction. In this case, the spectral shift moved toward the shorter wavelength.

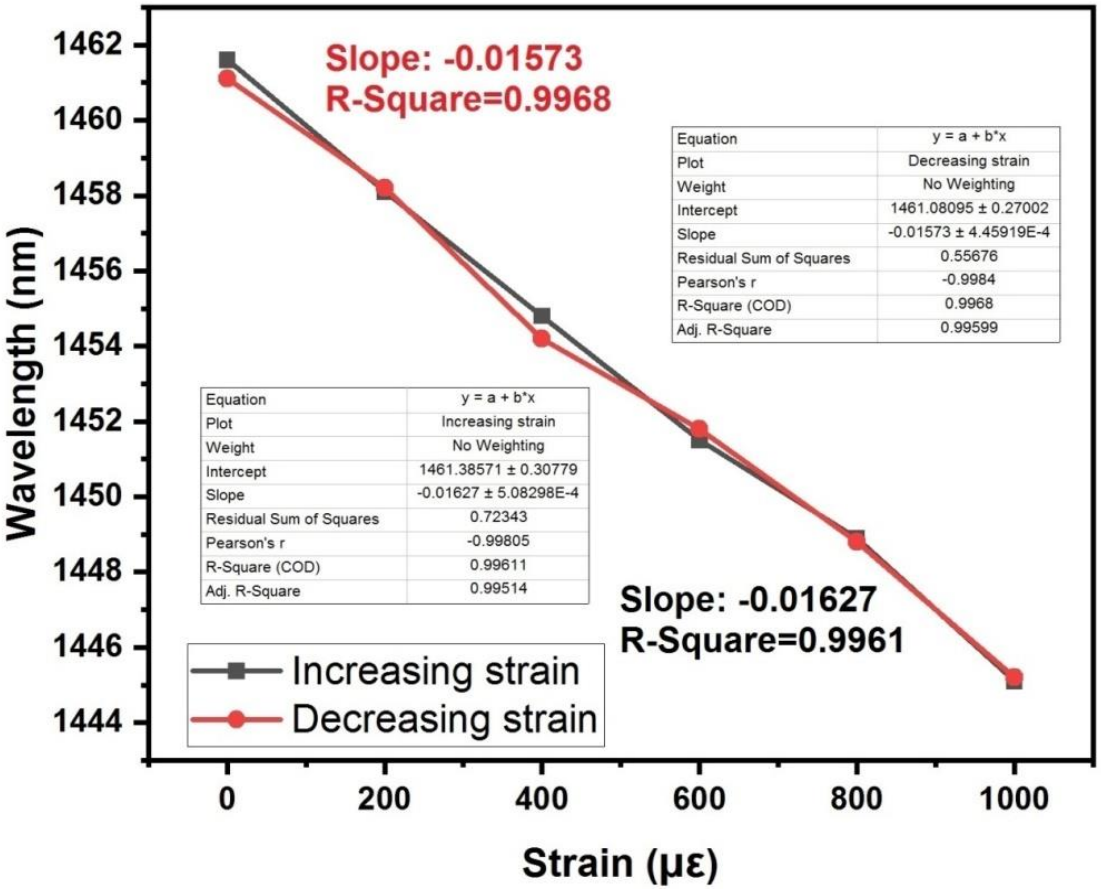

Figure(3.10):Linear fitting curve of strain sensor #1

3.4.1 Reproducibility and repeatability of the NCF based strain sensor

Repeatability is an important key in fabricating interferometric fiber sensors. It confirms the stability as an internal factor and reproducibility in mass production as an external factor. To do this, another strain sensor is structured after 24 hours. The second strain sensor is labeled sensor#2.This sensor is also examined.

The resonant dip of this sensor was at 1461.7 nm. Sensor#2 examined at the same lab under the same testing conditions. By increasing strain from 0-1000 με in steps of 200 μm, the exhibited wavelength shift headed toward shorter wavelengths as well. The spectral shift curve of sensor#2 is illustrated in Fig.(3.11).

The second NCF strain sensor followed an approximate behavior to the first sensor, it suffered a spectral shift to the shorter wavelengths which agreed with the first sensor's behavior. Accordingly, the reproducibility of the structure is confirmed for the same testing conditions.

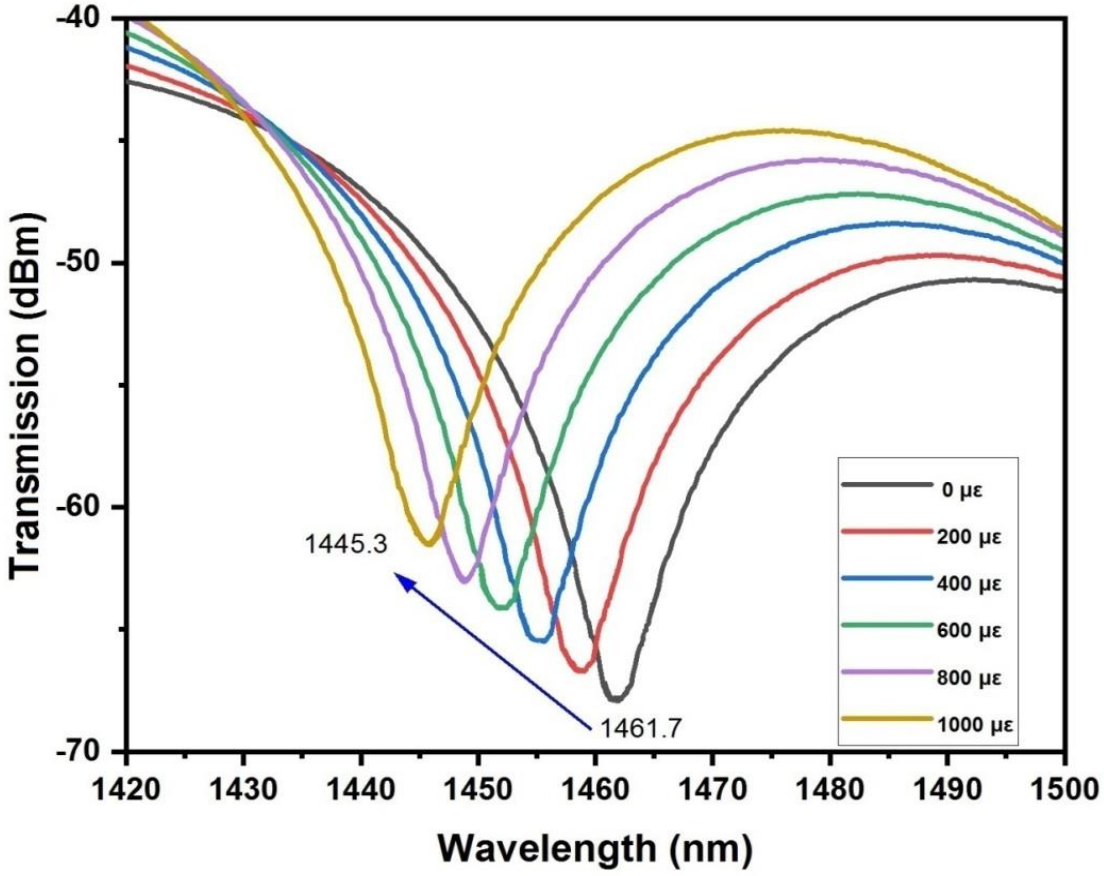

Figure(3.11):Transmission spectrum of strain sensor #2

From the calculated results, the regression coefficient of linear fitting is determined. Sensor #2 showed a wavelength sensitivity for straining and reducing strain of -16.37 pm με $^{-1}$ and 16.01 pm με $^{-1}$, respectively. The determined R^2 for both straining and reducing strain of sensor #2 are 0.9997 and 0.9956, respectively. The linear fitting curve of strain sensor #2 is illustrated in Fig.(3.12).

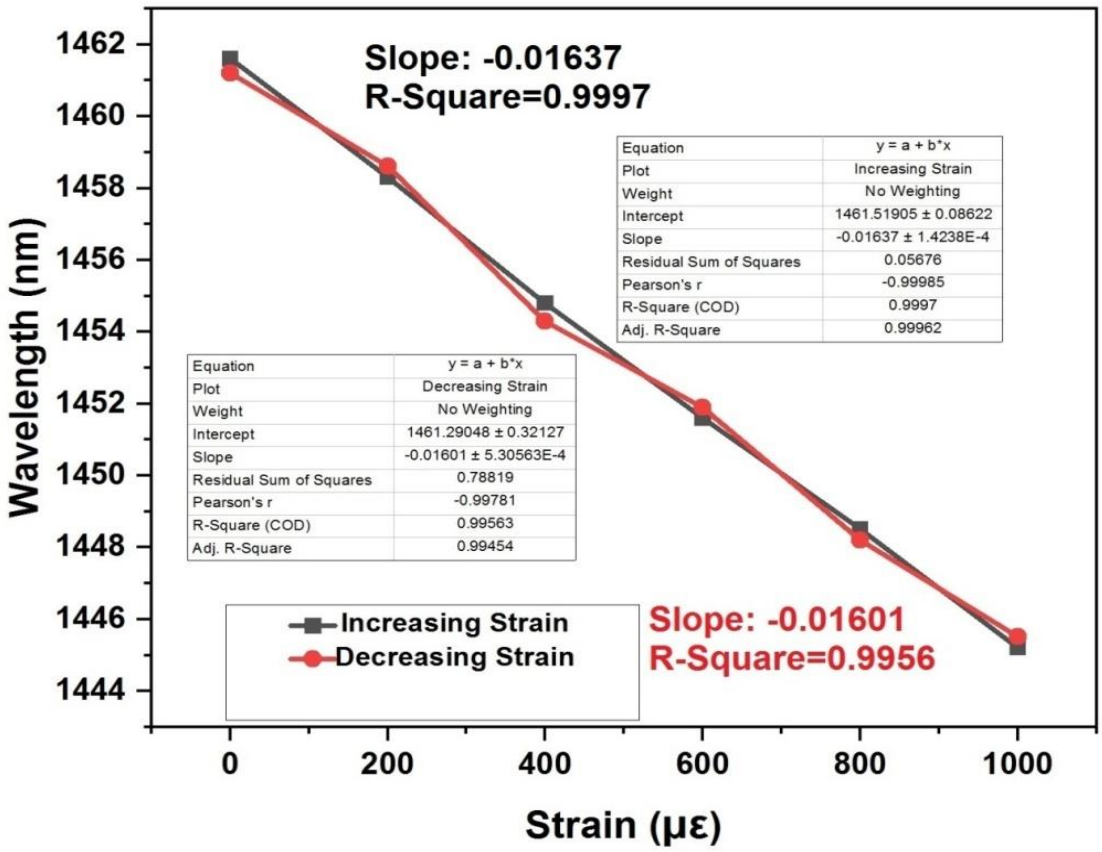

Figure(3.12):Linear fitting curve of strain sensor #2

3.4.2 Sensitivity comparison with another NCF sensing length strain sensor

In order to make a sensitivity comparison between various sensing lengths, a different NCF length is examined. A 35 mm NCF strain sensor is fabricated (sensor#3).This sensor revealed two interference dips at 1465.2 nm and 1533 nm of 19.23 dB and 14.1dB extinction ratios, respectively. The sensor bi-directionally strained in the range of 0-1000 με in steps of 200 μm as a total count of one step. The examination is conducted in the same lab utilizing same testing condition. Ensuring three dimensional alignments and avoiding bend to prevent result alteration. The 35 mm sensor exhibited a total wavelength shift of 15.2 nm at maximum strain value which

is 1000 με. Fig (3.13) shows the transmission spectrum of the 35 mm NCF. The obtained sensitivity of the sensor#3 is -15.11 pm $με^{-1}$ and -15.97 pm $με^{-1}$ for increasing and decreasing strain, respectively. The results are illustrated in Fig.(3.14)

.

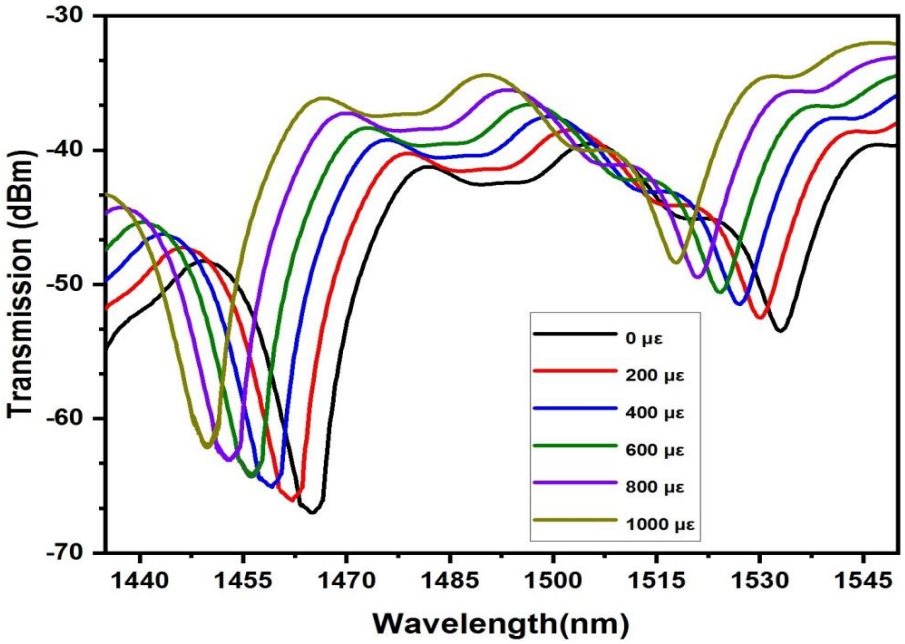

Figure(3.13):Transmission spectrum f strain sensor #3

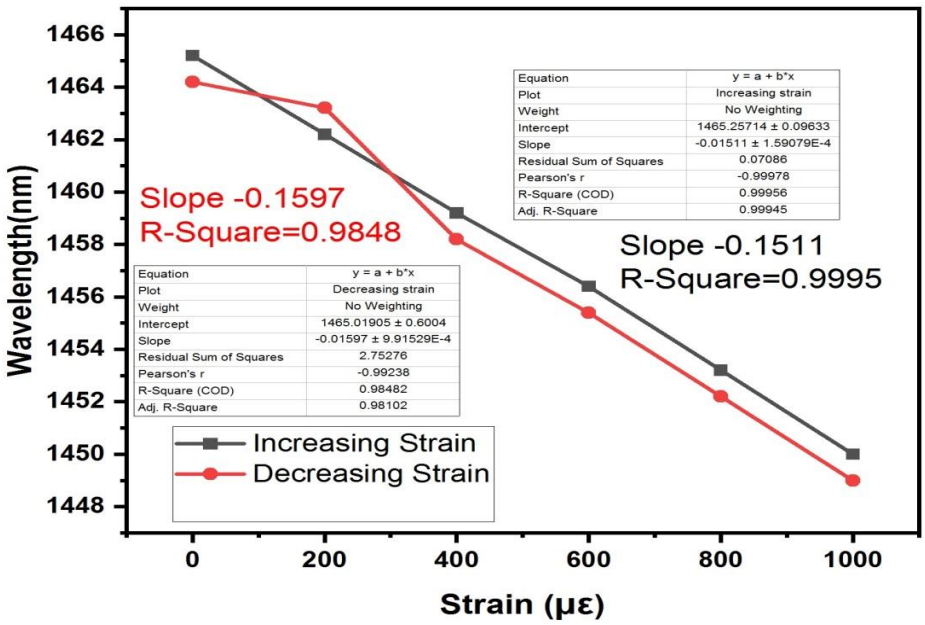

Figure(3.14):Linear fitting curve of strain sensor #3

To highlight the results of all three strain sensors for comparison purposes, the error bar graph is drawn for the 31 mm (sensor #1), the repeated 31 mm (sensor #2) and the 35 mm (sensor #3), respectively .From Fig.(3.15). The error bar shows that the

SNS strain sensor is precisely repeatable with a negligible error percentile. The error value is bouncing in the range of less than 1 pm.

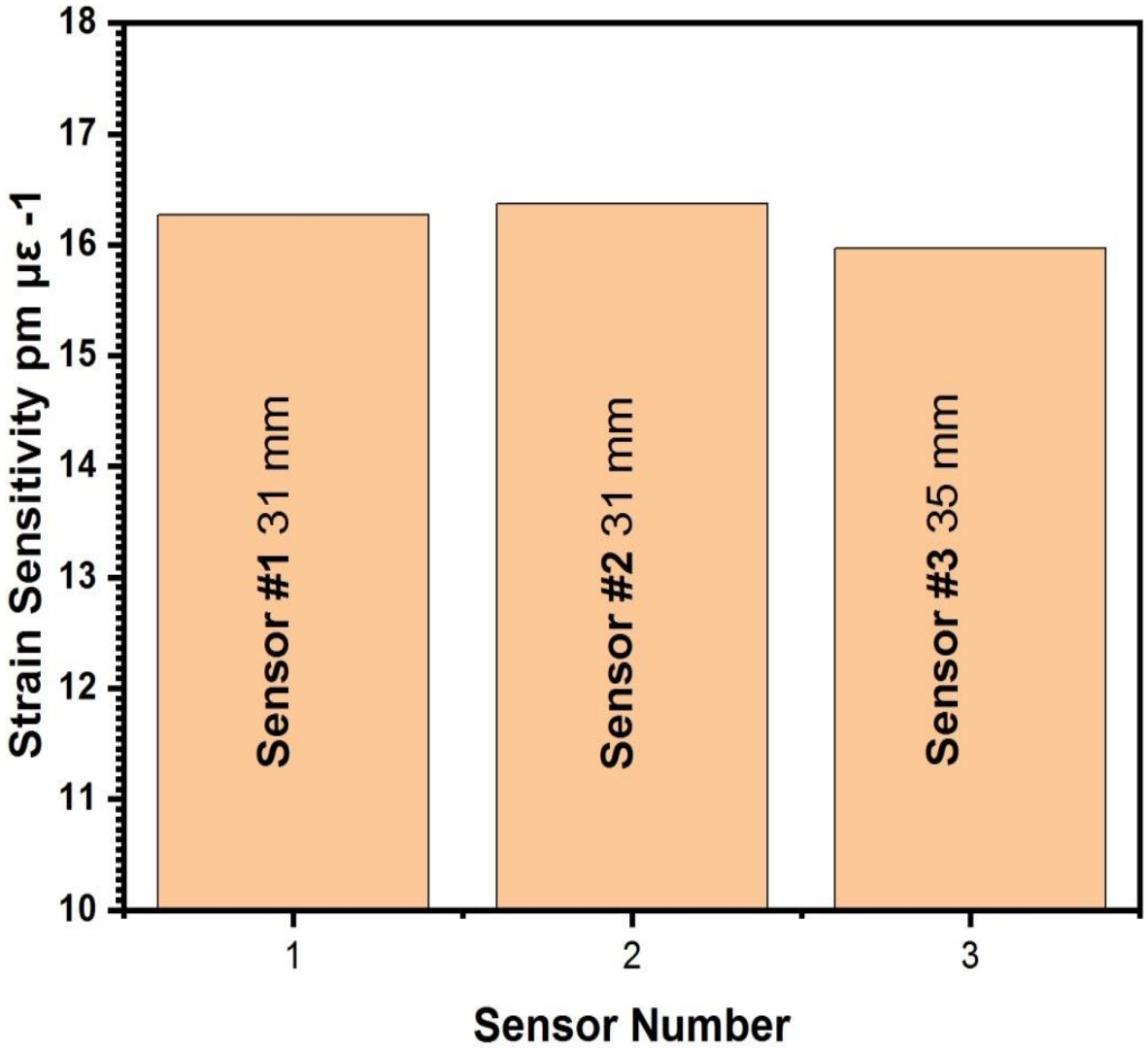

Figure (3.15):Error bar graph for three strain sensors

3.4.3 Temperature crosstalk analysis of SNS strain sensor results

In the cross sensitivity analysis of the strain sensor with temperature variation, the SNS strain sensor is situated on the hotplate. Temperature increased from 20-70 °C in steps 10°C of. The temperature wavelength shift is illustrated in Fig.(3.16). The calculated temperature sensitivity is about 3.97 pm /°C which is relatively low .The linear curve of temperature influence is illustrated in Fig.(3.17). The low temperature sensitivity can be due to low CTE and the high positive TOC of bare silica.

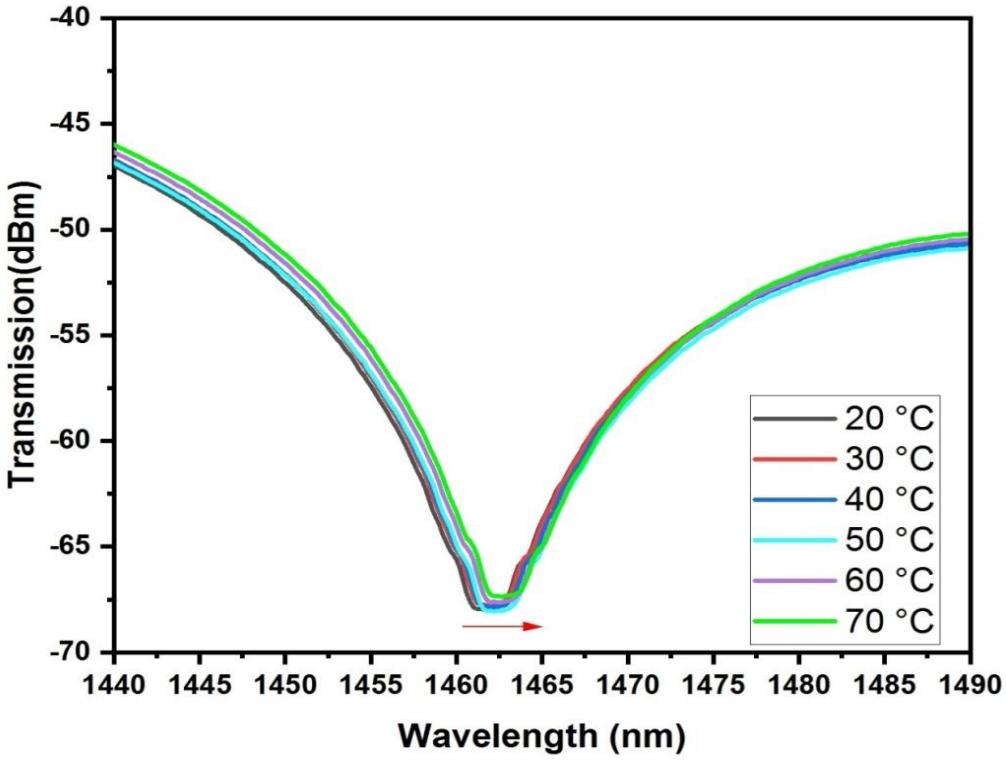

Figure(3.16):Interference wavelength shift of the strain sensor 2 due to thermal effect

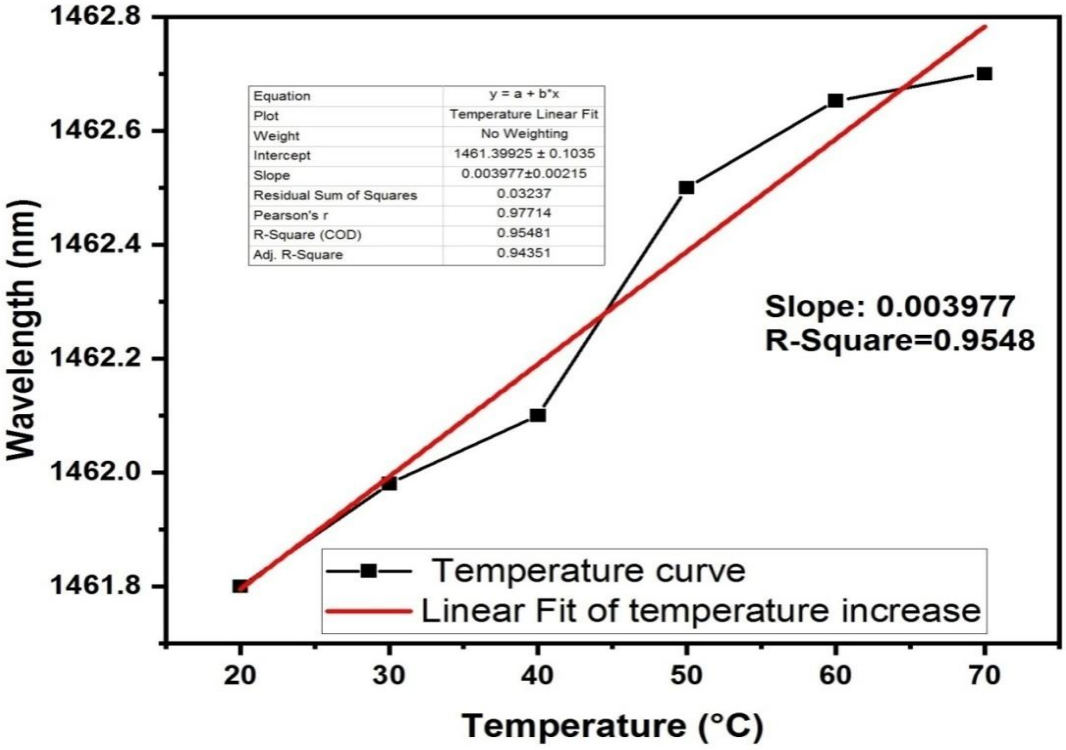

Figure(3.17):Linear fitting curve of the strain sensor 2 against temperature variation effect

The special structural properties of no-core fibers NCFs have broadened the sensation applications that rely on multimodal interference, evanescent wave absorption, self-image and nano-coatings. This fact promoted the usage of this special type of multimode fiber in many biological, physical and chemical fiber sensors.

Silica fiber which is the base material of the NCF has a low thermal expansion coefficient which explains the addition of coatings the fiber to increase temperature sensitivity.

Self-imaging is a constant behavior of multimodal waveguides, in which lead-in field is regenerated in one or more images at specific periods in the direction of propagation of the wave. When temperature increased, the NCF sensor interference dip exhibited a shift toward longer wavelengths (red-shift).This behavior is expected in multimode fiber sensors when the polymer jacket is stripped-off. The investigations agree with the previously published work [23].

3.5 Response and recovery time for the TSNS-PC sensor

The calculation of the response and recovery time is based on counting the total time for the dip wavelength to shift from the lower temperature limit to the upper temperature limit. The temperature is set to 30 ◦C then suddenly raised to 45◦C, the calculated response time was around 3.5 second for the dip wavelength to move from 1618 nm to 1589 nm .The temperature controller then turned off. The dip wavelength remained in the final shift position for approximately 8 seconds, then it started to shift towards the longer wavelengths as the temperature drops. The total time count for the wavelength shift to move from 30 ◦C to 45 ◦C then back to 30 ◦C is 20 seconds. The recovery time was around 16.5 seconds. Knowing each corresponding wavelength for each intermediate temperature, the recovery curve is down Fig. (3.18). the response and recovery time measurement for the real time TSNS-PC temperature sensor as in [final]

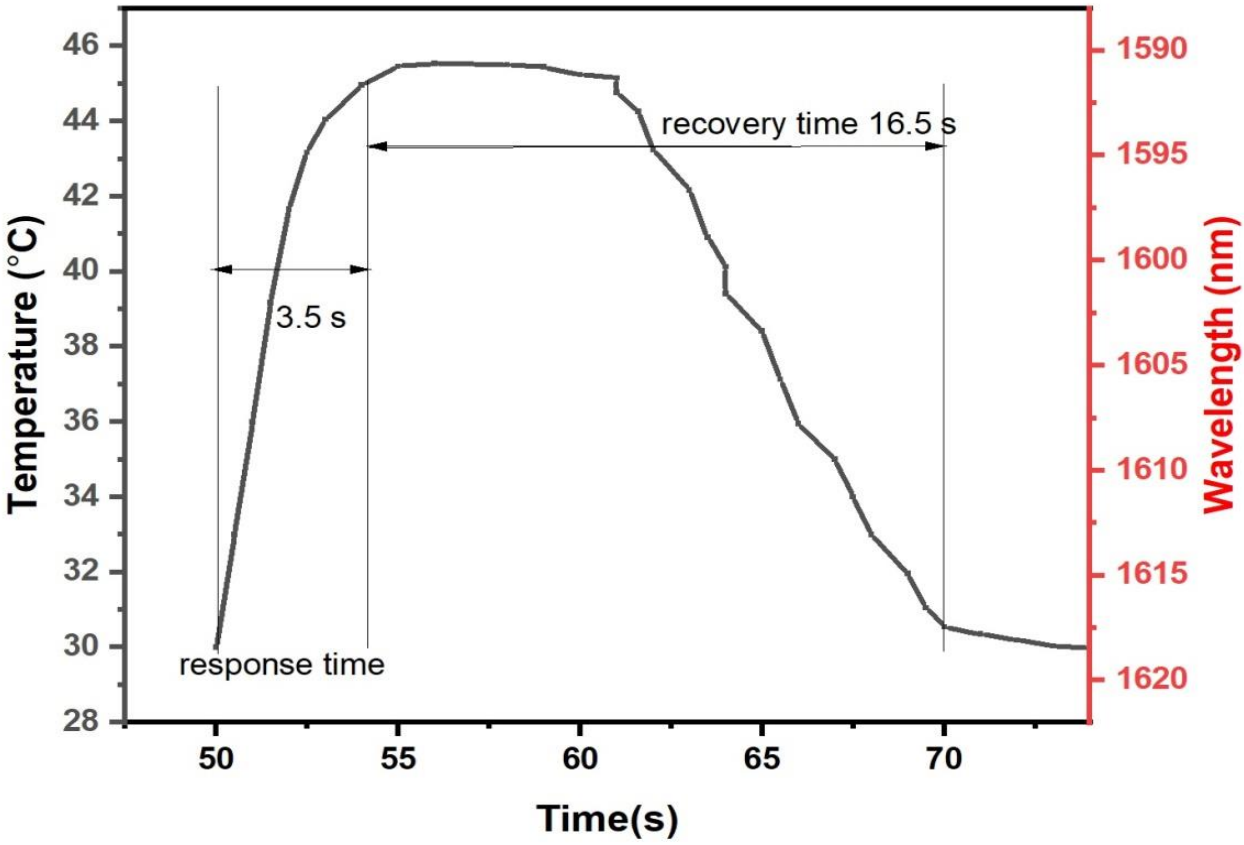

Figure(3.18) Response and recovery time curve for the TSNS-PC

3.6 Conclusion

In this work, the following goals are successfully achieved

-Two fiber-optic sensors for temperature and strain measurement based on NCF Mach-Zehnder interferometer have been designed and experimentally demonstrated.

-Two sensitivity enhancement techniques adapted to boost up the temperature sensitivity; inducing double bi-conical tapers and retaining the factory made polymer coating.

-The high temperature sensitivity is due to the high CTE , the high negative TOC of the polymer coating and the enhanced evanescent wave penetration to the outer media via tapering effect.

-With this novel structure high-sensitivity temperature sensor, the highest obtained sensitivity was around −1.9438nm/◦C and a high resolution of 0.0102 ◦C with a good response time of 3.5 seconds.

-The intensity profile behavior of the temperature sensor is investigated; it revealed a linear behavior without tapering effect and a polynomial behavior with tapering.

-The designed bi-directional uniaxial strain sensor exhibited a high sensitivity of -16.37 pm με -1 and a resolution of 0.8185, which to the best of our knowledge is the highest recoded so far in a similar structure.

-Repeatability and reproducibility of the strain sensor is examined, it revealed a great repeatability in the selected range.

-NCF sensing segment length influence on strain sensitivity is examined as well.

In brief, the sensors are cost effective, simple to fabricate, excellently repeatable, non-toxic and non-complex in structure which makes them perfect candidates in various thermometric and opto-mechanical sensing application in biomechanical, biomedical and engineering industry field.

3.7 Future work

1- Examining the influence of adding various heat sensitive coatings to the thermometric sensor.

2-Utilizing different diameter NCFs in the thermometric and the strain sensors and investigating the effect.

3-Studying the effect of adding nano-coatings to the thermometric and the strain sensors.

4-Examining the effect of adding heat insensitive coating to the strain sensor.

Publications

-Mohammad M. Hasan, Hanan J. Taher, Saif A. Mohammed ‘’**Highly sensitive fiber-optic temperature sensor based on tapered no-core fiber for biomedical and biomechanical applications’’** periodicals of engineering and natural science

Accepted 20 April 2021

Published 25 April 2021

-Mohammad M. Hasan, Hanan J. Taher’’ **Optical fiber bi-directional strain sensor based on coreless fiber’’** Springer nature journal of applied nanoscience

Accepted 19 July 2021

Published 29 July 2021

Mohammad M. Hasan, Hanan J. Taher **“The influence of no-core fiber length on** -optic **sensitivity in fiber-optic strain sensors ’’** Iraqi Journal of Laser

Accepted 10 August 2021

Published 20 August 2021

References

References:

[1]Ross-Pinnock, D., & Maropoulos, P. G. (2015). Review of industrial temperature measurement technologies and research priorities for the thermal characterisation of the factories of the future. In Proceedings of the Institution of Mechanical Engineers, Part B: Journal of Engineering Manufacture (Vol. 230, Issue 5, pp. 793–806). SAGE Publications. https://doi.org/10.1177/0954405414567929.

[2]Chen, W. (2019). Thermometry and interpretation of body temperature. In Biomedical Engineering Letters (Vol. 9, Issue 1, pp. 3–17). Springer Science and Business Media LLC. https://doi.org/10.1007/s13534-019-00102-2

[3]Bai, X., Yang, N., & Yang, Q. (2018). Temperature effect on the structural strains of an ancient Tibetan building based on long-term monitoring data. In Earthquake Engineering and Engineering Vibration (Vol. 17, Issue 3, pp. 641–657). Springer Science and Business Media LLC. https://doi.org/10.1007/s11803-018-0437-x

[4]Roriz, P., Carvalho, L., Frazão, O., Santos, J. L., & Simões, J. A. (2014). From conventional sensors to fibre optic sensors for strain and force measurements in biomechanics applications: A review. In Journal of Biomechanics (Vol. 47, Issue 6, pp. 1251–1261). Elsevier BV. https://doi.org/10.1016/j.jbiomech.2014.01.054.

[5] Schiavi, A., Cuccaro, R., & Troia, A. (2016). Strain-rate and temperature dependent material properties of Agar and Gellan Gum used in biomedical applications. In Journal of the Mechanical Behavior of Biomedical Materials (Vol. 53, pp. 119–130). Elsevier BV. https://doi.org/10.1016/j.jmbbm.2015.08.011.

[6] Bock, W. J., Nawrocka, M. S., Urbanczyk, W., Rostkowski, J., & Martynkien, T. (n.d.). Fiber-optic sensor for automotive applications. In Proceedings of IEEE Sensors,2004.IEEESensors,2004.IEEE. https://doi.org/10.1109/icsens.2004.1426148.

[7] Abad, S., González Torres, J., Rodriguez, R., Moreno, M. A., Araujo, F., & Pinto, F. (2017). Fiber optic sensing subsystem for temperature monitoring in space in-flight applications. In B. Cugny, Z.Sodnik, & N. Karafolas (Eds.), International Conference on Space Optics — ICSO 2014. SPIE. https://doi.org/10.1117/12.2304230.

[8] Ruffin, P. B. (2000). A review of fiber optics technology for military applications. In Novel Materials and Crystal Growth Techniques for Nonlinear Optical Devices: A Critical Review.Critical Review Collection. SPIE. https://doi.org/10.1117/12.419796.

[9] Wei, L., & Tjin, S. C. (2020). Special Issue "Fiber Optic Sensors and Applications": An Overview. In Sensors (Vol. 20, Issue 12, p. 3400). MDPI AG. https://doi.org/10.3390/s20123400.

[10] Yucel, M., Yucel, M., Gunduz, A. E., Goktas, H. H., & Ozturk, N. F. (2016). Using single-mode fiber as temperature sensor. In 2016 24th Signal Processing and CommunicationApplicationConference(SIU).IEEE.https://doi.org/10.1109/siu.2016.7495777.

[11]Tripathi, S. M., Kumar, A., Varshney, R. K., Kumar, Y. B. P., Marin, E., & Meunier, J.-P. (2009). Strain and Temperature Sensing Characteristics of Single-Mode–Multimode–Single-Mode Structures. In Journal of Lightwave Technology (Vol. 27, Issue 13, pp. 2348–2356). Institute of Electrical and Electronics Engineers (IEEE). https://doi.org/10.1109/jlt.2008.2008820.

[12] De, M., Gangopadhyay, T. K., & Singh, V. K. (2019). Prospects of Photonic Crystal Fiber as Physical Sensor: An Overview. In Sensors (Vol. 19, Issue 3, p. 464). MDPI AG. https://doi.org/10.3390/s19030464.

[13] Zhao, Y., Zhao, J., & Zhao, Q. (2020). Review of no-core optical fiber sensor and applications. In Sensors and Actuators A: Physical (Vol. 313, p. 112160). Elsevier BV. https://doi.org/10.1016/j.sna.2020.112160.

[14]Bakaic, M., Hanna, M., Hnatovsky, C., Grobnic, D., Mihailov, S., Zeisler, S. S., & Hoehr, C. (2020). Fiber-Optic Bragg Gratings for Temperature and Pressure Measurements in Isotope Production Targets for Nuclear Medicine. In Applied Sciences(Vol.10,Issue 13, p. 4610). MDPI AG. https://doi.org/10.3390/app10134610.

[15]Xie, L., Sun, B., Chen, M., & Zhang, Z. (2020). Sensitivity enhanced temperature sensor with serial tapered two-mode fibers based on the Vernier effect. In Optics Express(Vol.28,Issue22,p.32447).TheOpticalSociety.https://doi.org/10.1364/oe.403865.

[16] Korposh, S., James, S., Lee, S.-W., & Tatam, R. (2019). Tapered Optical Fibre Sensors: Current Trends and Future Perspectives. In Sensors (Vol. 19, Issue 10, p. 2294). MDPI AG. https://doi.org/10.3390/s19102294.

[17] Zhang, W., Zhu, L., Dong, M., Lou, X., & Liu, F. (2018). A Temperature Fiber Sensor Based on Tapered Fiber Bragg Grating Fabricated by Femtosecond Laser. In AppliedSciences(Vol.8,Issue12,p.2616).MDPIAG.https://doi.org/10.3390/app8122616.

[18] Zhao, X., Zhang, Y., Zhang, W., Li, Z., Yue, Y., & Yan, T. (2021). Ultrasensitive Fabry–Perot Strain Sensor Based on Vernier Effect and Tapered FBG-in-Hollow Silica Tube. In IEEE Sensors Journal (Vol. 21, Issue 3, pp. 3035–3041). InstituteofElectricalandElectronicsEngineers(IEEE).https://doi.org/10.1109/jsen.2020.3025795.

[19] Murugan, D., Bhatia, H., Sai, V. V. R., & Satija, J. (2020). P-FAB: A Fiber-Optic Biosensor Device for Rapid Detection of COVID-19. In Transactions of the Indian National Academy of Engineering (Vol. 5, Issue 2, pp. 211–215). Springer Science and Business Media LLC. https://doi.org/10.1007/s41403-020-00122-w.

[20] Lu, F., Lu, P., Badar, M., Wright, R. F., & Buric, M. P. (2020). Distributed fiber optic chemical sensor with a temperature compensation mechanism. In R. Katayama & Y. Takashima (Eds.), ODS 2020: Industrial Optical Devices and Systems. SPIE. https://doi.org/10.1117/12.2568773.

[21]Xiong, L., Guo, Y., Jiang, G., Zhou, X., Jiang, L., & Liu, H. (2021). Six-Dimensional Force/Torque Sensor Based on Fiber Bragg Gratings With Low Coupling. In IEEE Transactions on Industrial Electronics (Vol. 68, Issue 5, pp. 4079–4089).Institute of Electrical and Electronics Engineers(IEEE).https://doi.org/10.1109/tie.2020.2982107.

[22] Yang, D., Wang, J.-Q., Ren, W.-X., & Zhang, J. (2020). A Plastic Optical Fiber Sensing System for Bridge Deflection Measurement. In Sensors (Vol. 20, Issue 2, p. 480). MDPI AG. https://doi.org/10.3390/s20020480.

[23] Sulejmani, S., Sonnenfeld, C., Geernaert, T., Luyckx, G., Van Hemelrijck, D., Mergo, P., Urbanczyk, W., Chah, K., Caucheteur, C., Mégret, P., Thienpont, H., & Berghmans, F. (2013). Shear stress sensing with Bragg grating-based sensors in

microstructured optical fibers. In Optics Express (Vol. 21, Issue 17, p. 20404). The Optical Society. https://doi.org/10.1364/oe.21.020404.

[24] Zhang, Y., Xu, B., Wang, D., Guo, Y., Chen, M., Chen, W., Guo, P., Peng, X., & Li, J. (2021). Vibration Sensor Based on Hollow Biconical Fiber. In Sensors (Vol. 21, Issue 4, p. 1023). MDPI AG. https://doi.org/10.3390/s21041023.

[25]Rofianingrum, M. Y., Widiyatmoko, B., Kurniawan, E., Bayuwati, D., & Afandi, I. (2019). Fiber optic load sensor using microbend-deformer.In Journal of Physics: Series(Vol.1191,p.012007).IOP Publishing.https://doi.org/10.1088/1742-6596/1191/1/012007.

[26]Mokhtar, M. R., Owens, K., Kwasny, J., Taylor, S. E., Basheer, P. A. M., Cleland, D., Bai, Y., Sonebi, M., Davis, G., Gupta, A., Hogg, I., Bell, B., Doherty, W.,McKeague, S., Moore, D., Greeves, K., Sun, T., & Grattan, K. T. V. (2012). Fiber-Optic Strain Sensor System With Temperature Compensation for Arch Bridge Condition Monitoring. In IEEE Sensors Journal (Vol. 12, Issue 5, pp. 1470–1476). Institute of Electrical and Electronics Engineers (IEEE). https://doi.org/10.1109/jsen.2011.2172991.

[27] Bao, Y., Huang, Y., Hoehler, M., & Chen, G. (2019). Review of Fiber Optic Sensors for Structural Fire Engineering. In Sensors (Vol. 19, Issue 4, p. 877). MDPI AG. https://doi.org/10.3390/s19040877.

[28] Lai, C. C., Kam, J. C. P., Leung, D. C. C., Lee, T. K. Y., Tam, A. Y. M., Ho, S. L., Tam, H. Y., & Liu, M. S. Y. (2012). Development of a Fiber-Optic Sensing System for Train Vibration and Train Weight Measurements in Hong Kong. In Journal of Sensors (Vol. 2012, pp. 1–7). Hindawi Limited. https://doi.org/10.1155/2012/365165.

[29] Lawson, N. J., Correia, R., James, S. W., Partridge, M., Staines, S. E., Gautrey, J. E., Garry, K. P., Holt, J. C., & Tatam, R. P. (2016). Development and application of optical fibre strain and pressure sensors for in-flight measurements. In Measurement Science and Technology (Vol. 27, Issue 10, p. 104001). IOP Publishing. https://doi.org/10.1088/0957-0233/27/10/104001.

[30] Tian, K., Farrell, G., Wang, X., Yang, W., Xin, Y., Liang, H., Lewis, E., & Wang, P. (2017). Strain sensor based on gourd-shaped single-mode-multimode-single-mode hybrid optical fibre structure. In Optics Express (Vol. 25, Issue 16, p. 18885). The Optical Society. https://doi.org/10.1364/oe.25.018885.

[31] Zhang, C., Ning, T., Zheng, J., Xu, J., Gao, X., Lin, H., Li, J., & Pei, L. (2019). An optical fiber strain sensor by using of taper based TCF structure. In Optics & Laser Technology(Vol.120,p.105687).Elsevier BV.
https://doi.org/10.1016/j.optlastec.2019.105687.

[32] Yang, F., Wang, Z. K., & Wang, D. N. (2019). A highly sensitive optical fiber strain sensor based on cascaded multimode fiber and photonic crystal fiber. In Optical Fiber Technology(Vol.47,pp.102–106).ElsevierBV.
https://doi.org/10.1016/j.yofte.2018.11.029.

[33]Neumann1 E.-G.(988.)Single-Mode Fibers. Springer Berlin Heidelberg, [34] Shen, G., Qu, X., She, W., Yu, X., Sun, Q., & Chen, H. (1999). Study of UV-curable coatings for optical fibers. In Journal of Coatings Technology (Vol. 71, Issue 4,pp.53–57).Springer Science and Business Media LLC. https://doi.org/10.1007/bf02697896.

[35]Crisp J.(2005). Introduction to fiber optics. Elsevier; pp.15–16.

[36]Hui R.(2020) “Introduction,” in Introduction to Fiber-Optic Communications, Elsevier, pp. 3–15.

[37] Ahamed S. V.(2013). “Optical Fiber in Modern Networks,” in Intelligent Networks, Elsevier, 2013, pp. 93–106.

[38] Vukusic, J. I. (1986). Optical Fiber Communications: Principles and Practice. In Optica Acta: International Journal of Optics (Vol. 33, Issue 6, pp. 685–685). Informa UK Limited. https://doi.org/10.1080/716099703

[39] Zhao, Y., Zhao, J., & Zhao, Q. (2020). Review of no-core optical fiber sensor and applications. In Sensors and Actuators A: Physical (Vol. 313, p. 112160). Elsevier BV. https://doi.org/10.1016/j.sna.2020.112160.

[40]Pevec, S., & Donlagić, D. (2019). Multiparameter fiber-optic sensors: a review. In Optical Engineering (Vol. 58, Issue 07, p. 1). SPIE-Intl Soc Optical Eng. https://doi.org/10.1117/1.oe.58.7.072009.

[41]Hartog A. H.(2017). An Introduction to Distributed Optical Fibre Sensors. CRC Press.

[42]Lee, B. H., Kim, Y. H., Park, K. S., Eom, J. B., Kim, M. J., Rho, B. S., & Choi, H. Y. (2012). Interferometric Fiber Optic Sensors. In Sensors (Vol. 12, Issue 3, pp. 2467–2486). MDPI AG. https://doi.org/10.3390/s120302467.

[43]Zetie, K. P., Adams, S. F., & Tocknell, R. M. (2000). How does a Mach-Zehnder interferometer work? In Physics Education (Vol. 35, Issue 1, pp. 46–48). IOP Publishing. https://doi.org/10.1088/0031-9120/35/1/308.

[44]Chen, Q., Jin, C., Bao, Y., Li, Z., Li, J., Lu, C., Yang, L., & Li, G. (2014). A distributed fiber vibration sensor utilizing dispersion induced walk-off effect in a unidirectional Mach-Zehnder interferometer. In Optics Express (Vol. 22, Issue 3, p. 2167). The Optical Society. https://doi.org/10.1364/oe.22.002167.

[45] Khan, S., Le Calvé, S., & Newport, D. (2020). A review of optical interferometry techniques for VOC detection. In Sensors and Actuators A: Physical (Vol. 302, p. 111782). Elsevier BV. https://doi.org/10.1016/j.sna.2019.111782.

[46] Park, M., Lee, S., Ha, W., Kim, D.-K., Shin, W., Sohn, I.-B., & Oh, K. (2009). Fabrication of Intrinsic Fiber Mach-Zehnder Interferometer by Imbedding Micro Air-cavity. In Conference on Lasers and Electro-Optics/International Quantum Electronics Conference. Conference on Lasers and Electro-Optics. OSA. https://doi.org/10.1364/cleo.2009.jwa94.

[47]Hu J. J. D, Wong R. Y.-N., and Shum P. P., (2018)"Photonic Crystal Fiber–Based Interferometric Sensors," in Selected Topics on Optical Fiber Technologies and Applications, InTech.

[48] Flores, R., Janeiro, R., & Viegas, J. (2019). Optical fibre Fabry-Pérot interferometer based on inline microcavities for salinity and temperature sensing. In Scientific Reports (Vol. 9, Issue 1). Springer Science and Business Media LLC. https://doi.org/10.1038/s41598-019-45909-2.

[49]Grattan K. T. V. and B. T. Meggitt, Eds. (2000) Optical Fiber Sensor Technology. Springer US, pp. 7–8 ,.

[50]Freise, A., & Strain, K. (2010). Interferometer Techniques for Gravitational-Wave Detection. In Living Reviews in Relativity (Vol. 13, Issue 1). Springer Science and Business Media LLC. https://doi.org/10.12942/lrr-2010-1.

[52]Lefèvre, H. C. (2014). The fiber-optic gyroscope, a century after Sagnac's experiment: The ultimate rotation-sensing technology? In Comptes Rendus Physique (Vol. 15, Issue 10, pp. 851–858). Elsevier BV. https://doi.org/10.1016/j.crhy.2014.10.007.

[53] Post E. J. (1967). Sagnac effect, Rev. Mod. Phys. 39, 475–493.

[54]Mansuripur M., "The Sagnac interferometer," in Classical Optics and Its Applications, Cambridge University Press, pp. 182–196.

[55] Schubert, C., Abend, S., Gersemann, M., Gebbe, M., Schlippert, D., Berg, P., & Rasel, E. M. (2021). Multi-loop atomic Sagnac interferometry. In Scientific Reports (Vol. 11, Issue 1). Springer Science and Business Media LLC. https://doi.org/10.1038/s41598-021-95334-7.

[56]Polykarpov A. and A. Tiwari,(2014)"Chapter 1. Photocured Materials:A General Perspective," in Photocured Materials, Royal Society of Chemistry, , pp. 1–14.

[57] Zhang, Z., Zhao, P., Lin, P., & Sun, F. (2006). Thermo-optic coefficients of polymers for optical waveguide applications. In Polymer (Vol. 47, Issue 14, pp. 4893–4896). Elsevier BV. https://doi.org/10.1016/j.polymer.2006.05.035.

[58] Lian, X., Wu, Q., Farrell, G., & Semenova, Y. (2020). High-sensitivity temperature sensor based on anti-resonance in high-index polymer-coated optical fiber interferometers. In Optics Letters (Vol. 45, Issue 19, p. 5385). The Optical Society. https://doi.org/10.1364/ol.403050.

[59] Sampath, U., Kim, D., Kim, H., & Song, M. (2018). Polymer-coated FBG sensor for simultaneous temperature and strain monitoring in composite materials under cryogenic conditions. In Applied Optics (Vol. 57, Issue 3, p. 492). The Optical Society. https://doi.org/10.1364/ao.57.000492.

[60] Marrujo-Garcia, S., Hernandez-Romano, I., Torres-Cisneros, M., Monzon-Hernandez, D., & May-Arrioja, D. (2019). Curvature and sensitivity enhanced temperature polymer-coated multimode interference sensor. In P. D. LeVan, A. K. Sood, & P. Wijewarnasuriya (Eds.), Infrared Sensors, Devices, and Applications IX. SPIE. https://doi.org/10.1117/12.2529317.

[61] Tian, K., Farrell, G., Lewis, E., Wang, X., Liang, H., & Wang, P. (2018). A high sensitivity temperature sensor based on balloon-shaped bent SMF structure with its original polymer coating. In Measurement Science and Technology (Vol. 29, Issue 8, p. 085104). IOP Publishing. https://doi.org/10.1088/1361-6501/aac992

[62] Nurulain S., Norazmi R. Nor Mazlee, Salim M. ,and Hadi M.. (2017) "A Review on Optical Fibre Sensor Topology and Modulation Technique.".

[63]Smith M. D.(2015) Fibre interferometry for differential measurements. Engineering and Physical Sciences,.

[64] Wang, F., Zhu, H., Li, Y., Zhao, H., Wang, X., & Liu, Y. (2016). Comparative study on a core-offset fiber temperature sensor between the faraday rotation mirror structure and the double coupling structure. In Optics Communications (Vol. 367, pp. 286–291). Elsevier BV. https://doi.org/10.1016/j.optcom.2016.01.077.

[65] He, X. L., Wang, D. H., Wang, X. B., Xia, Q., Li, W. C., Liu, Y., Wang, Z. Q., & Yuan, L. B. (2019). A Cascade Fiber Optic Sensors for Simultaneous Measurement of Strain and Temperature. In IEEE Sensors Letters (Vol. 3, Issue 11, pp. 1–4). Institute of Electrical and Electronics Engineers (IEEE). https://doi.org/10.1109/lsens.2019.2949048.

[66] Madhav, K. V., Semenova, Y., & Farrell, G. (2010). Macro-bend optical fiber linear displacement sensor. In F. Berghmans, A. G. Mignani, & C. A. van Hoof (Eds.), Optical Sensing and Detection. SPIE. https://doi.org/10.1117/12.854631.

[67] Urrutia, A., Goicoechea, J., & Arregui, F. J. (2015). Optical Fiber Sensors Based on Nanoparticle-Embedded Coatings. In Journal of Sensors (Vol. 2015, pp. 1–18). Hindawi Limited. https://doi.org/10.1155/2015/805053.

[68] Wilczyński, K., Wysokiński, K., Stańczyk, T., Tenderenda, T., Markiewicz, K., Mąkowska, A., Szostkiewicz, Ł., Śmietana, M., & Nasiłowski, T. (2018). Metal-coated fibers for sensing in harsh environment. In 26th International Conference on Optical Fiber Sensors. Optical Fiber Sensors. OSA. https://doi.org/10.1364/ofs.2018.the8.

[69] Xu, B., Li, J., Li, Y., Xie, J., & Dong, X. (2014). Liquid Seal for Temperature Sensing with Fiber-Optic Refractometers. In Sensors (Vol. 14, Issue 8, pp. 14873–14884). MDPI AG. https://doi.org/10.3390/s140814873.

[70] Yang, Y., Averardi, A., & Gupta, N. (2019). An intensity modulation based fiber-optic loop sensor for high sensitivity temperature measurement. In Sensors and Actuators A: Physical (Vol. 297, p. 111554). Elsevier BV. https://doi.org/10.1016/j.sna.2019.111554.

[71] Tian, K., Farrell, G., Wang, X., Xin, Y., Du, Y., Yang, W., Liang, H., Lewis, E., & Wang, P. (2018). High sensitivity temperature sensor based on singlemode-no-core-singlemode fibre structure and alcohol. In Sensors and Actuators A: Physical (Vol. 284, pp. 28–34). Elsevier BV. https://doi.org/10.1016/j.sna.2018.10.016.

[72] S. M. Kadhim*1, K. A. S. & N. H. J. (2018). Optical Fiber Sensor With Ag-Nps Cladding For Temperature Sensing. Zenodo. https://doi.org/10.5281/ZENODO.1290493.

[73] Kuang, K. S. C., Quek, S. T., Koh, C. G., Cantwell, W. J., & Scully, P. J. (2009). Plastic Optical Fibre Sensors for Structural Health Monitoring: A Review of Recent Progress. In Journal of Sensors (Vol. 2009, pp. 1–13). Hindawi Limited. https://doi.org/10.1155/2009/312053

[74]Ghetia S. , Gajjar R. and Trivedi(2013).Classification of Fiber Optical Sensors. P.

[75]Wang, K., Dong, X., Kohler, M. H., Kienle, P., Bian, Q., Jakobi, M., & Koch, A. W. (2021). Advances in Optical Fiber Sensors Based on Multimode Interference (MMI): A Review. In IEEE Sensors Journal (Vol. 21, Issue 1, pp. 132–142). Institute of Electrical and Electronics Engineers (IEEE). https://doi.org/10.1109/jsen.2020.3015086.

[76]Matias I. R., Ikezawa S., and Corres J., Eds., (2017)Fiber Optic Sensors. Springer International Publishing.

[77]Mohammed, W. S., Smith, P. W. E., & Gu, X. (2006). All-fiber multimode interference bandpass filter. In Optics Letters (Vol. 31, Issue 17, p. 2547). The Optical Society. https://doi.org/10.1364/ol.31.002547

[78]Hatta A. M.,(2009). "Singlemode-multimode-singlemode optical fibre structures for optical sensing," Ph.D. dissertation, Dublin Institute of Technology.

[79]P. Roriz and A. B. Lobo Ribeiro, (2018) "Fiber Optical Sensors in Biomechanics," in Opto-Mechanical Fiber Optic Sensors, Elsevier, pp. 263–300.

[80]Samset, E., Mala, T., Ellingsen, R., Gladhaug, I., Søreide, O., & Fosse, E. (2001). Temperature measurement in soft tissue using a distributed fibre Bragg-grating sensor system. In Minimally Invasive Therapy & Allied Technologies (Vol. 10, Issue 2, pp. 89–93). Informa UK Limited. https://doi.org/10.1080/13645700152601379.

[81] Dennison, C. R., Wild, P. M., Dvorak, M. F., Wilson, D. R., & Cripton, P. A. (2008). Validation of a Novel Minimally Invasive Intervertebral Disc Pressure Sensor Utilizing In-Fiber Bragg Gratings in a Porcine Model. In Spine (Vol. 33, Issue 17, pp. E589–E594). Ovid Technologies (Wolters Kluwer Health). https://doi.org/10.1097/brs.0b013e31817c55e2.

[82]Webb, D. J., Hathaway, M. W., Jackson, D. A., Jones, S., Zhang, L., & Bennion, I. (2000). First in-vivo trials of a fiber Bragg grating based temperature profiling system. In Journal of Biomedical Optics (Vol. 5, Issue 1, p. 45). SPIE-Intl Soc Optical Eng. https://doi.org/10.1117/1.429967.

[83]Xu J.(2005). High temperature high bandwidth fiber optic pressure sensors [Ph.D. thesis]. Faculty of Virginia Polytechnic Institute and State University.

[84]Wehrle, G., Nohama, P., Kalinowski, H. J., Torres, P. I., & Valente, L. C. G. (2001). A fibre optic Bragg grating strain sensor for monitoring ventilatory movements. In Measurement Science and Technology (Vol. 12, Issue 7, pp. 805–809). IOP Publishing. https://doi.org/10.1088/0957-0233/12/7/309.

[85] Udd E.(1991). Fiber optic sensors: an introduction for engineers and scientists. NY: Wiley Interscience.

[86] Jackson, D. A., & Jones, J. D. C. (1986). Fibre Optic Sensors. In Optica Acta: International Journal of Optics (Vol. 33, Issue 12, pp. 1469–1503). Informa UK Limited. https://doi.org/10.1080/713821914.

[87]Swee Chuan Tjin, Jianzhong Hao, Yu-. (2001). A Pressure Sensor Using Fiber Bragg Grating. In Fiber and Integrated Optics (Vol. 20, Issue 1, pp. 59–69). Informa UK Limited. https://doi.org/10.1080/01468030119652.

[88]Tjin, S. C., Tan, Y. K., Yow, M., Lam, Y.-Z., & Hao, J. (2001). Recording compliance of dental splint use in obstructive sleep apnoea patients by force and temperature modelling. In Medical & Biological Engineering & Computing (Vol. 39, Issue 2, pp. 182–184). Springer Science and Business Media LLC. https://doi.org/10.1007/bf02344801.

[89] Frias, C., Frazão, O., Tavares, S., Vieira, A., Marques, A. T., & Simões, J. (2009). Mechanical characterization of bone cement using fiber Bragg grating sensors. In Materials & Design (Vol. 30, Issue 5, pp. 1841–1844). Elsevier BV. https://doi.org/10.1016/j.matdes.2008.07.035.

[90] Li, C., Liu, Y., Qu, S., & Chen, M. (2021). Temperature fiber sensor without cross sensitivity based on the multi-thin-no-thin-multi fiber coated with PDMS. In Journal of Physics D: Applied Physics (Vol. 54, Issue 45, p. 455101). IOP Publishing. https://doi.org/10.1088/1361-6463/ac1bd6.

[91] Bhardwaj, V., Gangwar, R. K., & Singh, V. K. (2016). Silicone rubber-coated highly sensitive optical fiber sensor for temperature measurement. In Optical Engineering (Vol. 55, Issue 12, p. 126107). SPIE-Intl Soc Optical Eng. https://doi.org/10.1117/1.oe.55.12.126107.

[92]Li, E., & Peng, G.-D. (2008). Wavelength-encoded fiber-optic temperature sensor with ultra-high sensitivity. In Optics Communications (Vol. 281, Issue 23, pp. 5768–5770). Elsevier BV. https://doi.org/10.1016/j.optcom.2008.08.022.

[93]Manfred K. (2004). "Strain Measurement with Fiber Bragg Grating Sensors.

[94]Al-Janabi, D. I., Salman, A. M., & Al-Janabi, A. (2020). High-sensitivity balloon-like thermometric sensor based on bent single-mode fiber. In Measurement

Science and Technology (Vol. 31, Issue 11, p. 115106). IOP Publishing. https://doi.org/10.1088/1361-6501/ab9458.

[95]He, J., Liao, C., Yang, K., Liu, S., Yin, G., Sun, B., Zhou, J., Zhao, J., & Wang, Y. (2015). High-Sensitivity Temperature Sensor Based on a Coated Single-Mode Fiber Loop. In Journal of Lightwave Technology (Vol. 33, Issue 19, pp. 4019–4026). Institute of Electrical and Electronics Engineers (IEEE). https://doi.org/10.1109/jlt.2015.2456153.

[96]Xin Q.(2013).“Durability and reliability in diesel engine system design,” in Diesel Engine System Design, Elsevier pp. 113–202.

[97]Gordelier, T., Thies, P. R., Rinaldi, G., & Johanning, L. (2020). Investigating Polymer Fibre Optics for Condition Monitoring of Synthetic Mooring Lines. In Journal of Marine Science and Engineering (Vol. 8, Issue 2, p. 103). MDPI AG. https://doi.org/10.3390/jmse8020103.

[98] Guzmán-Sepúlveda, J. R., Guzmán-Cabrera, R., & Castillo-Guzmán, A. A. (2021). Optical Sensing Using Fiber-Optic Multimode Interference Devices: A Review of Nonconventional Sensing Schemes. In Sensors (Vol. 21, Issue 5, p. 1862). MDPI AG. https://doi.org/10.3390/s21051862.

[99] Campanella, C., Cuccovillo, A., Campanella, C., Yurt, A., & Passaro, V. (2018). Fibre Bragg Grating Based Strain Sensors: Review of Technology and Applications. In Sensors (Vol. 18, Issue 9, p. 3115). MDPI AG. https://doi.org/10.3390/s18093115.

[100] Alvarez, M., & Lechuga, L. M. (2010). Microcantilever-based platforms as biosensing tools. In The Analyst (Vol. 135, Issue 5, p. 827). Royal Society of Chemistry (RSC). https://doi.org/10.1039/b908503n.

[101] Childs, P. R. N., Greenwood, J. R., & Long, C. A. (2000). Review of temperature measurement. In Review of Scientific Instruments (Vol. 71, Issue 8, pp. 2959–2978). AIP Publishing. https://doi.org/10.1063/1.1305516.

[102] Lee, J. E.-Y., Zhu, Y., & Seshia, A. A. (2008). A bulk acoustic mode single-crystal silicon microresonator with a high-quality factor. In Journal of Micromechanics and Microengineering (Vol. 18, Issue 6, p. 064001). IOP Publishing. https://doi.org/10.1088/0960-1317/18/6/064001.

[103] Noda, K., Hoshino, K., Matsumoto, K., & Shimoyama, I. (2006). A shear stress sensor for tactile sensing with the piezoresistive cantilever standing in elastic material. In Sensors and Actuators A: Physical (Vol. 127, Issue 2, pp. 295–301). Elsevier BV. https://doi.org/10.1016/j.sna.2005.09.023.

[104] Jiangfeng Wu, Fedder, G. K., & Carley, L. R. (2004). A low-noise low-offset capacitive sensing amplifier for a 50-/spl mu/g//spl radic/Hz monolithic CMOS MEMS accelerometer. In IEEE Journal of Solid-State Circuits (Vol. 39, Issue 5, pp. 722–730). Institute of Electrical and Electronics Engineers (IEEE). https://doi.org/10.1109/jssc.2004.826329.

[105] Timoshenko, S. (1925). Analysis of Bi-Metal Thermostats. In Journal of the Optical Society of America (Vol. 11, Issue 3, p. 233). The Optical Society. https://doi.org/10.1364/josa.11.000233.

[106] Lai, J., Perazzo, T., Shi, Z., & Majumdar, A. (1997). Optimization and performance of high-resolution micro-optomechanical thermal sensors. In Sensors and Actuators A: Physical (Vol. 58, Issue 2, pp. 113–119). Elsevier BV. https://doi.org/10.1016/s0924-4247(96)01401-x.

[107] Shin, D. D., Dong-Gun Lee, Mohanchandra, K. P., & Carman, G. P. (n.d.). Thin film NiTi fluidic-thermostat array. In The 13th International Conference on Solid-State Sensors, Actuators and Microsystems, 2005. Digest of Technical Papers. TRANSDUCERS ’05. The 13th International Conference on Solid-State Sensors, Actuators and Microsystems, 2005. Digest of Technical Papers. TRANSDUCERS ’05. IEEE. https://doi.org/10.1109/sensor.2005.1496479.

[108] Wijngaards, D. D. L., de Graaf, G., & Wolffenbuttel, R. F. (2004). Single-chip micro-thermostat applying both active heating and active cooling. In Sensors and Actuators A: Physical (Vol. 110, Issues 1–3, pp. 187–195). Elsevier BV. https://doi.org/10.1016/j.sna.2003.10.084.

[109] Meijer, G. C. M., Guijie Wang, & Fruett, F. (2001). Temperature sensors and voltage references implemented in CMOS technology. In IEEE Sensors Journal (Vol.

1, Issue 3, pp. 225–234). Institute of Electrical and Electronics Engineers (IEEE). https://doi.org/10.1109/jsen.2001.954835 .

[110] Blauschild, R. A., Tucci, P. A., Muller, R. S., & Meyer, R. G. (1978). A new NMOS temperature-stable voltage reference. In IEEE Journal of Solid-State Circuits (Vol. 13, Issue 6, pp. 767–774). Institute of Electrical and Electronics Engineers (IEEE). https://doi.org/10.1109/jssc.1978.1052048.

[111] Tortonese, M., Barrett, R. C., & Quate, C. F. (1993). Atomic resolution with an atomic force microscope using piezoresistive detection. In Applied Physics Letters (Vol. 62, Issue 8, pp. 834–836). AIP Publishing. https://doi.org/10.1063/1.108593.

[112] Linnemann, R., Gotszalk, T., Hadjiiski, L., & Rangelow, I. W. (1995). Characterization of a cantilever with an integrated deflection sensor. In Thin Solid Films (Vol. 264, Issue 2, pp. 159–164). Elsevier BV. https://doi.org/10.1016/0040-6090(94)05829-6.

[113] Brugger, J., Despont, M., Rossel, C., Rothuizen, H., Vettiger, P., & Willemin, M. (1999). Microfabricated ultrasensitive piezoresistive cantilevers for torque magnetometry. In Sensors and Actuators A: Physical (Vol. 73, Issue 3, pp. 235–242). Elsevier BV. https://doi.org/10.1016/s0924-4247(98)00240-4.

[114] Behrens, I., Doering, L., & Peiner, E. (2003). Piezoresistive cantilever as portable micro force calibration standard. In Journal of Micromechanics and Microengineering (Vol. 13, Issue 4, pp. S171–S177). IOP Publishing. https://doi.org/10.1088/0960-1317/13/4/325.

[115] Onoe, H., Gel, M., Hoshino, K., Matsumoto, K., & Shimoyama, I. (2005). Direct Measurement of the Binding Force between Microfabricated Particles and a Planar Surface in Aqueous Solution by Force-Sensing Piezoresistive Cantilevers. In Langmuir (Vol. 21, Issue 24, pp. 11251–11261). American Chemical Society (ACS). https://doi.org/10.1021/la051666f.

[116] Ma, L., Kang, Z., Qi, Y., & Jian, S. (2015). Fiber-optic temperature sensor based on a thinner no-core fiber. In Optik (Vol. 126, Issues 9–10, pp. 1044–1046). Elsevier BV. https://doi.org/10.1016/j.ijleo.2015.02.084.

[117] Bhardwaj, V., Gangwar, R. K., & Singh, V. K. (2016). Silicone rubber-coated highly sensitive optical fiber sensor for temperature measurement. In Optical Engineering (Vol. 55, Issue 12, p. 126107). SPIE-Intl Soc Optical Eng. https://doi.org/10.1117/1.oe.55.12.126107.

[118] Hsu, J.-M., Chen, J.-Z., & Zheng, W.-H. (2016). Highly Sensitive Temperature Fiber Sensor Based on Mach-Zehnder Interferometer. In Fiber and Integrated Optics (Vol. 35, Issues 5–6, pp. 230–238). Informa UK Limited. https://doi.org/10.1080/01468030.2016.1214992.

[119] Zhenan, J., Weiwei, D., Yinggang, L., Jingle, Z., & Kang, L. (2017). Tapered multi-mode fiber temperature sensor based on simultaneous response of wavelength and intensity. In Journal of Applied Optics (Vol. 38, Issue 2, pp. 628–632). Journal of Applied Optics. https://doi.org/10.5768/jao201738.0208001.

[120] Zhou, T., Zhang, Y., Han, B., Zhang, A., & Fu, D. (2018). Low cost non-adiabatic tapered fiber for high-sensitive temperature sensing. In Optical Fiber Technology (Vol. 45, pp. 53–57). Elsevier BV. https://doi.org/10.1016/j.yofte.2018.06.004.

[121] Liao, Y.-C., Liu, B., Liu, J., Wan, S.-P., He, X.-D., Yuan, J., Fan, X., & Wu, Q. (2019). High Temperature (Up to 950 °C) Sensor Based on Micro Taper In-Line Fiber Mach–Zehnder Interferometer. In Applied Sciences (Vol. 9, Issue 12, p. 2394). MDPI AG. https://doi.org/10.3390/app9122394.

[122] May-Arrioja, D. A., Ruiz-Perez, V. I., Lopez-Cortes, D., & Lozano-Crisostomo, N. (2019). Linear multimode interference fiber temperature sensor using the liquid in glass thermometer principle. In Applied Optics (Vol. 58, Issue 14, p. 3856). The Optical Society. https://doi.org/10.1364/ao.58.003856.

[123] Dong, J., Sang, M., Wang, S., Xu, T., Wang, Y., & Liu, T. (2020). A Novel Mach–Zehnder Interferometric Temperature Sensor Based on a Symmetrical Double-Grooved Structure. In IEEE Sensors Journal (Vol. 20, Issue 24, pp. 14850–14856). Institute of Electrical and Electronics Engineers (IEEE). https://doi.org/10.1109/jsen.2020.3010338.

[124] Wang, Q., Meng, H., Fan, X., Zhou, M., Liu, F., Liu, C., Wei, Z., Wang, F., & Tan, C. (2020). Optical fiber temperature sensor based on a Mach-Zehnder interferometer with single-mode-thin-core-single-mode fiber structure. In Review of

Scientific Instruments (Vol. 91, Issue 1, p. 015006). AIP Publishing. https://doi.org/10.1063/1.5128485.

[125] Wang, F., Pang, K., Ma, T., Wang, X., & Liu, Y. (2020). Folded-tapered multimode-no-core fiber sensor for simultaneous measurement of refractive index and temperature. In Optics & Laser Technology (Vol. 130, p. 106333). Elsevier BV. https://doi.org/10.1016/j.optlastec.2020.106333.

[126] Al-Hayali, S. K., & Al-Janabi, A. H. (2020). All fiber-optic temperature sensor based on cladding etched no-core fiber coated with nanostructured copper oxide-polyvinyl alcohol thin film. In Optik (Vol. 220, p. 165154). Elsevier BV. https://doi.org/10.1016/j.ijleo.2020.165154.

[127] Liu, Z., Yin, B., Liang, X., Bai, Y., Tan, Z., Liu, S., Li, Y., Liu, Y., & Jian, S. (2014). Axial strain and temperature sensing characteristics of the single–coreless–single mode fiber structure-based fiber ring laser. In Applied Physics B (Vol. 117, Issue 2, pp. 571–575). Springer Science and Business Media LLC. https://doi.org/10.1007/s00340-014-5869-z.

[128] Ma, L., Qi, Y., Kang, Z., & Jian, S. (2014). All-Fiber Strain and Curvature Sensor Based on No-Core Fiber. In IEEE Sensors Journal (Vol. 14, Issue 5, pp. 1514–1517). Institute of Electrical and Electronics Engineers (IEEE). https://doi.org/10.1109/jsen.2014.2298553.

[129] Sun, Y., Liu, D., Lu, P., Sun, Q., Yang, W., Wang, S., Liu, L., & Zhang, J. (2017). Dual-Parameters Optical Fiber Sensor With Enhanced Resolution Using Twisted MMF Based on SMS Structure. In IEEE Sensors Journal (Vol. 17, Issue 10, pp. 3045–3051). Institute of Electrical and Electronics Engineers (IEEE). https://doi.org/10.1109/jsen.2017.2673959.

[130] Yan, S.-C., Zhao, Y., Chen, M.-Q., & Liu, Q. (2020). Optical fiber strain sensor with double S-tapers. In Instrumentation Science & Technology (Vol. 49, Issue 3, pp. 313–326). Informa UK Limited. https://doi.org/10.1080/10739149.2020.1840387.

[131] Yan, S.-C., Zhao, Y., Chen, M.-Q., & Liu, Q. (2020). Optical fiber strain sensor with double S-tapers. In Instrumentation Science & Technology (Vol. 49, Issue 3, pp. 313–326). Informa UK Limited. https://doi.org/10.1080/10739149.2020.1840387.

[132] Zhang, S., Geng, T., Wang, S., Niu, H., Li, X., Deng, S., Wang, Z., Sun, C., Ma, Y., Yang, W., Sun, W., & Yuan, L. (2020). High-Sensitivity Strain and Temperature Simultaneous Measurement Sensor Based on Multimode Fiber Chirped Long-Period Grating. In IEEE Sensors Journal (Vol. 20, Issue 24, pp. 14843–14849). Institute of Electrical and Electronics Engineers (IEEE). https://doi.org/10.1109/jsen.2020.3010071.

[133] Wang, Y., Zhou, Y., Wang, X., Chen, D., Lian, Z., Lu, C., & Tam, H.-Y. (2020). Simultaneous measurement of temperature and strain based on a hollow core Bragg fiber. In Optics Letters (Vol. 45, Issue 22, p. 6122). The Optical Society. https://doi.org/10.1364/ol.403722.

[134] Lian, X., Wu, Q., Farrell, G., & Semenova, Y. (2020). High-sensitivity temperature sensor based on anti-resonance in high-index polymer-coated optical fiber interferometers. In Optics Letters (Vol. 45, Issue 19, p. 5385). The Optical Society. https://doi.org/10.1364/ol.403050.

[135] Huang, Y., Wang, T., Deng, C., Zhang, X., Pang, F., Bai, X., Dong, W., Wang, L., & Chen, Z. (2017). A Highly Sensitive Intensity-Modulated Optical Fiber Magnetic Field Sensor Based on the Magnetic Fluid and Multimode Interference. In Journal of Sensors (Vol. 2017, pp. 1–7). Hindawi Limited. https://doi.org/10.1155/2017/9573061.

[136] Ma, L., Qi, Y., Kang, Z., & Jian, S. (2014). All-Fiber Strain and Curvature Sensor Based on No-Core Fiber. In IEEE Sensors Journal (Vol. 14, Issue 5, pp. 1514–1517). Institute of Electrical and Electronics Engineers (IEEE). https://doi.org/10.1109/jsen.2014.2298553.

[137] Zhou, T., Zhang, Y., Han, B., Zhang, A., & Fu, D. (2018). Low cost non-adiabatic tapered fiber for high-sensitive temperature sensing. In Optical Fiber Technology(Vol.45,pp.53–57).ElsevierBV. https://doi.org/10.1016/j.yofte.2018.06.004.

[138] Lian, X., Wu, Q., Farrell, G., & Semenova, Y. (2020). High-sensitivity temperature sensor based on anti-resonance in high-index polymer-coated optical

fiber interferometers. In Optics Letters (Vol. 45, Issue 19, p. 5385). The Optical Society. https://doi.org/10.1364/ol.403050.

[139] Hernandez-Romano, I., Monzon-Hernandez, D., Moreno-Hernandez, C., Moreno-Hernandez, D., & Villatoro, J. (2015). Highly Sensitive Temperature Sensor Based on a Polymer-Coated Microfiber Interferometer. In IEEE Photonics Technology Letters (Vol. 27, Issue 24, pp. 2591–2594). Institute of Electrical and Electronics Engineers (IEEE). https://doi.org/10.1109/lpt.2015.2478790.

[140]Hernandez-Romano, I., Monzon-Hernandez, D., Moreno-Hernandez, C., Moreno-Hernandez, D., & Villatoro, J. (2015). Highly Sensitive Temperature Sensor Based on a Polymer-Coated Microfiber Interferometer. In IEEE Photonics Technology Letters (Vol. 27, Issue 24, pp. 2591–2594). Institute of Electrical and Electronics Engineers (IEEE). https://doi.org/10.1109/lpt.2015.2478790.

[141] P. Wang, H. Zhao, X. Wang, G. Farrell, and G. Brambilla, “A Review of Multimode Interference in Tapered Optical Fibers and Related Applications,” Sensors, vol. 18, no. 3, p. 858, Mar. 2018, doi: 10.3390/s18030858. [Online]. Available: http://dx.doi.org/10.3390/s18030858

[142] Khaleel, W. A., & Al-Janabi, A. H. M. (2017). High-sensitivity sucrose erbium-doped fiber ring laser sensor. In Optical Engineering (Vol. 56, Issue 2, p. 026116). SPIE-Intl Soc Optical Eng. https://doi.org/10.1117/1.oe.56.2.026116.

[143 Alsweefe, H., Al-Hayali, S. K., & Al-Janabi, A. (2018). Efficient humidity sensor based on an etched no-core fiber coated with copper oxide nanoparticles. In Journal of Nanophotonics (Vol. 12, Issue 04, p. 1). SPIE-Intl Soc Optical Eng. https://doi.org/10.1117/1.jnp.12.046018.

Appendices

Appendix

(A)

THORLABS

Laser Diode Current and Temperature Controller

ITC4000 Series Operation Manual

2018

1 General Information

The ITC4000 Series is a high power precision laser diode and temperature controller series with a USB 2.0 interface for driving laser diodes up to 20A laser current.

Special highlights of the ITC4000 Series Laser Diode and Temperature Controllers are:

- Operate with anode- or cathode-grounded lasers and photodiodes
- Current (photodiode) and voltage (thermopile) feedback inputs
- The laser diodes can be operated in constant current as well as in constant power mode
- CW mode with modulation up to 100kHz
- Internal DDS generator for sine, square, triangle waveforms
- External modulation input
- QCW mode with pulse width down to 100µs
- QCW trigger input and trigger output
- Interlock for automatic switch off by an external emergency switch or by a cable interruption
- Laser Diode Enable input
- High power TEC with excellent temperature stability and PID Auto-Tune function
- Temperature loop monitoring for laser protection
- A wide variety of protection features safeguard the laser diode and the TEC element from damage.
- USB interface for remote operation supporting the USBTMC protocol
- SCPI compliant command set
- VXIpnp Instrument Drivers for various programming environments including NI-LabVIEW™, NI-LabWindows™/CVI and MS-Visual Studio
- Power efficient by active power management

This part of the operation manual contains specific information on how to operate the ITC4000 Series Laser Diode and Temperature Controller. A general description is followed by an explanation of how to operate the unit manually. The instrument provides a USB 2.0 Full Speed interface according to the USB 2.0 specification, the USBTMC specification and the USBTMC USB488 specification.

Related documents:

- LDC4000 Series Operation Manual available at www.thorlabs.com
- TED4000 Series Operation Manual available at www.thorlabs.com
- Series 4000 Programmers Reference Manual at www.thorlabs.com

© 2018 Thorlabs

Appendix

(B)

THORLABS

LM14S2
Butterfly Laser Diode Mount

User Guide

Chapter 8 Specifications

Performance Specifications	
Laser Specifications	
Lasers Supported	14 Pin-Butterfly
Maximum Laser Current	5 A
Laser Pin Configurations	User Configurable
RF Modulation Frequency	100 kHz to 500 MHz
RF Input Connection	SMA
RF Input Impedance	25 Ω (On Bias-T Adapter)
Maximum RF Power	200 mW or Limit of Laser Diode
Laser Polarity	Anode Grounded (See Section 4.7)
TEC Specifications	
Maximum TEC Current	5 A
Maximum TEC Voltage	Laser Specific
TEC Heating / Cooling Capacity	Laser Specific
Typical Temperature Range (LD Dependent)	0 to 70 °C
Temperature Sensors	Laser Specific

Physical Specifications	
Size (Not Including Ports)	3.5" x 3.5" x 1.25" (88.9 mm x 88.9 mm x 31.75 mm)
Weight	0.6 lb (0.27 kg)

Appendix

(C)

Superluminescent Diode
1550 nm, Butterfly Package

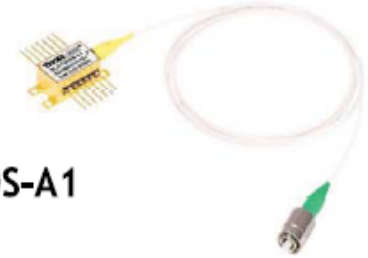

SLD1550S-A1

Description

The SLD1550S-A1 is a 1550 nm, low-power, broadband Superluminescent Diode (SLD) with a near-Gaussian spectral profile and low ripple. This SLD is housed in a standard 14-pin butterfly package with FC/APC-connectorized, nonpolarization-maintaining fiber. An integrated thermistor allows for temperature control, thus stabilizing the power and spectrum.

Specifications

CW; T_{CHIP} = 25° C, T_{CASE} = 0 to 65° C

SLD1550S-A1				
	Symbol	Min	Typical	Max
Center Wavelength	λ_C	1520 nm	1550 nm	1580 nm
Operating Current	I_{OP}	-	450 mA	500 mA
ASE Power*	P_{ASE}	0.75 mW	1.0 mW	-
Optical 3 dB Bandwidth*	BW	100 nm	110 nm	-
RMS Gain Ripple *	δG	-	-	0.1 dB
Forward Voltage*	V_F	-	1.6 V	2.0 V
TEC Operation (Typical / Max @ T_{CASE} = 25 °C / 65 °C)				
- TEC Current	I_{TEC}	-	0.35 A	1.5 A
- TEC Voltage	V_{TEC}	-	0.5 V	3.5 V
- Thermistor Resistance	R_{TH}	-	10 kΩ	-

*@I_{OP}

Performance Plots

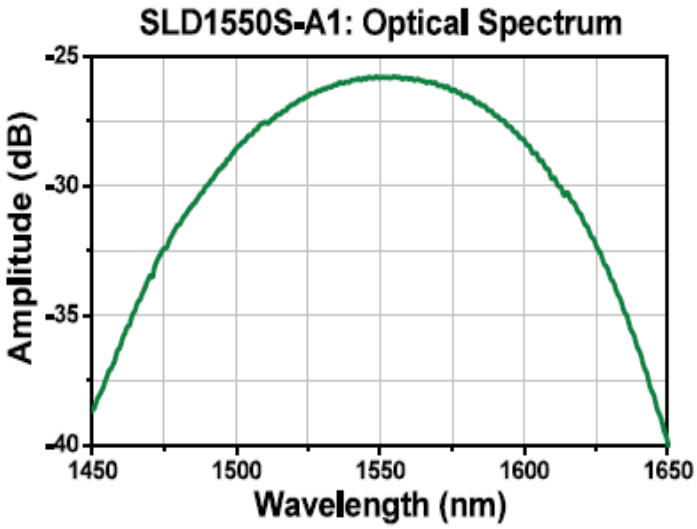

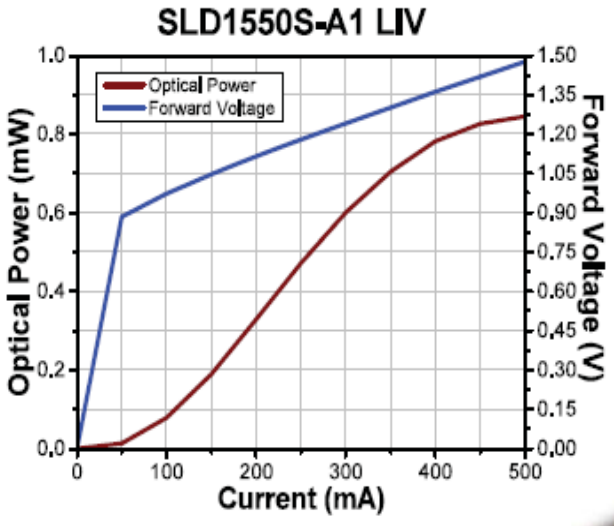

Drawings

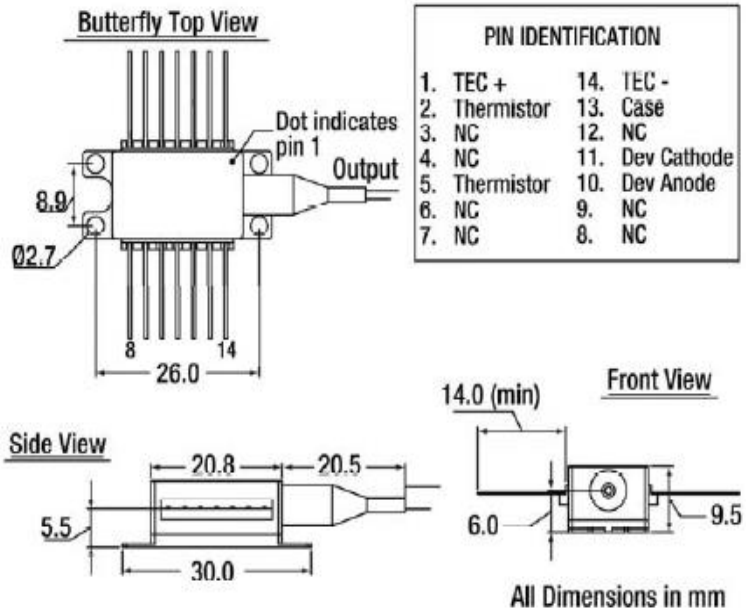

Note: Output isolator and monitor photodiode are available options for butterfly-packaged diodes. Please contact Technical Support for more information.

Appendix

(D)

Coreless Termination Fiber

FG125LA
FG250LA
FG400LA

Description

These coreless silica termination fibers can be spliced to the ends of standard fiber to reduce back reflections or prevent damage to the fiber end face. A return loss of greater than 65 dB is achieved by splicing 0.25 m of coreless fiber to the desired component.

Specifications

Specifications			
Item #	FG125LA	FG250LA	FG400LA
Wavelength Range	400 - 2400 nm		
Return Loss	>65 dB with 0.25 m		
Glass Diameter	125 ± 1 µm	250 ± 10 µm	400 ± 15 µm
Coating Diameter	250 µm ± 5%	400 ± 20 µm	550 ± 20 µm
Coating	Acrylate		
Glass Refractive Index	1.467287 @ 436 nm 1.458965 @ 589.3 nm 1.450703 @1020 nm 1.444 @1550 nm		
Operating Temperature	-40 to 85 °C		
Proof Test Level	>100 kpsi		
Recommended Stripping Tool	T06S13 or FTS4	T12S16	T18S25

Appendix

(E)

Corning® SMF-28® Ultra Optical Fiber

Product Information

CORNING

Corning® SMF-28® Ultra optical fiber is an ITU-T Recommendation G.652.D compliant optical fiber with Corning's enhanced low-loss and bend fiber technologies. This full-spectrum fiber has bend performance that exceeds the ITU-T Recommendation G.657.A1 standard and still splices the same as the installed base of standard single-mode fibers such as SMF-28e+ fiber. SMF-28 Ultra fiber offers industry-leading specifications for attenuation, macrobend loss, and polarization mode dispersion values, which provide a solid foundation for new network deployments as well as upgrades to existing networks. Since Corning brought the first fiber to market more than 40 years ago, Corning's leadership in single-mode fiber innovation has been unparalleled.

Optical Specifications

Maximum Attenuation

Wavelength (nm)	Maximum Value* (dB/km)
1310	≤ 0.32
1383**	≤ 0.32
1490	≤ 0.21
1550	≤ 0.18
1625	≤ 0.20

* Alternate attenuation offerings available upon request.
** Attenuation values at this wavelength represent post-hydrogen aging performance.

Attenuation vs. Wavelength

Range (nm)	Ref. λ (nm)	Max. α Difference (dB/km)
1285 – 1330	1310	0.03
1525 – 1575	1550	0.02

The attenuation in a given wavelength range does not exceed the attenuation of the reference wavelength (λ) by more than the value α.

Macrobend Loss

Mandrel Radius (mm)	Number of Turns	Wavelength (nm)	Induced Attenuation* (dB)
10	1	1550	< 0.50
10	1	1625	< 1.5
15	10	1550	≤ 0.05
15	10	1625	≤ 0.30
25	100	1310, 1550, 1625	≤ 0.01

*The induced attenuation due to fiber wrapped around a mandrel of a specified radius.

Point Discontinuity

Wavelength (nm)	Point Discontinuity (dB)
1310	≤ 0.05
1550	≤ 0.05

Cable Cutoff Wavelength (λ_{cc})

$\lambda_{cc} \leq 1260$ nm

Mode-Field Diameter

Wavelength (nm)	MFD (μm)
1310	9.2 ± 0.4
1550	10.4 ± 0.5

Dispersion

Wavelength (nm)	Dispersion Value [ps/(nm·km)]
1550	≤ 18.0
1625	≤ 22.0

Zero Dispersion Wavelength (λ_0): 1304 nm ≤ λ_0 ≤ 1324 nm
Zero Dispersion Slope (S_0): S_0 ≤ 0.092 ps/(nm²·km)

Polarization Mode Dispersion (PMD)

	Value (ps/√km)
PMD Link Design Value	≤ 0.04*
Maximum Individual Fiber PMD	≤ 0.1

*Complies with IEC 60794-3: 2001, Section 5.5, Method 1, (m = 20, Q = 0.01%), September 2001.

The PMD link design value is a term used to describe the PMD of concatenated lengths of fiber (also known as PMD_Q). This value represents a statistical upper limit for total link PMD. Individual PMD values may change when fiber is cabled.

How to Order

Contact your sales representative, or call the Optical Fiber Customer Service Department:
Ph: 1-607-248-2000 (U.S. and Canada)
+44-1244-525-320 (Europe)
Email: cofic@corning.com
Please specify the fiber type, attenuation, and quantity when ordering.

وزارة التعليم العالي و البحث العلمي
جامعة بغداد
معهد الليزر للدراسات العليا

متحسس مبني على الليف البصري منزوع القلب لقياس درجة الحرارة و الانفعال

رسالة مقدمة الى

معهد الليزر للدراسات العليا /جامعة بغداد/لأستكمال متطلبات نيل شهادة ماجستير علوم في الليزر/ الهندسة الميكانيكية

من قبل

محمد مزاحم حسن داؤد

بكالوريوس هندسة ميكانيكية –2007

بأشراف

ا.م دكتور حنان جعفر طاهر

1443 هـ **2021 م**

الخلاصة

اثبتت المتحسسات الضوئية المصنوعة من الالياف البصرية في العقدين الاخيرين انها الوسيلة المثلى لقياس الكثير من المتغيرات الفيزيائية والكيميائية و الميكانيكية. اذ تمتاز بدقة عالية ،و وزن خفيف ،وقابلية تضمين دقيقة، والمناعة ضد التداخل الكهرومغناطيسي ومقاومة التأكل الكيميائي ضد اغلب الاحماض و القواعد. تلك الخصائص المميزة رجحت استخدامها بدل بالمتحسسات الالكترونية التقليدية في الكثير من التطبيقات الصناعية و الطبية . في هذا العمل تم اقتراح و عرض متحسسين، الاول متحسس حرارة يعتمد على مبدأ مقياس تداخل ماخ زيندربأستخدام الليف البصري المنزوع القلب المستدق.اذ تم لحام جزء بطول 2.96 سم تقريبا من الليف البصري منزوع القلب بي ليفين احاديين و تم توليد نهايات مستدقة عند نقطتي اللحام باستخدام جهاز لحام ضوئي. ثم تم تصنيع متحسس انفعال يعتمد على مبدأ ماخ زيندر و ذلك بلحام جزء بطول 31 ملم من الليف البصري منزوع القلب بقطر 125 مايكرومتر بين ليفين بصريين احاديي الطول الموجي واستخدام مساكات خاصة لليف البصري مثبتة على منصات مايكرومترية خاصة لتطبيق الاستطالة و توليد الانفعال المايكرومتري. في متحسس الحرارة تم الاحتفاظ بالغطاء البوليمر الواقي للجزء المتحسس لتمكين توظيف طريقتين لزيادة حساسية الحرارة ، اللحام المستدق و الاحتفاظ بالغطاء البوليمرذو معامل تمدد حراري اعلى من السيليكا-جيرمانيوم . كانت حساسية الحرارة المستحصلة من متحسس الحرارة تساوي 1.943- نانوميتر لكل درجة حرارة سيليزية مع دقة تصل الى 0.01 سيليزي و زمن استجابة 3.5 ثانية في مدى قياس حرارة من 30 الى 45 درجة حرارة سيليزية.اما في متحسس الانفعال تم تطبيق استطالة خطية باتجاهين متعاكسين و على احداثي واحد بمدى استطالة من 0 الى 1000 مايكرومتر، فكانت الحساسية المستحصلة 16.37- بيكومتر لكل وحدة استطالة و تعتبر هذه القراءة المستحصلة لحساسية الانفعال باستخدام الليف البصري المنزوع القلب الاعلى لحد الان على حد علمنا اذ كانت الدقة المستحصلة لمتحسس الانفعال 0.8 بيكومتر . المتحسسين يمكن تصنيعهما بسهولة و بكلفة قليلة و قابلية اعادة تصنيع عالية و تكرارية اداء ممتازة ، اذ من الممكن استخدامهما في الكثير من التطبيقات الطبية والهندسية كتطبيقات الطب الحياتي و تطبيقات ميكانيك الاحياء و الكثير من التطبيقات الصناعية الدقيقة.